MODELING OF HIGH STRAIN RATE AND STRAIN LOCALIZATION IN FCC SINGLE CRYSTALS: MULTISCALE DISLOCATION DYNAMICS ANALYSES

By:

MU'TASEM A. SHEHADEH

A dissertation submitted in partial fulfillment of the requirement for the degree of

DOCTOR OF PHILOSOPHY

WASHINGTON STATE UNIVERSITY

School of Mechanical and Materials Engineering

May 2005

To the faculty of Washington State University

The members of the committee appointed to examine the dissertation of MU'TASEM SHEHADEH find it satisfactory and recommend that it be accepted.

_____

Chair

_____

_____

ACKNOWLEDGEMENTS

I am extremely grateful to Allah, who alone made this accomplishment possible and provided me the strength to achieve it. I wish to express my deepest gratitude to my advisor, professor Hussein Zbib for his continuous support, encouragement and guidance throughout the years, and helping me to gain the experience that one must have in the academic field. Thanks are due to Dr. Sinisa Mesarovic, for serving on my dissertation committee, for the fruitful discussions we had about issues related to the current work and for the peer review of the manuscript. I would like also to thank Dr. Balasingam Muhunthan and Dr. Laith Tashman for serving on my dissertation committee.

I would also like to acknowledge the collaboration with Lawrence Livermore National Laboratory (LLNL). Special thanks go to Dr. Eduardo Bringa for the long-fruitful discussions that we had, and for his valuable comments especially on issues related to the mechanism of homogenous nucleation of dislocations. In addition, I also have to thank Dr. Tomas Diaz de la Rubia for his support.

In the School of Mechanical and Materials Engineering (MME), I would like to thank my officemates: Shafique Khan, Firas Akasheh and Sreekanth Akarapu for the interesting discussions that we had. I would also like to thank the administrative and technical staff in MME for their continuous help. In particular, I would like to mention Janet Danforth, Gayle Landeen, Mary Simenson, Micheal Shook and Giac Pham.

Special thanks go to my life-long friend Murad Alholy. Together we lived all the details of doctorate students' life, and together we went through a very rich experience at Washington State University (WSU).

Finally, special acknowledgements go to my parents, brothers and sisters for constant and life-long love, encouragement and support. To my parents, I thank you for your endless patience and sacrifice.

MODELING OF HIGH STRAIN RATE AND STRAIN LOCALIZATION IN FCC SINGLE CRYSTALS: MULTISCALE DISLOCATION DYNAMICS ANALYSES

Abstract

By Mu'tasem A. Shehadeh, Ph.D.

Washington State University

May 2005

Chair: Hussein M. Zbib

In this work, the deformation process in FCC single crystals under high strain rate ranging between 10^5 s^{-1} to 10^8 s^{-1} is investigated using a multiscale model of plasticity that couples discrete dislocation dynamics and finite element analyses. Computer simulations are carried out to mimic the shock loading condition involved in high intensity laser experiments. In the first part of this study, the effects of peak pressure, shock pulse duration, crystal anisotropy and the nonlinear elastic properties on the interaction between shock waves and preexisting dislocation sources are investigated. Our calculations show that the dislocation density is proportional to strain rate, pulse duration and crystal orientation, and that the dislocation density increases with pressure proportional to a power law of 1.70 for pressure greater than 30 GPa. The results suggest

that while the inclusion of pressure-dependent elastic properties for isotropic media leads to faster wave propagation speed, incorporating the effect of crystal anisotropy in the elastic properties results in orientation dependent wave speed and peak pressure. The relaxed configurations of dislocation microstructures showed the formation of micro bands coincident with the {1 1 1} whose characteristics are strain rate and orientation dependent.

In the second part of this study, shock-induced dislocation nucleation is investigated. Shock waves with strength ranging from 10 to 60 GPa are launched in copper perfect crystals resulting in the nucleation of large number of dislocation loops at the wave front. Once the dislocation loops are nucleated, they grow in all directions in their slip planes forming a three dimensional microstructures consisting of dislocation entanglements and weak cellular structure. By this plasticity mechanism, we found that uniaxially compressed material relaxes to a hydrostatically compressed state (1D $\rightarrow$3D) as observed in the experiment.

In the third part of this study, the effect of finite element boundary condition on wave propagation is investigated by implementing periodic boundary condition and comparing its results with free and confined boundary conditions. The results show that confined and periodic boundary conditions based on node-to-node matching are suitable to model shock wave propagation. Mesh sensitivity analyses for steep and ramp shock waves show that the convergence in the ramp wave occurs at relatively coarse mesh density when compared to the steep wave. The effect of lattice rotation on strain localization was also investigated. The results show that more strain localization occurs when slip rotation is taken into account.

TABLE OF CONTENTS

LIST OF FIGURES

LIST OF TABLES

DEDICATION

This dissertation is dedicated to my parents and to all my brothers and sisters. It is also dedicated to all those who struggle for justices and dignity.

CHAPTER 1

Introduction

1.1 Introduction

High strain rate processes refer to events in which the material is subjected to a rapid deposition or transmission of energy in a small region through the propagation of shock waves. Shock waves are supersonic disturbances that lead to large changes in pressure (compression), density and internal energy almost instantaneously. The time over which the material can achieve these abrupt changes ranges between hundreds of nanoseconds to fractions of nanoseconds depending on the extremity of the loading condition.

Shock waves can be generated by different means such as mechanical from high-speed impact, chemical from explosives, radiative from high intensity laser or nuclear from neutrons. Shock waves can propagate in one, two or three dimensional geometries, however most of the research attention has been focused on the propagation of one dimensional wave, as it is extremely difficult to carry out precise measurements in two and three dimensional geometries. The main types of one dimensional shock waves are planar, cylindrical and spherical shock waves where the compression occurs in a surface, a line, and a point respectively. The experimental measurements for the planar shock wave are relatively simple compared to spherical and cylindrical waves where geometrical attentions need to be incorporated.

Under shock loading condition, the material undergoes changes in its mechanical, physical and mechanical properties. In solid mechanics, we are mainly interested in developing fundamental understanding of the material response under extreme conditions and the deformation process accompanied by shock propagation. By that we can improve our understanding to the deformation process under extreme conditions and design novel materials with enhanced mechanical properties.

1.2 Plane Wave Loading

Plane wave loading is achieved by loading of half space with lateral dimensions extending to infinity as shown in figure 1.1. Half spaces however, do not exist in real life, therefore, in the experiments where the specimens have finite dimensions, this loading condition is attained by making the measurements at the center of the specimens over a very short period of time before the arrival of waves reflected from the edges. In general, such loading generates a uniaxial strain in the material, resulting in the propagation of large amplitude three-dimensional state of stress.

The main elements to investigate the mechanical response in shock experiments are the application of controlled loading and the precise measurements of the material response and the wave structure (Graham 1993). Wave profile measurements are carried out by constructing wave snapshots or wave histories. Wave snapshots are constructed by recording the variation in the wave profile as a function of distance at the same time, whereas wave histories are constructed by recording the variation in the wave amplitude as a function of time at the same position. The ideal shock profile (exhibited by normal

fluids) consists of a discontinuous shock front, plateau at the peak pressure whose duration is equivalent to the pulse duration and a release part as shown in figure 1.2a. This kind of idealization is used when the behavior of the solid material is assumed to be fluid like. In real solids however, the wave profile is different as different peculiarities are exhibited such as plastic deformation. Shock waves are usually classified as weak, moderate and strong. When the shock strength exceeds the critical value of plastic flow stress defined as the Hugoniot elastic limit (HEL), yielding phenomenon occurs and leaves elastic precursor that separates the elastic and plastic regimes on the wave profile (See figure 1.2b). It is worth mentioning that although the HEL in metals is low, it can be very high in ceramics; take for example sapphire where HEL ~ 20 GPa (Meyers 1994).

1.3 Rankin Hugoniot Jump Conditions

In this section, we derive the jump conditions using the hydrodynamics treatments of fluids assuming uniaxial compression of the material. In strong shocks, the amplitude of pressure greatly exceeds the yield stress and so the shear modulus of the material can be neglected. The generation of shock waves can be simply envisioned as successive motion of a piston in a cylinder of a unit cross sectional area as shown in figure 1.3. The motion of the piston takes the matter from its ambient conditions (P_0, ρ_0, E_0) to the highly compressed state (P, ρ, E) over a period of time equals Δt where P, ρ, E are pressure, mass density, and internal energy per unit mass.

During a time interval of Δt the wave front has moved a distance $U_s \Delta t$ where U_s is the wave propagation speed. The piston however, has moved a distance $U_p \Delta t$, where

U_p is the piston (particle) velocity. Hence the matter contained in region $U_s \Delta t$ is now contained in region $(U_s - U_p) \times \Delta t$. The conservation of mass states that matter can neither be created nor destroyed, hence one can obtain:

$$\rho_0 U_s = \rho(U_s - U_p), \text{ or } \frac{\rho_0}{\rho} = 1 - \frac{U_p}{U_s} \qquad 1.1$$

Newton's second law states that force is equal to the rate change of momentum $(F\Delta t = \Delta(\text{mass} \times \text{velocity}))$. When a shock travels a distance $U_s \times \Delta t$, it accelerates a mass $\rho_0 U_s \Delta t$ to a particle velocity of U_p. Because the area is unity, the impulse $F\Delta t = (P - P_0)\Delta t$, assuming P_0 equals to zero, we obtain;

$$P = \rho_0 U_s U_p \qquad 1.2$$

The energy conservation requires that the work done by the piston on the matter is equal to the change in its kinetic and internal energies. When the piston moves a distance $U_p \Delta t$, the work done is equal to $PU_p \Delta t$. The change in the kinetic energy acquired by that mass element is therefore $\frac{1}{2}(\rho_0 U_s \Delta t) U_p^2$. The change in the internal energy between the undisturbed and shocked states can be expressed as $\rho_0 U_s \Delta t(E - E_0)$. From this discussion the energy equation can be expressed in the following form:

$$PU_p = \frac{1}{2}(\rho_0 U_s) U_p^2 + \rho_0 U_s (E - E_0) \qquad 1.3$$

Using equations 1.1 and 1.2, equation 1.3 can be rearranged such that:

$$E - E_0 = \frac{1}{2} P(V - V_0) \qquad 1.4$$

Where $V = 1/\rho$. In shock wave community, equations 1.1, 1.2 and 1.4 are usually called the Rankine-Hugoniot jump conditions. It is worth mentioning that the experimental data of a large number of materials shows that relationship between the shock velocity and the particle velocity is linear with a slope that is material dependent.

1.3 Stress Analysis

Stress analysis of the state of stress under shock loading condition is essential to comprehend the deformation process under extreme conditions. The state of stress in a planar shock wave involves uniaxial strain compression. Suppose that the material is compressed uniaxially in the z-direction, then $\varepsilon_{zz} \neq 0$ and all other stain components are zero. If no plastic deformation (no dislocations) is involved in the wave propagation, linear elasticity theory predicts the following relations:

$$\sigma_{xx} = \sigma_{yy} = \frac{\upsilon}{1-\upsilon}\sigma_{zz} \tag{1.5}$$

$$\tau = \frac{1}{2}(\sigma_{zz} - \sigma_{yy}) \tag{1.6}$$

$$p_m = -\frac{1}{3}(\sigma_{xx} + \sigma_{yy} + \sigma_{zz}) \tag{1.7}$$

Where υ is Poisson's ratio and τ is the maximum shear stress at the wave front and p_m is the hydrostatic pressure. In the shock wave loading of solids, the longitudinal component of the stress is defined as the pressure ($P = -\sigma_{zz}$) since it is the driving force of the shock wave, in fluids however the pressure is equal to the hydrostatic pressure. When the applied pressure exceeds the HEL, the material deforms plastically. Plastic deformation is mainly produced by a microscopic mechanism controlled by the activities of dislocations.

Dislocation activities are the fundamental mechanism for relieving strain in crystalline materials, hence it is expected that the dislocation activities will cause the stresses to have different values than those given by the elasticity theory.

1.5 Dislocation Dynamics

According to the dislocation theory, plastic deformation in crystals is achieved by the generation and transport of dislocations (see figure 1.4). Dislocations are line defects that can move on specific planes in certain directions depending on the crystallographic structure of the crystal. In fcc crystals for example, dislocations move on $\{111\}$ planes in $\langle 110 \rangle$ directions. Geometrically a dislocation line is defined by its Burgers vector (b) and line sense (ξ). The Burgers vector is the displacement of the atoms that occurs in the crystal as the dislocation moves. The line sense is a unit vector tangent to the dislocation line. When the Burgers vector is normal to the line sense the dislocation is defined as edge dislocation and when it is parallel to the line sense it is defined as screw dislocation. The dislocation can be a line extending until it reaches a free surface or an interface or it can be a closed loop within the crystal. As the dislocation is a line defect, it is associated with an internal strain field that varies as the inverse of the distance from its core

This fundamental understanding of dislocation mechanisms has been used to simulate the collective behavior of large number of dislocations in single crystals. Discrete dislocation dynamics (DD) simulation codes have been introduced in the last two decades as powerful numerical tools to simulate plasticity of single crystals based on the fundamental physical laws that govern dislocation motion and interaction. At

Washington State University, professor Zbib and collaborators have developed one of the few well-known three-dimensional DD codes. In this framework, plastic deformation of single crystals is obtained by the explicit evaluation of dislocation evolution history. Dislocation lines and curves are represented by discrete straight segments that interact with each other over short and long ranges. The Peach-Koehler (PK) force resulted from different sources is calculated on each dislocation segment. This includes the forces exerted on the dislocation from externally applied stresses, the stress fields from the immediate neighboring segments and other dislocations that may be present in the computational cell. As a dislocation moves, it may encounter local obstacles such as stacking fault tetrahedra, defect clusters and vacancies. Furthermore, the dislocation has to overcome internal drag, and local barriers such as the Peierls stresses.

The calculated PK force is used to advance the dislocation segment based on a linear mobility law. The dislocation mobility can be extracted from experimental data, or calculated by atomistic simulations. For high strain rate loading, the dynamics of the dislocations follows a Newtonian equation of motion as will be explained in the next chapters. Another important consideration for DD simulations is dealing with close dislocation-dislocation interactions such as annihilation and formation of jogs and junctions.

1.6 Deformation Mechanisms

There are three regimes of deformation, which are controlled by the applied pressure (strain rate). These deformation regimes are thermal activation, phonon drag and

shear wave speed limit. Figure 1.5 shows the transition in the mode of deformation by plotting the dislocation velocity as a function of flow stress. Here we give a brief description of these regimes.

Thermal Activation: At low strain rate, dislocation overcomes the short-range obstacle discussed above by the assistance of thermal energy. After the dislocation gets over the obstacle, it moves a distance λ till it encounters another barrier. In this case, the dislocation velocity can be written as:

$$\bar{v} = \frac{\lambda}{t_r + t_w} \qquad 1.9$$

Here, t_r is the running time between obstacles and t_w is the waiting time for the thermal kick. Apparently, t_w will decrease as the applied stress (strain rate) increases, therefore the thermal activation mechanism becomes less effective.

Phonon Drag: At high strain rates, the applied stress becomes large enough that the dislocations will have no time to wait for a thermal kick. In this regime, the dislocation has to overcome another barrier provided by drag forces, which result from the interaction between the dislocations and the elastic vibrations of the crystal (phonons).

Shear Wave Speed Limit: At ultra high strain rate, the dislocation velocity is limited by the shear wave speed. This speed limit comes about as the stress field of the dislocation becomes infinite when the dislocation speed approaches the shear wave velocity. A detailed treatment of this speed limit with the introduction of the concept the dislocation effective mass can be found in (Weertman 1961).

1.7 Dislocations under Shock Loading

Under low strain rate, low pressure loading, the onset of plasticity occurs by means of multiplication and motion of preexisting dislocations when the applied shear stress τ becomes large enough to move the dislocations. Under high strain rate loading however, high amplitude wave propagates with a state of shear stress exceeding the shear strength of the crystal therefore; plasticity may be induced by the multiplication and motion of preexisting dislocations or by the homogenous nucleation of small dislocation loops on or behind the wave front. The generation of the dislocation at the wave front relaxes the crystal, transforming the state of stress from uniaxial strain as given in equation 1.4 to a hydrostatically compressed state. In other words, the introduction of high density of defects at the wave front results in a fluid like behavior of the solid material by means of plasticity mechanism

$$\sigma_{xx} = \sigma_{yy} = \sigma_{zz} + 2\bar{\tau} \qquad 1.10$$

Here, $\bar{\tau}$ is the flow stress of the lattice.

There are several models that address the fundamental problem of homogenous nucleation of dislocations at the wave front. Smith (1958) proposed that infinite edge dislocations are nucleated at the wave front moving with the wave front (supersonic dislocation). Meyers (1978) suggested a model of dislocation loops nucleated periodically at the wave front as the wave advances in the lattice as depicted in figure 1.6. The nucleated loops move behind the wave front sub-sonically as the dislocation speed is limited by the shear wave speed limit.

1.8 Study Rationale

Extensive research has been carried out over the years to study the materials' response to shock loading. Historically, most of the research was carried out on the continuum scale by carrying out experiments or developing constitutive models based on the results of the experiments. With the advances in the experimental techniques such as the introduction of the in situ X-ray diffraction and the use of laser as sources to generate shocks, and with the advent of powerful computers, attention has been switched toward the investigation of the deformation process of different length and time scales and then trying to connect these scales together using multiscale models. Moreover, the material's response to extreme conditions involves many uncertainties that neither current experiments nor current theoretical models can resolve. These uncertainties maybe resolved by the collaboration of experimentalists, theoreticians and materials modelers to resolve these uncertainties.

Extensive work has been carried out in the national laboratories such as LLNL using all possible tools (experiments, theories, massive powerful parallel computers via molecular dynamics (MD) simulations to investigate the deformation mechanisms under extremely high strain rates, high pressure loading at different spatial and temporal scales with the focus on the atomistic and continuum scales. None of these modeling efforts to our knowledge, however, has been directed to investigate the deformation mechanism under shock loading on the micro scale.

In this dissertation, multiscale dislocation dynamics plasticity model (MDDP) developed at WSU by Zbib and coworkers is used as a tool to develop more insight and

to improve our understanding to plastic deformation under extreme shock loading conditions. The model is discussed in some details in chapter 2 and chapter 3. In this effort, we try to develop fundamental understanding to shock-induced plastic deformation in fcc single crystals and address some issues that are uncertain or cannot be attacked using current experimental techniques or beyond the capabilities of MD simulations. To date, the most advanced laser experiments can be used to generate peak pressure up to 100 GPa. On the other hand, MD simulations are limited in its spatial and temporal capabilities as fractions of micrometer and sub nanosecond can be simulated. It is worth mentioning however, that in the next few years the National Ignition Facility (NIF) at LLNL will be operational and using this huge laser facility where 192 powerful laser beams can be focused on a very small piece of material (mm's), many of current uncertainties can hopefully be resolved and by that we can compare our simulation results with the experiments and then make any necessary modifications.

It is worth mentioning that the version of the MDDP model that we started this work with could not be used to address shock wave-dislocation interaction. In this work therefore, the model has been modified to account for the following issues:

- Under shock loading condition, the material's properties become pressure dependent. A model that takes into account this pressure dependent behavior has been implemented in the new version of the code.
- When this work was started, the model was based on the assumption that the material is isotropic. However, cubic single crystal exhibits anisotropy in its response. The model therefore has been modified to account for this anisotropy effect.

- We include a model for homogeneous nucleation of dislocations based on large-scale atomistic simulations of shock loading. This homogenous nucleation model allows simulating shock induced plasticity in both perfect and defected single crystals. Before implementing this model, the simulations had to start with an initial distribution of dislocation loops or sources.
- Slip rotation was accounted for in the current model by updating the slip systems at each time step.
- Periodic boundary condition in the finite element (FE) code has been implemented to investigate the effect of different boundary conditions on the wave propagation and the induced plasticity.

1.9 Organization of the Study

After this brief introduction, I would like to introduce the main contents of the current work. This dissertation discusses the interaction process between dislocations and shock waves and it is written using paper format option. Each chapter to follow represents a technical paper that has been accepted or submitted for publication or a subscript that is in preparation for submission.

1- In chapter 2, the effects of different shock wave and materials' properties on the interaction process between dislocations and shock waves in isotropic media are investigated. Although the focus in this chapter is on the development of the dislocation microstructure, the model captures the main features of any

constitutive model applicable to shock loading, i.e. the constitutive model is modified and becomes of nonlinear type to account for materials' nonlinearity resulting from the changes in the elastic properties and mass density under high pressure. The effects of several parameters including peak pressure and pulse duration on dislocation microstructure are investigated.

2- In chapter 3, the effect of crystals anisotropy on wave propagation and dislocation microstructure is investigated. Moreover, the issue of shock wave attenuations has been addressed.

3- In chapter 4, the issue of homogenous nucleation of dislocation is addressed for the first time in the context of multiscale dislocation dynamics simulations. The results of dislocation dynamics are compared with multi-million molecular dynamics simulations and the most recent high intensity laser experiments carried out ay Lawrence Livermore National Laboratory.

4- In chapter 5, numerical and strain localization issues are investigated. This includes the role of finite element boundary condition on wave propagation, the effect of loading history of wave convergence and the role of lattice rotation on the deformation process.

References

Weertman, J., 1961, Response of metals to high velocity deformation. Ed P G Shewmon and V F Zackay (New York: Interscience), p 205.

Graham, R. A., 1993, *Solids Under High-Pressure Shock Compression*, Springer-Verlag, New York, p.15.

Meyers, M. A., 1994, *Dynamic Behavior of Materials*, (New York: John Wiley & Sons), p. 119.

Meyers, M. A., 1978, *Scripta Met*., **12**,21.

Smith, C. S., 1958,*Trans. AIME*, **vol. 212**, 99 574-578.

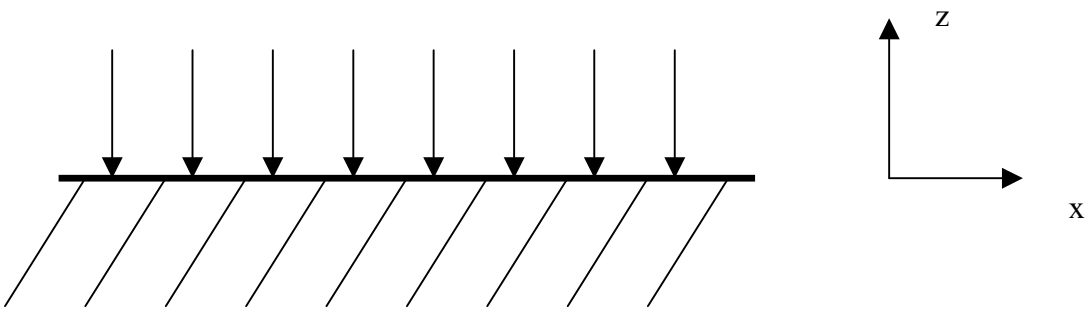

Figure 1.1. Uniaxial strain loading of half plane

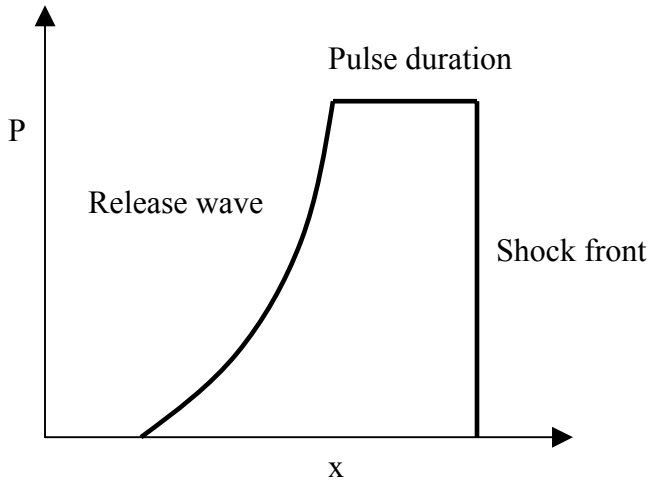

(a)

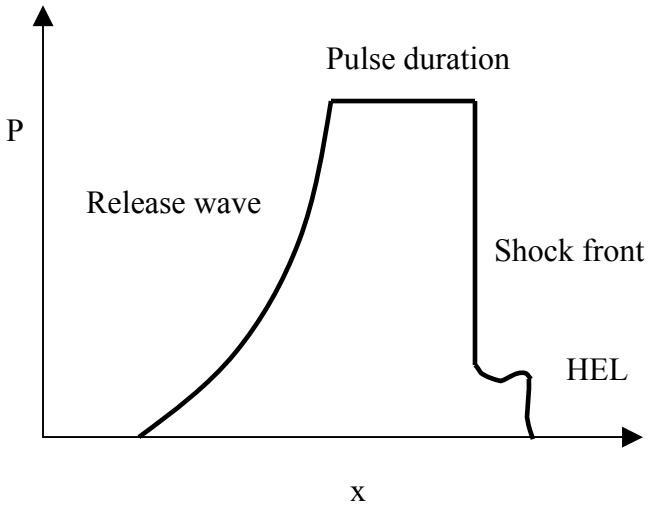

(b)

Figure 1.2. (a) Ideal wave profile (b) Effect of yielding on the wave profile

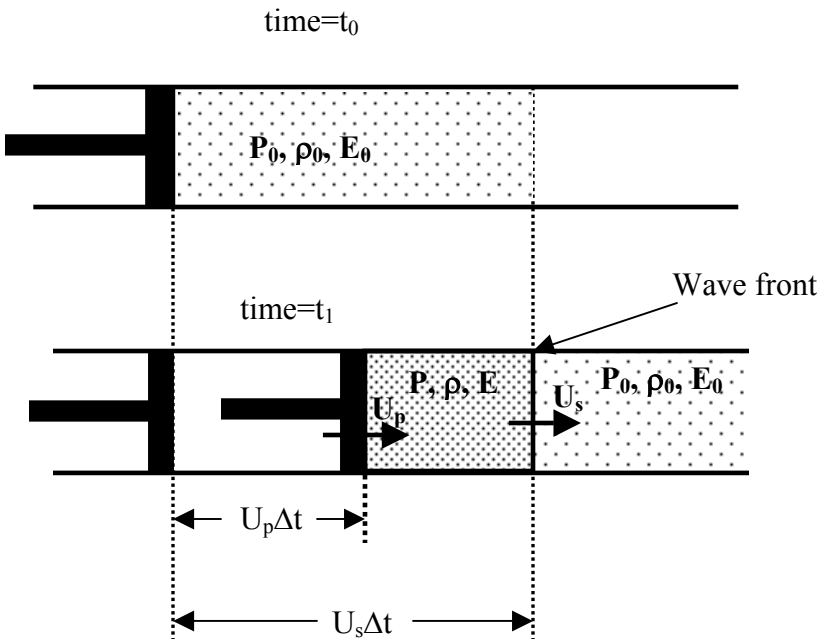

Figure 1.3. Rigid piston drives a shock wave into a compressible fluid

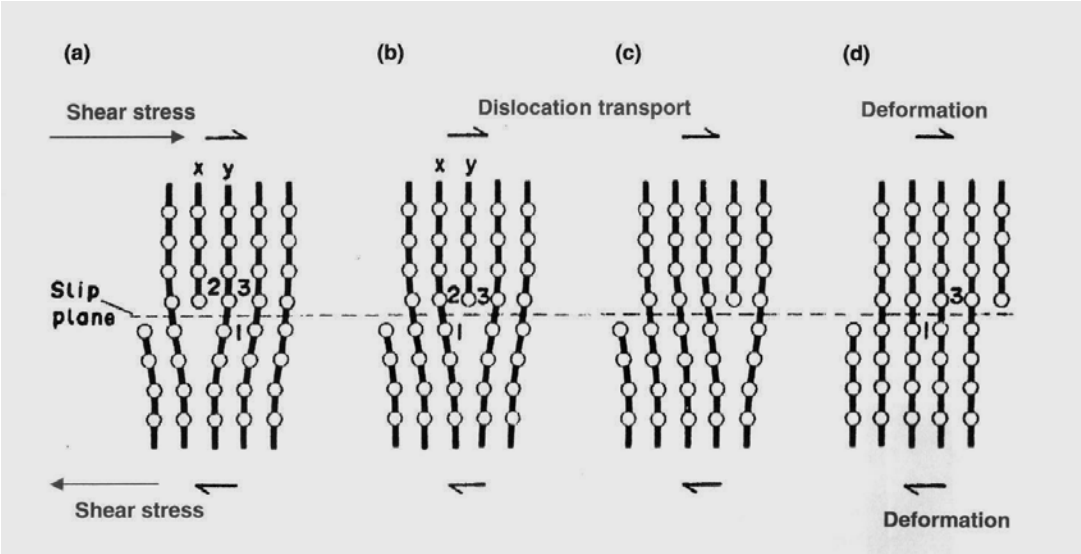

Figure 1.4. Dislocation motion in the crystal lattice

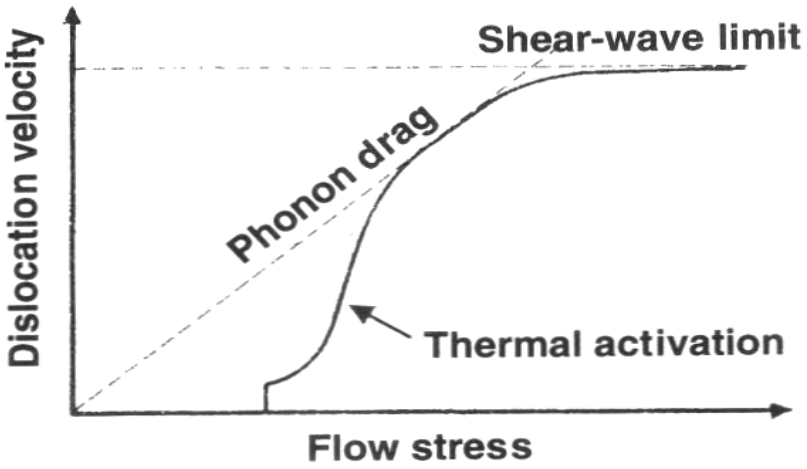

Figure 1.5. Regimes of deformation

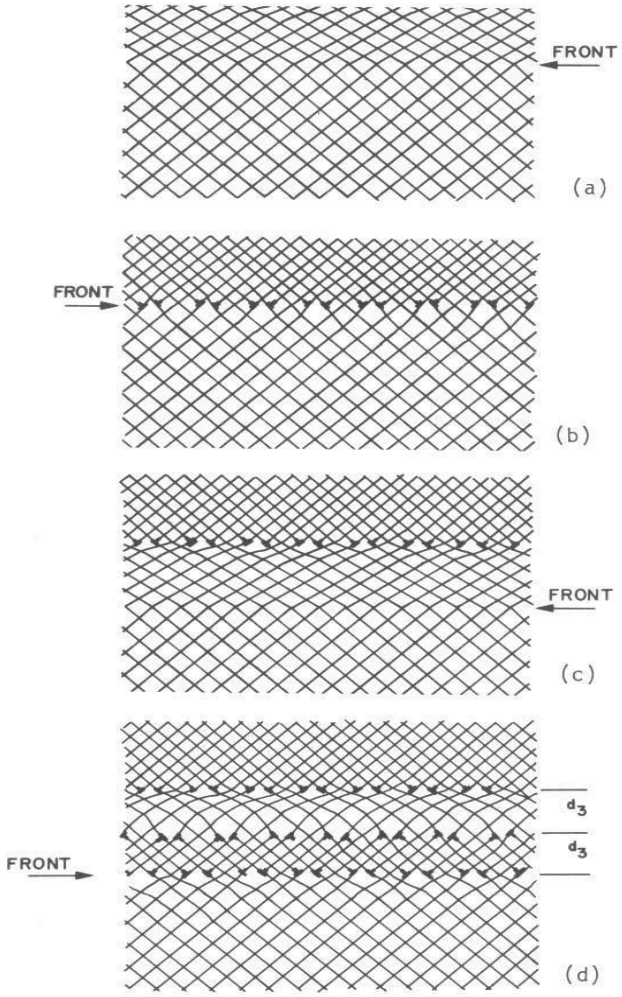

Figure 1.6. Dislocation nucleation at the wave front as proposed by Meyers (1978)

CHAPTER 2

Modeling the Dynamic Deformation and Patterning in FCC Single Crystals at High Strain Rates: Dislocation Dynamics Plasticity Analysis

2.1 Introduction

The response of materials to high strain rates and the deformation processes that occur under shock loading conditions are of interests in many applications, e.g. explosive metalworking, explosive welding, and high intensity laser interaction with solid targets. Shock waves are supersonic disturbances that lead to large changes in compression, particle velocity and internal energy almost instantaneously (Gupta 1999). Under shock conditions, a uniaxial strain state of deformation is induced in the material resulting in the propagation of a high pressure wave. When the applied pressure exceeds the Hugoniot elastic limit, the material deforms plastically as a result of dislocation motion and multiplication. In general, dislocations move on their slip planes with velocities that increase with the rate of deformation. However, due to the relativistic effect, the dislocations are limited to move at velocities less than the shear wave velocity. Weertman (1961) derived expressions for total, kinetic and strain energies of dislocation lines as a

function of velocity, and derived an expression for the effective mass of a fast moving dislocation. The dislocations accommodate high strain rates and restrictions on their velocity by high rates of multiplications and or nucleation. It is also observed that with high rate of strain, dislocations tend to multiply in heterogeneous patterns that lead to shear banding. Coffey (1992) examined the microscopic processes responsible for shear band formation including the rate at which a source can create dislocations. In addition, he examined the localized confinement of these dislocations and the very large energy dissipation rates associated with the very high velocity dislocations.

The interaction process between shock waves and dislocations leads to the formation of different microstructures such as dislocation cells (Wright *et al*. 1981, Meyers *et al*. 2003), micro twins (Meyers *et al*. 2001) and heavy deformation bands coincident with the slip planes (Mogileviskii and Bushnev 1990, Rivas *et al*. 1995). It is believed that the microstructure generated by shock waves depends on a number of parameters such as peak pressure, pulse duration, crystallographic orientation, and stacking fault energy (*SFE*). Meyers *et al*. (2001, 2002) presented a mechanism for dislocation generation that provides a realistic production of dislocations at different shock strengths.

Deformation process under high strain rate is a complex multiscale dynamic problem. Therefore, experiments at different scales were conducted to get more insight into the deformation process under extreme conditions. In the recent years, high intensity laser experiments have been introduced as an excellent tool to probe the materials' response to shocks at ultra high strain rates ($> 10^6$ s^{-1}). Kalantar *et al.* (2000, 2001) used intense laser to shock load copper single and polycrystals to study their response at high

strain rates. Loveridge *et al.* (2001) used x-ray diffraction with sub nanosecond resolution to measure the lattice parameters of silicon and copper single crystals. Copper single crystal shocked along [2 0 0] axis exhibited compression along [2 0 0] and [0 2 0] indicating prompt transition to plastic flow, whereas the response for silicon was purely elastic. Meyers *et al.* (2003) observed that the substructures generated by short pulse laser (5 nanoseconds duration) are very similar to those generated by plate impact experiments where the pulse duration is in the microsecond time scale. The effect of temperature on the dynamic tensile strength of aluminum single crystals was investigated (Kanel *et al.* 2001).

The advancements in the experimental capabilities over the years have improved our understanding of the dynamic response of materials. However, current experimental capabilities cannot address material response at pressure larger than 100 GPa. Until new experiments are designed, theories and models suitable for each length scale can be used and linked to perform multiscale simulations.

In the atomistic scale, molecular dynamic (MD) simulations have been used to investigate the deformation process in single crystals. Horstemeyer *et al.* (2001, 2002) carried out MD simulations to examine the effects of size scale, strain rate, and crystal orientation on the deformation of fcc single crystals. Kadau *et al.* (2002) conducted a multimillion MD simulation to study the shock induced phase transition in iron. Large-scale MD simulations were used to study plasticity induced in shock loaded fcc crystals and the dislocation structure behind the shock front (Bringa *et al*. 2003). A combined MD and finite element (FE) approach was introduced to study the propagation of laser induced pressure in a solid (Smirnova *et al.* 1999). Current MD capabilities can simulate

sizes in the submicron scale as no more than billions of atoms can be modeled (Clifton and Bathe 1999). Dislocation dynamics (DD) however, can simulate sizes of few microns, exceeding by an order of magnitude the capabilities of MD simulations.

DD has emerged as an excellent numerical tool to simulate the collective behavior of dislocations in a bulk material. Over the last 15 years, several DD models have been developed to simulate plastic deformation in single crystals, see for example (Kubin and Canova 1992, Schwarz and LeGoues 1997, Zbib *et al*. 1998, Ghoneim and Sun 1999). Van der Giessen and Needleman (1995) developed a model that couples two dimensional DD with a continuum FE model. A computational framework that couples three dimensional DD with a continuum FE analysis was developed based on an elasto-viscoplastic model (Yasin *et al*. 2001). These authors and others addressed various plastic deformation problems including hardening mechanisms, size effects, and dislocation-particles interaction, but none of them has addressed the problem of dislocations interaction with shock wave.

In our attempt to understand the response of fcc single crystal to high strain rates, multiscale dislocation dynamics model developed at Washington State University (WSU) by Zbib and coworkers (Rhee *et al.* 1998, Zbib *et al.* 1998, Yasin *et al.* 2001, Zbib *et al*. 2003) is used to study the interaction between stress waves and dislocations. In this study, the effects of strain rate, shock pulse duration and the dependence of elastic properties on pressure are investigated.

2.2 Multiscale Dislocation Dynamics Plasticity (MDDP)

The MDDP model merges two length scales, the nano-microscale where plasticity is determined by explicit three dimensional discrete dislocation dynamics (DD) analyses providing the material length scale, and the continuum scale where energy transport is based on basic continuum mechanics laws. The result is a hybrid elasto-viscoplastic simulation model coupling discrete DD with FE analysis. The MDDP methodology has been developed by Zbib and co-workers (2001-2004), here we give a very brief description of the basic equations governing dislocation-waves interaction.

Within the continuum framework, the governing equations are based on representative volume element (RVE) where the material obeys the basic laws of continuum mechanics, i.e. linear momentum balance and energy balance:

$$div\, S = \rho \dot{v} \tag{2.1}$$

$$\rho\ C_v \dot{T} = K\nabla^2 T + S.\dot{\varepsilon}^p \tag{2.2}$$

In the nano-microscale, DD analyses are used to determine the plasticity of single crystals by explicit three dimensional evaluations of dislocations motion and interaction among themselves and among other defects such as point and cluster defects, microcracks, microvoids, etc. In DD, dislocations are discretized into segments of mixed character. The dynamics of the dislocation is governed by a "*Newtonian*" equation of motion, consisting of an inertia term, damping term, and driving force arising from short-range and long-range interactions. As the dislocation moves, it has to overcome internal drag, and local barriers such as the Peierls stress. The dislocation may encounter local obstacles such as stacking fault tetrahedra, defect clusters and vacancies that interact with

the dislocation at short ranges and affect its local dynamics. In summary, the dislocation may encounter the following set of forces:

- Drag force, $B\boldsymbol{v}$, where B is the drag coefficient and $\boldsymbol{v}$ is the dislocation velocity.
- Peierls stress $\boldsymbol{F}_{Peierls.}$
- Force due to externally applied loads, $\boldsymbol{F}_{external.}$
- Dislocation-dislocation interaction force $\boldsymbol{F}_{D.}$
- Dislocation self-force $\boldsymbol{F}_{self.}$
- Dislocation-obstacle interaction force $\boldsymbol{F}_{obstacel.}$
- Image force $\boldsymbol{F}_{image.}$
- Osmotic force $\boldsymbol{F}_{Osmotic}$ resulting from non-conservative motion of dislocation (climb) and results in the production of intrinsic point defects.
- Thermal force $\boldsymbol{F}_{thermal}$ arising from thermal fluctuations.

As mentioned above, the velocity $\boldsymbol{v}$ of a dislocation segment is governed by a first order differential equation consisting of an inertia term, a drag term and a driving force vector such that:

$$m_s \dot{v} + \frac{1}{M_s(T,p)} v = F_s \qquad \text{with} \qquad m_s = \frac{1}{v}\left(\frac{dW}{dv}\right) \tag{2.3}_1$$

$$F_s = F_{Peirels} + F_D + F_{Self} + F_{External} + F_{Obstacle} + F_{Im\,age} + F_{Osmotic} + F_{Thermal} \tag{2.3}_2$$

In the above equation the subscript s stands for the segment, m_s is defined as the effective dislocation segment mass density, M_s is the dislocation mobility which could depend both on the temperature T and the pressure P, and W is the total energy per unit length of a moving dislocation (elastic energy plus kinetic energy). Hirth *et al*. (1998) derived

expressions for the effective mass per unit dislocation length for screw $(m_s)_{\text{screw}}$ and edge $(m_s)_{\text{edge}}$ dislocations when moving at a high speed.

Determination of the time step under extreme dynamic loading conditions is critical. In DD, the time step is dictated by the shortest flight distance for short-range interaction between dislocations and the time step used in dynamic FE modeling. In this analysis, the critical time (t_c) and the time step (δt) for both DD and FE which yields a stable solution are given by $t_c = \frac{l}{C_l}$, $\delta t = \frac{t_c}{10}$ where l is the characteristic length which is the shortest dimension in the FE mesh. In our calculations, t_c can be as small as 1×10^{-10} second and thus δt is one order of magnitude less. This time step is very suitable to simulate ultra high strain rate loading involved in laser based experiments in which the pulse duration is the order of few nanoseconds. More details of the model can be found in Zbib and de la Rubia (2002).

It is apparent that the momentum equation generates elastic stress wave with a specific shape by applying certain boundary conditions in the FE code. The elastic wave exerts a driving force on the dislocations giving rise to $\boldsymbol{F}_{external.}$ which, can be expressed as:

$$F_{External} = \left(\sigma^a . b\right) \times \zeta \tag{2.4}$$

where σ^a is the stress applied on the dislocation by the stress wave, b is the Burgers vector, and ζ is the line sense of the dislocation line. An interaction process between the dislocations and the stress wave takes place resulting in changes in the wave profile and the formation of dislocation microstructure.

2.3 MDDP Simulations

MDDP simulations are performed to investigate the deformation process at high strain rates in copper and aluminum single crystals. Material properties used in this work can be found in table 2.1. The simulations are designed to mimic uniaxial strain loading at extreme conditions of high strain rates ranging between 10^5 s^{-1} to 10^7 s^{-1}, and short pulse durations of few nanoseconds (Loveridge *et al.* 2001). As illustrated in figure 2.1, the simulation setup consists of a block with dimensions 2.5 μm ×2.5 μm ×25 μm. In order to achieve the uniaxial strain involved in shock loading, the four sides of the block are confined so that they can move in the loading direction only. The bottom surface is rigidly fixed. A velocity-controlled boundary condition (v_p) with a zero rise time is applied on the upper surface over a short period of time (t^*) to generate the stress wave. The upper surface is then released and the simulations continue for the elastic wave to interact with the existing dislocation sources.

The average strain rate in the entire domain is defined as:

$$\dot{\bar{\varepsilon}} = \frac{v_p}{L_z} \tag{2.5}$$

where L_z is the length of the computational cell in the loading direction. It is worthy to mention that although equation (2.5) gives the average strain rate in the entire domain, the local values of strain rate can reach much higher values depending on the FE mesh density. The loading and the boundary conditions are summarized in the following equations;

$$u_z(t) = -v_p t \qquad 0 \le t \le t^*, \qquad \text{at } z = \frac{L_z}{2} \tag{2.6}$$

$$u_z(t) = 0 \qquad \text{at } z = -\frac{L_z}{2}$$

$$\begin{aligned} u_x(t) &= 0, \quad at \quad x = -\frac{L_x}{2}, \frac{L_x}{2} \\ u_y(t) &= 0, \quad at \quad y = -\frac{L_y}{2}, \frac{L_y}{2} \end{aligned} \tag{2.7}$$

Where L_x, L_y, and L_z are the dimensions of the computational cell in the x, y and z directions respectively, u_x, u_y, and u_z are the displacement components.

Frank-Read loops distributed on different slip planes are used as agents for dislocation generation. For copper and aluminum, 0.50 to 0.80 μm source lengths are used. In DD code, the boundary condition for the RVE is either reflective boundary condition, which ensures the continuity of the dislocation curves, or periodic boundary condition that ensures the conservation of dislocation flux across the boundaries as well as continuity. In FE analysis however, the sides are constrained to move only in the z direction so that a uniaxial strain consistent with the shock experiment is achieved. In order for the boundary conditions in FE and DD to be consistent, periodic FE boundary condition is implemented as well. This implementation of periodic FE boundary condition yields a relaxed state of stress with low peak pressure when compared to the experiment. Furthermore, both shear and longitudinal waves are generated which is discordant with plane wave characteristics. More details of boundary condition effects on wave propagation and dislocation microstructures will be presented in chapter 5.

The main focus of this study is the interaction between the transmitted wave and dislocation sources. However, when the stress wave hits the rigid base, it reflects to the material block and interacts with the dislocations again. In order to isolate the effect of the reflected waves, the length of the cell (25 μm) is chosen such that once the wave front

reaches the bottom surface, the value of the stresses in the position where the dislocations are located is very small so that there is enough time for the dislocations to relax. A better solution to isolate the effect of the reflected wave would be by implementing a suitable non-reflective FE boundary condition.

Under high strain rate loading, the elastic properties of metals depend on the applied pressure (Steinberg *et al*. 1980). In order to better simulate the physical problem, any constitutive model must account for this effect. In MDDP code, the experimental results of Hayes *et al*. (1999) for the shear modulus (G) and Poisson's ratio (ν) of copper are fitted in the constitutive equation to account for the dependence of elastic properties on pressure such that:

$$G = \begin{cases} G_0 + 0.89P & 0 < P < 60 \\ G_0 + 53.4 + 0.40P & 60 < P < 100 \end{cases} \tag{2.8}$$

$$v = v_0 + 1.70 \times P \times 10^{-12} \tag{2.9}$$

where, P is the peak pressure in GPa, G_0 and v_0 are the shear modulus and Poisson's ratio under normal static loading conditions.

In the current study, two different set of simulations are performed: (a) different values of v_p are applied on the upper surface for the same pulse duration to simulate different strain rates, (b) the same v_p is applied for different t^* to simulate different pulse durations.

2.4 Results and Discussion

The uniaxial strain compression applied on the material results in propagating three dimensional state of stress, which can be decomposed into mean and deviatoric stresses. Figure 2.2 shows the mean stress snapshots of a wave propagating in copper single crystal shocked to 4×10^5 s^{-1} for 2.0 nanoseconds (ns) duration. The wave profile consists of 1) a wave front that increases from zero to the peak value of stress 2) fluctuations about the peak stress for period of time corresponds to the pulse duration, and 3) a release part where the stress decreases from its peak value to zero. As the wave propagates in the crystal, the peak stress decays from its initial value of 3.35 GPa to 3.25 GPa. The decay in the peak stress can be attributed to energy dissipation during the process of dislocation generation and motion. Furthermore, additional peaks appear in the wave profile as a result of the FE mesh size effect.

The dependence of elastic properties on pressure as indicated by equation 2.8 and equation 2.9 resulting in material nonlinearity, which is accounted for by adjusted the FE stiffness matrix at each time step. Wave profiles generated by linear and nonlinear models as seen in figure 2.3 reveal that the quantitative features of the two models are similar. However, the nonlinear model predicts faster wave propagation and higher value of peak pressure.

The current simulations are performed assuming wave propagation in isotropic medium. Including cubic symmetry exhibited by fcc single crystals in FE analyses can refine the present calculations. The effect of crystal anisotropy on the shock wave-dislocation interaction will be discussed in chapter 3. See (Shehadeh *et al*. 2005).

As the shock wave advances in the material, it encounters the dislocation sources and an avalanche of dislocations occurs the instant the wave hits the sources. The dislocations continue to emit from the sources at very high speeds, inducing very large energy dissipation rate leading to a local temperature increase as illustrated in figure 2.4. Eventually, the level of stress drops dramatically, consequently, the rate of production diminishes and a relaxation process takes place. During the relaxation process, the contribution of dislocation annihilation becomes noticeable, and curved dislocations retract to stable configurations, therefore, dislocation density saturates.

The regimes of shock wave-dislocations interaction can be deduced from the dislocation density history as shown in figure 2.5. The regimes of interaction are marked as A, B and C to denote no interaction, avalanche of dislocations and relaxation regimes respectively. Similar features of the interaction processes can be extracted from the evolution of plastic strain as presented in figure 2.6a, which shows that the local values of plastic strain keep increasing till the relaxation process takes place where plastic strain saturates. Moreover, two peaks appear suggesting the existence of localized deformation regions, as the dislocation density in these regions is very high. The dislocation activities cause stresses to have different values than those predicted by elasticity theory (Weertman 1981). Figure 2.6b shows the wave profiles for perfectly elastic (no dislocations) and elastic-plastic (with dislocation) models. Obviously, the dislocation activities result in reducing the values of the effective shear stress revealing that shocks induce material softening.

Under high strain rate deformation conditions, it is expected that the dislocations move subsonically or even as fast as the shear wave velocity. The random motion of

dislocations on their slip planes causes random changes in the local dislocation velocities. A histogram of the instantaneous speed of the dislocations as they interact with a wave front launched at strain rate 5×10^{6} s^{-1} is shown in figure 2.7. The calculations show that about 92% of the dislocations move at speed less than 500 m s^{-1}; that is about 0.22 of the shear wave velocity in copper. Among these dislocations, about 25% are immobile (zero speed), and a very small percentage of dislocations (1.5%) move at speed faster than 0.80 of the shear wave velocity. The average speed of these dislocations whose global density is $\sim 2.50\times10^{11}$ m^{-2} is 285 m s^{-1}, whereas for a higher density of 1.50×10^{12} m^{-2}, the average dislocation speed is 85 m s^{-1}. This is consistent with Orowan equation in which the average dislocation speed decreases with increasing the dislocation density.

The effect of strain rate and pulse duration on the evolution of dislocation density and the resulting microstructure were investigated in copper samples oriented in the (001) orientation. Figure 2.8a shows that the rate of dislocation multiplication increases with strain rate. Moreover, the relaxation regime as discussed in figure 2.4 does not appear for strain rates larger than 10^{6} s^{-1}. DD involves massive computations that in the case of very high strain rate the computational capabilities of our machines cannot reach the point where the relaxation process takes place. Morphologies of the resulting dislocation microstructures obtained from slices within the computational cell at different strain rates are depicted in figure 2.8b. For the lowest strain rate (7×10^{5} s^{-1}), irregular dislocation entanglements were formed as the combination of stress level and pulse duration (1.3 ns) is not sufficient for the dislocation to organize in a regular microstructure. As the rate of deformation increases (>10^{6} s^{-1}), the level of stress renders so high that it allows the

dislocation to form long deformation bands of submicron dimension coincident with the slip planes. The thickness of these bands appears to correlate inversely with strain rate.

Shock pulse duration is an important parameter in controlling the microstructure of the dislocations. Pulse duration is related to the time required for the dislocations to reorganize (Meyers 1994). Histories of dislocation densities for different pulse durations can be seen in figure 2.9a. Based on our calculations, the saturation density of dislocations increases with pulse duration in the nanosecond time scale. These results are consistent with the findings of Wright *et al*. (1988) on plate-impact experiments conducted in the microsecond range. Morphologies of the dislocation microstructure at different pulse durations are shown in figure 2.9b. Irregular dislocations entanglements were formed at the shortest pulse duration. As the pulse duration increases, these entanglements become more distinguishable and can develop deformation bands within which areas of high dislocation density surrounded by low dislocation density areas are formed.

In materials with high dislocation mobility such as copper, dislocation patterns proceed through the rapid motion of dislocations in a very small volume of the specimen (Zaiser 2001). In order to quantitatively understand the underlying microstructure of the material, it is very important to describe relevant features of the three dimensional form of the microstructure (Ohser and Mucklick 2000). In this study, the local dislocation density distribution is investigated by extracting data from thin slices parallel to the x, y and z-axes. Figure 2.10a shows a thin slice in the x-z plane in which networks of lines are formed and then the local dislocation densities are calculated at evenly spaced positions. In these calculations, the dislocation density at every position relative to the average

density is calculated and named as relative local densities which is analogous to the most simply thought of pair distribution function (Allen and Tildesley 1997).

Figure 2.10b shows that distinguished peaks of high relative dislocation densities appear in the locations where the local dislocation densities are about one order of magnitude higher than the average value (1.2×10^{14} m^{-2}). The local distributions of dislocation densities indicate that the dislocation microstructure is not homogenous within the computational cell suggesting the existence of two subareas with different dislocation density properties. The first one, in which dislocation density is high, occupies a very small portion of the computational cell. The second one occupies most of the computational cell with low dislocation density.

Pattern configurations (number and position of peaks) can be affected by the imposed strain rate. In fcc materials, there are 12 different slip systems, which can contribute to the deformation process. Table 2.2 lists the slip systems as combinations of the slip planes and slip directions. (001) orientation has the highest symmetry among all orientations with four possible slip planes that have identical Schmid factor of 0.4082. In this orientation, eight slip systems can be activated. The contribution of each slip system to the plastic deformation at different strain rates is investigated by plotting the dislocation density distribution of each slip system. Figure 2.11 indicates that while the same slip systems are activated, the contribution of each one of them to the deformation process is greatly affected by the applied strain rate. This may be attributed to the interaction process between the dislocations on different slip systems.

The effects of material properties i.e. the elastic constants (G, ν) and the mass density ($\bar{\rho}$) on the wave propagation and interaction with dislocations is investigated by

performing simulations for copper and aluminum under the same loading conditions. Figure 2.12 illustrates that the wave propagates in aluminum is faster than in copper, consequently, wave-dislocations interaction starts in aluminum before it starts in copper. The saturation dislocation density in copper however, is larger than that of aluminum as the peak pressure generated in copper is greater than that in aluminum.

2.5 Summary of the Results

In this section we present a summary of the simulation results for copper and aluminum single crystals. As mentioned before, stress waves are generated by applying velocity controlled boundary condition (v_p) on the upper surface of the computational cell. The FE part of the code calculates the state of stress produced by the imposed particle velocity. The pressure produced is then used to find the corresponding particle velocity given in (Meyers 1994) which is denoted by U_p. For most metals, shock velocity (U_s) is directly proportional to the particle velocity via the relationship:

$$\boldsymbol{U_s = C_o + SU_p} \tag{2.10}$$

where C_o is sound velocity at zero pressure, and S is an empirical parameter determined by experiments as given in table 2.1. The pressure ($-\sigma_{33}$) is then calculated using the momentum equation, which is given by:

$$\boldsymbol{-\sigma_{33} = \hat{\rho}_0 U_p U_s} \tag{2.11}$$

The longitudinal elastic wave velocities were calculated and compared with their corresponding theoretical values. Summary of the calculations for a (5×5×50) FE mesh size is listed in table 2.3. The values of the peak pressure obtained from our calculations

are in a very good agreement with the corresponding theoretical values given by equation 2.11. However, the speeds of the calculated longitudinal elastic wave are underestimated. This can be attributed to the effect of FE mesh size. Figure 2.13 shows that as the mesh size increases, the wave profile converges and the wave velocity approaches its theoretical value.

2.6 Conclusions

This work is the first of its kind that uses multiscale dislocation dynamics plasticity simulations to study shock wave-dislocation interaction in fcc single crystals. These simulations are designed to mimic the loading conditions in recent laser based experiments, where the pulse duration is few nanoseconds. It is shown that avalanche of dislocations is a natural consequence of the interaction between dislocations and stress waves. The results of our calculations show that dislocation density is proportional to strain rate and pulse duration; however, the dislocation microstructure is controlled mainly by strain rate. Dislocation micro bands coincident with the {1 1 1} planes are formed at strain rate larger than 10^6 s^{-1}, whereas, dislocation entanglements were formed at strain rates lower than 10^6 s^{-1}. It is also observed that the inclusion of pressure dependent elastic properties in the FE constitutive equation influences the shape of the wave profile. Statistical analyses of the local dislocation densities allow accounting for the heterogeneous and intermittent nature of plastic flow, which may give better insight to understand pattern formation in crystalline materials. The instantaneous speed distribution of the dislocations interacting with a wave front launched at 10^6 s^{-1} shows

that the speed of more than 90% of the dislocations is less than 500 m s^{-1}, and that a very small percentage of the dislocations move at speed approaching the shear wave velocity. The current model can be modified to incorporate many issues that appear in high strain problem, such as the effect of temperature on phonon drag and the effect of dislocation climb on pattern formation.

References

Allen, M. P., and Tildesley, D. J., 1997, *Computer Simulations of Liquids*, (Oxford Science Publications: Oxford).

Bringa, E. M., Wirth, B. D., Caturla, M. J., Stolken, J., and Kalantar, D., 2003, *Nucl. Instr. and Meth. In Phys.* **B202**, 56.

Clifton, R. J. and Bathe, N., 1999, *Shock Compression of Condensed Matter*, edited by M. D. Furnish, L. C. Chhbildas and R. S., Hixson (Melville, New York), pp. 19-26.

Coffey, C. S. 1992, *Shock Waves and High Strain Rate Phenomena in Materials*, edited by M. A. Meyers, L. E. Murr and K. P., Staudhammer (Dekker, New York), pp. 669-690.

Ghoneim, N.M., and Sun, L.Z., 1999, *Phys. Rev.*, **B 60**, 128.

Gupta, Y.M., 1999, *Multiscale Modeling of Materials*, edited by V. Bulatov, T. de la Rubia, R. Philips, E. Kaxiras, and N. Ghoniem (Material Research Society, 1998) pp. 139-149.

Hayes D., Hixson, R. S., McQueen, R.G., 1999, *Shock Compression of Condensed Matter*, edited by M. D. Furnish, L. C. Chhbildas and R. S., Hixson (Melville, New York), pp. 483-488.

Hirth, J. P., Zbib, H. M., and Lothe, J., 1998, *Model. Simul. Mater. Sci. Eng.*, **6**, 165.

Horstemeyer. M. F., Baskes, M. I., and Plompton, S. J., 2001*, Acta Mater*., **49**, 4363.

Horstemeyer. M. F., Baskes, M. I., Godfrey, A., and Hughes, D. A., 2002, *International Journal of Plasticity*, **18**, 203.

Kadau, K., Germann, T. C., Lomdhal, P. S., and Holian, B., 2002, *Science*, **296**, 1681.

Kalantar, D. H., Remington, B. A., Colvin, J. D., Mikaelian, K.O., Weber, S. V., Wiley, L.G., Wark, J. S., Loveridge, A., Allen, A.M., Hauer, A. A., and Meyers, M. A., 2000, *Physics of Plasmas,* **7 (5)**, 1999.

Kalantar, D. H., Allen, A. M., Gregori, F., Kad, B., Kumar, M., Lorenz, K. T., Loveridge, A., Meyers, M. A., Pollaine, S., Remington, B. A., and Wark, J. S., 2001, *Shock Compression of Condensed Matter*, edited by M. D. Furnish, N. N. Thadhani and Y. Horie (Melville, NewYork), pp. 615-618.

Kanel, G. I., Razorenov, S. V., Baumung, K., and Singer, J., 2001, J. *App. Phys*., **90**, 136.

Kubin, L.P., and Canova, G., 1992, *Scripta Metall. Mater*., **27**, 957.

Loveridge-Smith, A., Allen, A., Belak, J., Boehly, T., Hauer, A., Holian, B., Kalantar, D., Kyrala, G., Lee, R.W., Lomdahl, P., Meyers, M. A., Paisley, D., Pollaine, S., Remington, B., Swift, D. C., Weber, S., and Wark, J. S., 2001, *Phys. Rev.Lett*., **86(11)**, 2349.

Meyers, M. A., 1994, *Dynamic Behavior of Materials*, (New York: John Wiley & Sons).

Meyers, M. A., Gregori, F., Kad, B. K., Schneider, M. S., Kalantar, D. H., Remington, B. A., Wark, J.S., Boehly, T., and Ravichandran G., 2001, *Shock Compression of condensed Matter*, edited by M. D. Furnish, N. N. Thadhani and Y. Horie (Melville, NewYork), pp. 619-622.

Meyers, M. A., Benson, D.J., Vohringer, O., Kad, B. K., Hue, Q., and Fu, H.-H., 2002, *Materials Science and Engineering*, **A322**, 194.

Meyers, M. A., Gregori, F., Kad, B. K., Schneider, M. S., Kalantar, D. H., Remington, B. A., Ravichandran G., Boehly, T., and Wark, J., 2003, *Acta Materialia*, **51(5),** 1211.

Mogilevskii, M. A. and Bushnev, L. S., 1990, *Combustion, Explosion, and Shock Waves*, **26**, 215.

Ohser, J., and Mucklich. F., 2000, *Statistical Analysis of Microstructures in Materials Science*, (New York: John Wiley & Sons, Ltd).

Rhee, M., Zbib, H. M., Hirth, J. P., Huang, H., and de la Rubia, T.D., 1998, *Modeling and Simulations in Maters.Sci. & Eng*., **6**,467.

Rivas, J. M., Quinones, S. A., Murr, L. E., 1995, *Scripta Metallurgica et Materialia*, **33(1)**, 101.

Schwarz, K. W., and LeGoues, F. K., 1997, *Phys. Rev. Lett*., **79,** 1877.

Shehadeh, M. A., Zbib, H. M., and de la Rubia, T., 2005, *Int. J. Plasticity*. In press.

Smirnova, J. A., Zhigilei, L. V., Garrison, B. J., 1999, *Computer Science Communications*, **118**, 11.

Steinberg, D. J., Cochran, S. G., and Guinan, M. W., 1980, *J. App. Phys*. **51**, 1498.

Van der Giessen, E., Needleman, A., 1995, *Model. Simul. Mater. Sci. Eng*., **3**, 689.

Weertman, J.,1961, Response of metals to high velocity deformation, edited by P. G. Shewmon and V. F. Zackay (New York: Interscience). p 205.

Wright, R. N., Mikkola, D. E., and Larouchie S., 1981, *Shock Waves and high Strain Rate Phenomena in Metals*, edited by M. Meyers, L. E., and Murr (Plenum, NewYork) pp 703-716

Wright, R. N., and Mikkola, D. E., 1985*, Metallurgical Transactions*, **16 A**, 891.

Zaiser, M., 2001, *Materials Science and Engineering*, **A309**. 304.

Zbib, H. M., Rhee, M., and Hirth, J. P., 1998, *Int. J. Mech. Sci*., **40**,113.

Zbib, H. M., and de la Rubia, T. D., 2002, *International Journal of Plasticity*, **18**, 1133.

Zbib, H. M., Shehadeh, M., Khan, S.M., and Karami, G., 2003, *International Journal for Multiscale Computational Engineering*, **1**, 73.

Yasin, H., Zbib, H. M., and Khaleel, M. A., 2001, *Materials Science and Engineering*, **A309**, 29.

Table 2.1 Material and shock properties for copper and aluminum

Material	G(GPa)	ν	ρ(kg/m^3)	Cp(J/kg.K)	K (W/m.K)	S
Cu	46.6	0.32	8900	385	398	1.49
Al	25.0	0.345	2700	900	274	1.34

Table 2.2 Slip systems in fcc metals.

Slip System	Burgers Vector	Slip Plane
1	$[\bar{1}10]$	$(\bar{1}\,\bar{1}\,1)$
2	$[\bar{1}10]$	$(1\,1\,1)$
3	$[0\,1\,\bar{1}]$	$(\bar{1}11)$
4	$[0\,1\,\bar{1}]$	$(1\,1\,1)$
5	$[\bar{1}0\,\bar{1}]$	$(\bar{1}11)$
6	$[\bar{1}0\,\bar{1}]$	$(\bar{1}\,\bar{1}\,1)$
7	$[10\,\bar{1}]$	$(1\bar{1}1)$
8	$[10\,\bar{1}]$	$(1\,1\,1)$
9	$[0\,\bar{1}\,\bar{1}]$	$(1\bar{1}1)$
10	$[0\,\bar{1}\,\bar{1}]$	$(\bar{1}\,\bar{1}\,1)$
11	$[\bar{1}\,\bar{1}\,0]$	$(1\bar{1}1)$
12	$[\bar{1}\,\bar{1}\,0]$	$(\bar{1}11)$

Table 2.3. Summary of the calculations for copper and aluminum

Material	Copper				Aluminum			
Vp (m/s)	**35.7**	**71.4**	**357.6**	**715.2**	**46.3**	**92.6**	**463.3**	**926.6**
Ave Strain Rat (1/s)	**5×10^{5}**	**1×10^{6}**	**5×10^{6}**	**1×10^{7}**	**5×10^{5}**	**1×10^{6}**	**5×10^{6}**	**1×10^{7}**
Computed Axial Stress (σ_{33}) GPa	**2.22**	**4.39**	**22.20**	**43.21**	**1.20**	**2.45**	**12.60**	**25.04**
Longitudinal Elastic Wave Speed (m/s): Theoretical	**3790**	**3970**	**4310**	**4820**	**5017**	**5170**	**5820**	**5875**
Computes Elastic Wave Speed (m/s): From the code	**3300**	**3346**	**3737**	**4155**	**4672**	**5144**	**5285**	**5651**
Vp (m/s) Theoretical	**57.5**	**113.3**	**524**	**908**	**70.44**	**143**	**649**	**1281**
Theoretical axial stress (σ33) G.Pa	**1.95**	**3.93**	**21.02**	**41.06**	**0.97**	**2.00**	**10.26**	**23.19**
Dislocation Density ($1/m^2$)	**4×10^{12}**	**7×10^{12}**	**1.6×10^{13}**	**2.5×10^{13}**		**2.5×10^{13}**	**2.0×10^{13}**	**2.1×10^{13}**
Temp Rise	**13**	**33**	**103**	**190**	**10**	**41**	**104**	**186**

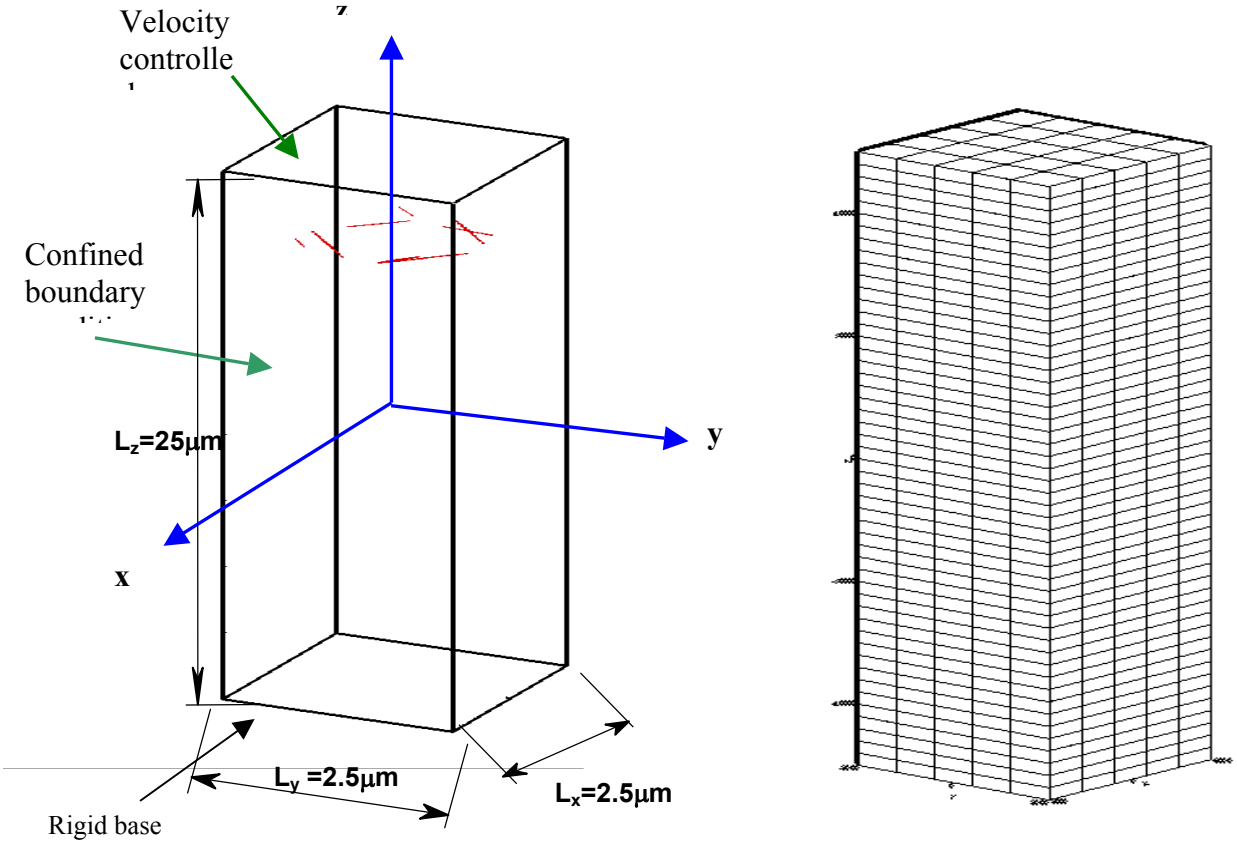

Figure 2.1. Setup of the simulation cell and the finite element mesh.

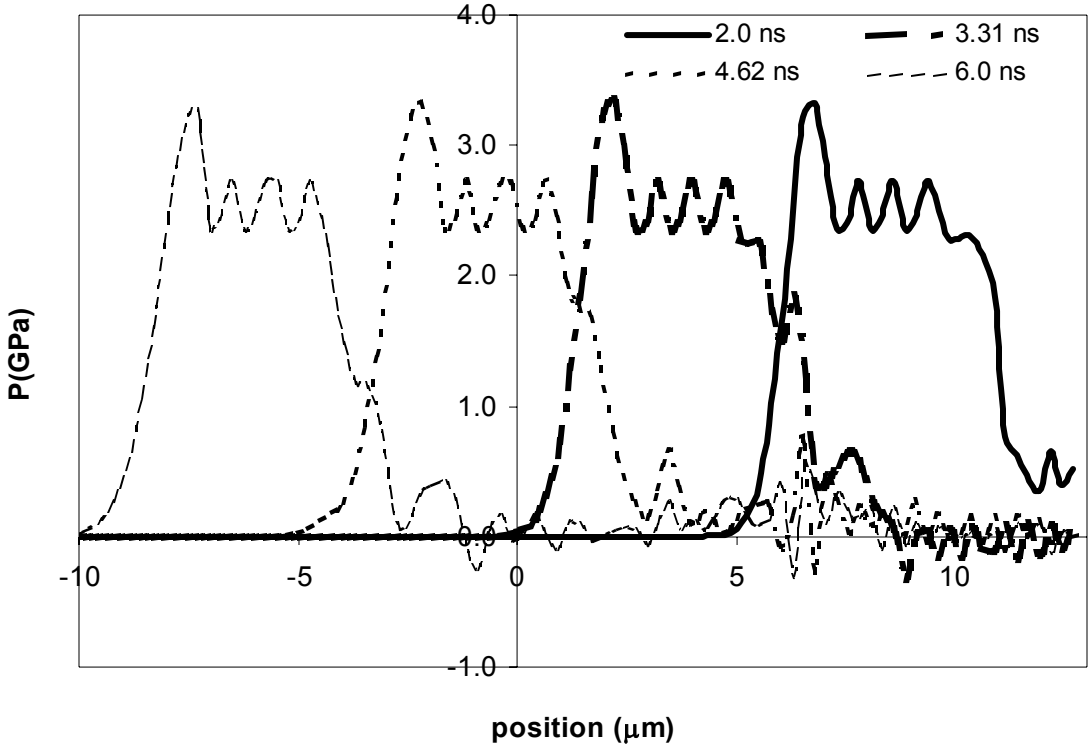

Figure 2.2. Stress snapshots in copper crystal shocked to strain rate 4×10^5 s^{-1} for 2.0 nanoseconds.

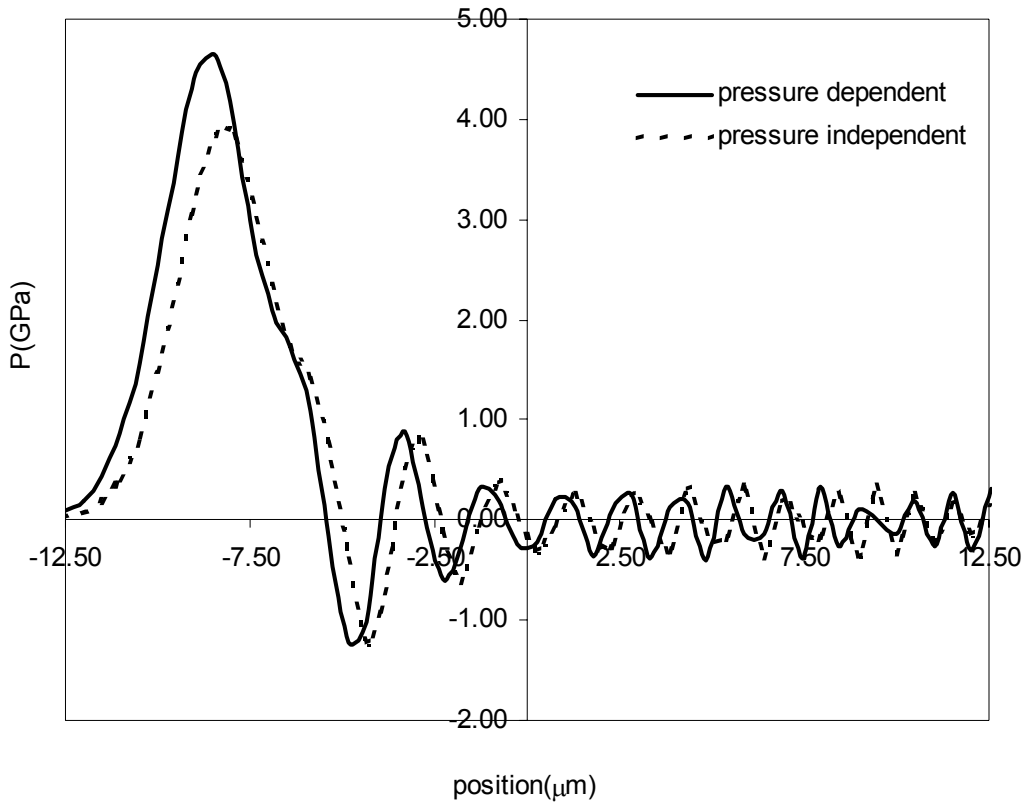

Figure 2.3. The effect of pressure-dependent elastic properties on the mean stress profile of copper shocked to strain rate 7×10^{5} s^{-1} for 1.3 nanoseconds.

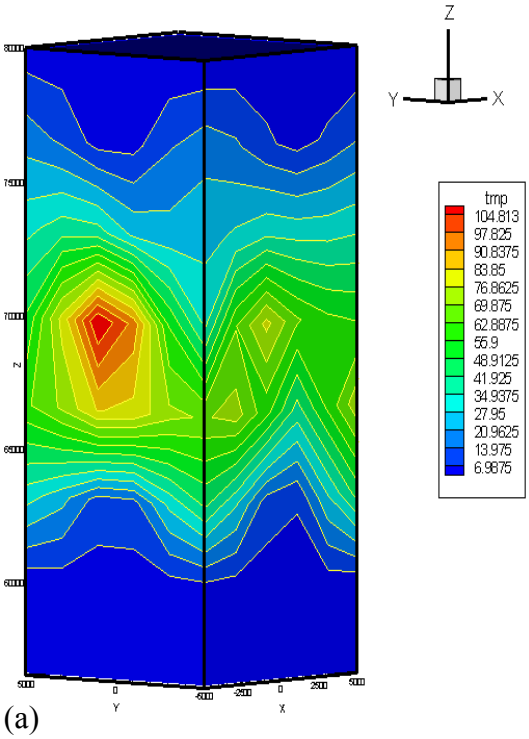

(a)

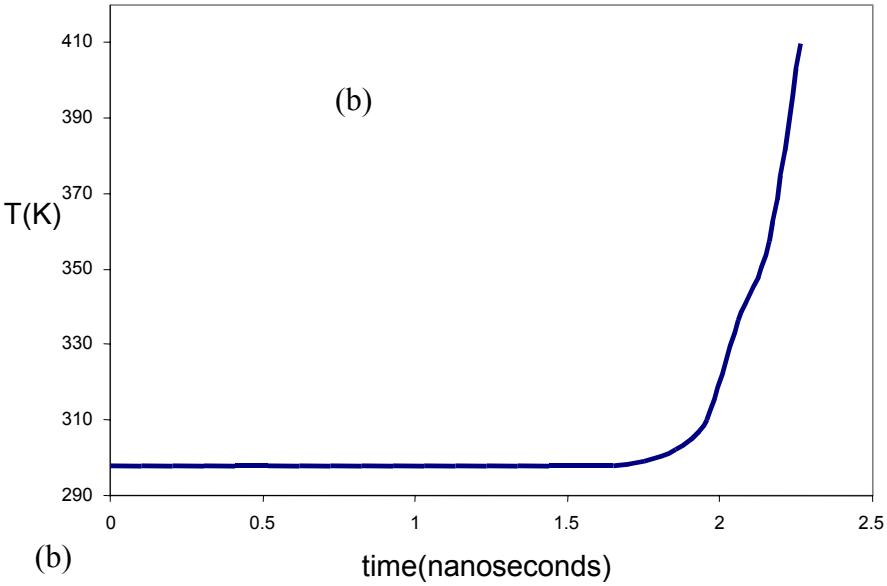

(b)

Figure 2.4. Simulation results in aluminum single crystal at ultrahigh strain rate ($5\times10^{6}s^{-1}$). (a) Contour plot of temperature distribution in the computational cell. (b) Temperature history of the element of highest temperature increase.

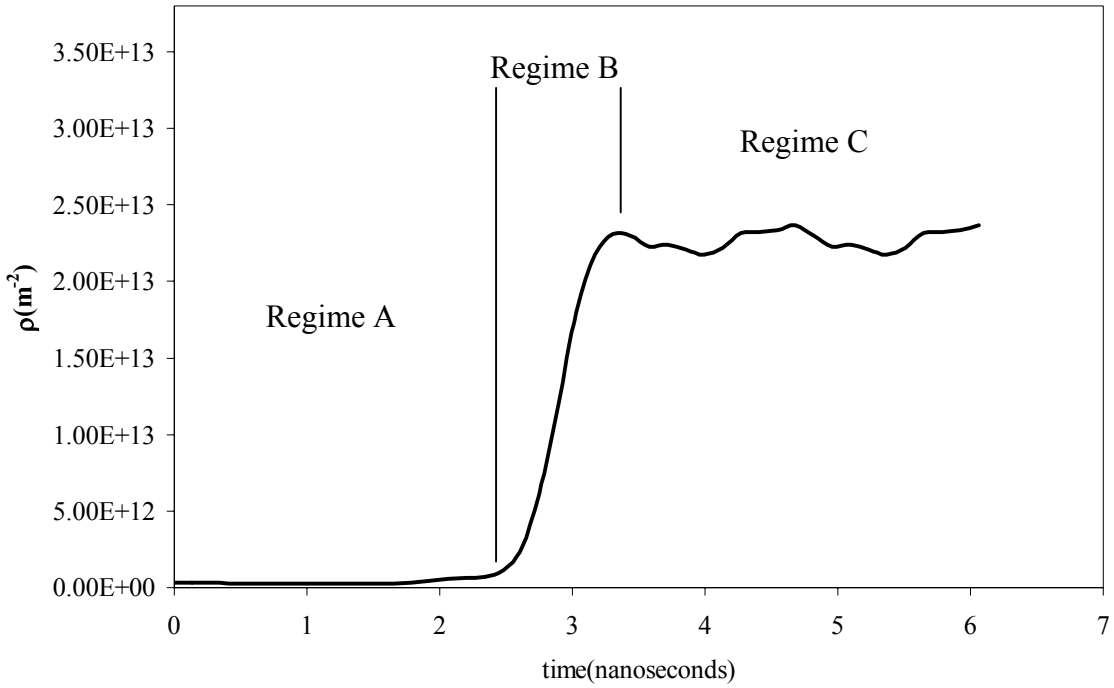

Figure 2.5. Dislocation density history for copper shocked to strain rate $1\times10^{6}\ s^{-1}$ for 1.8 nanoseconds.

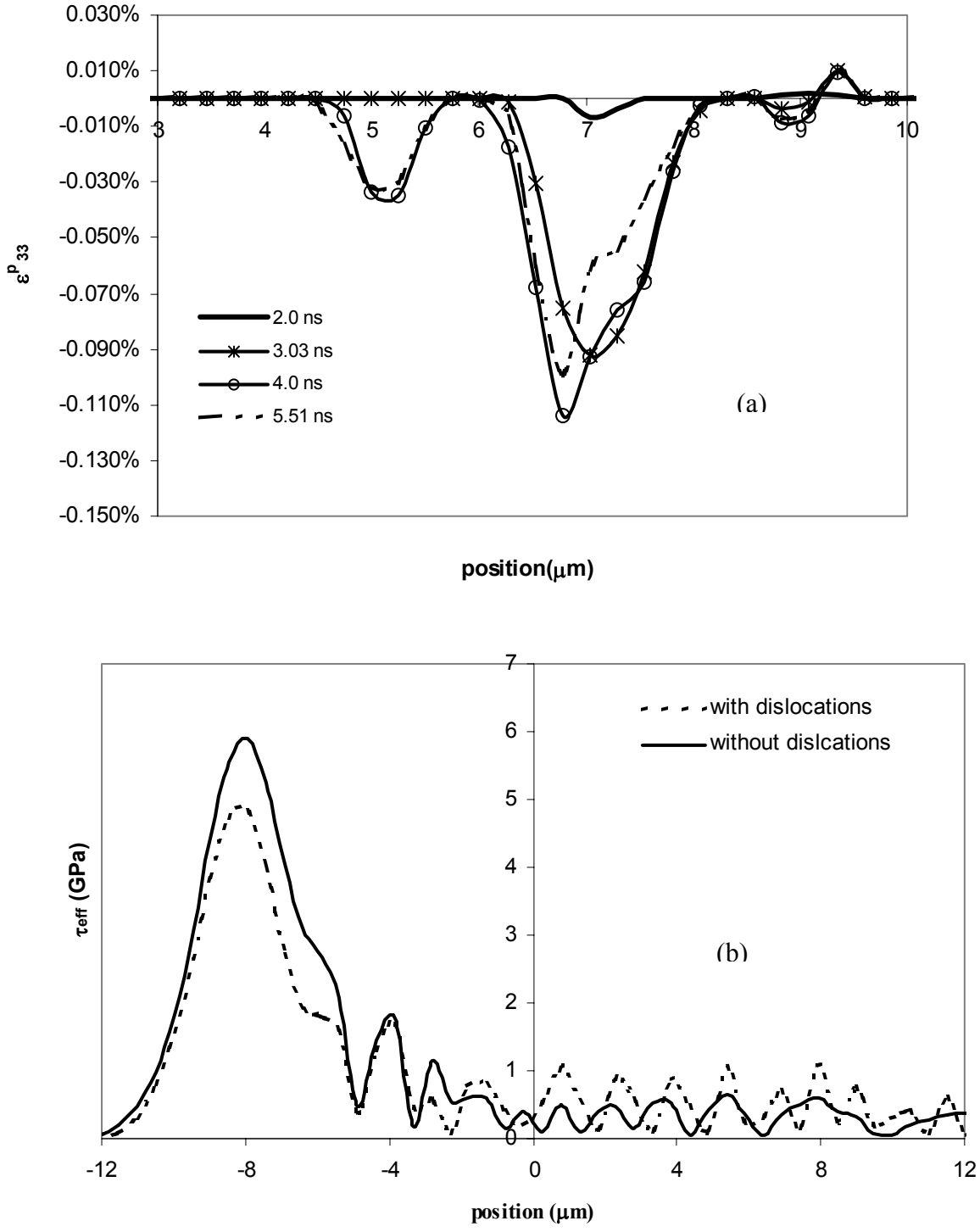

Figure 2.6. (a) Snapshot of plastic strain (ε^p_{33}) evolution in copper single crystal shocked to 4 $\times 10^5$ s^{-1} for 2 nanosecond (b) The effect of dislocations activities on the effective shear stress in copper.

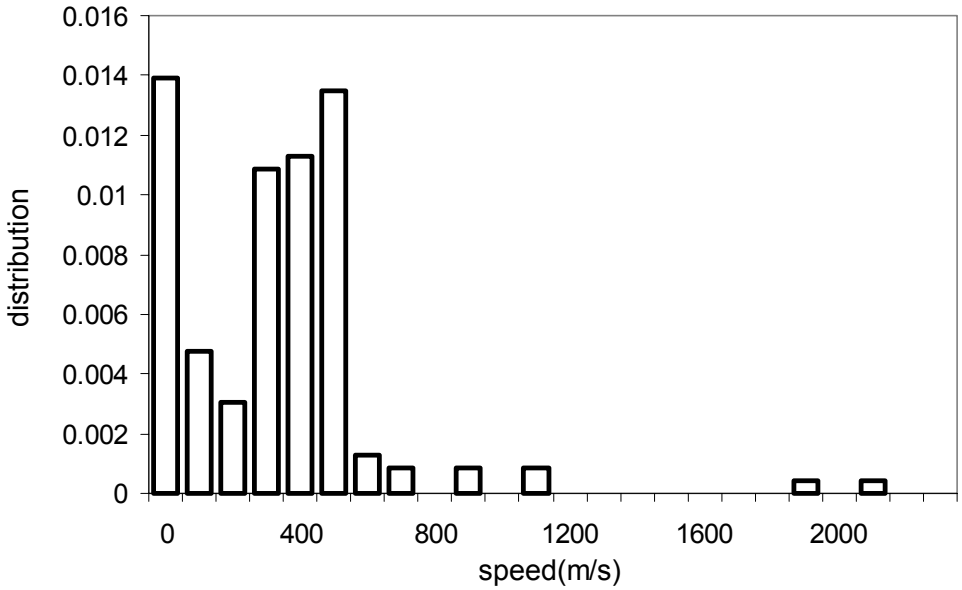

Figure 2.7. The distribution of dislocation velocity as the wave front interacts with the sources at $\dot{\varepsilon}=5\times10^{6}\ s^{-1}$

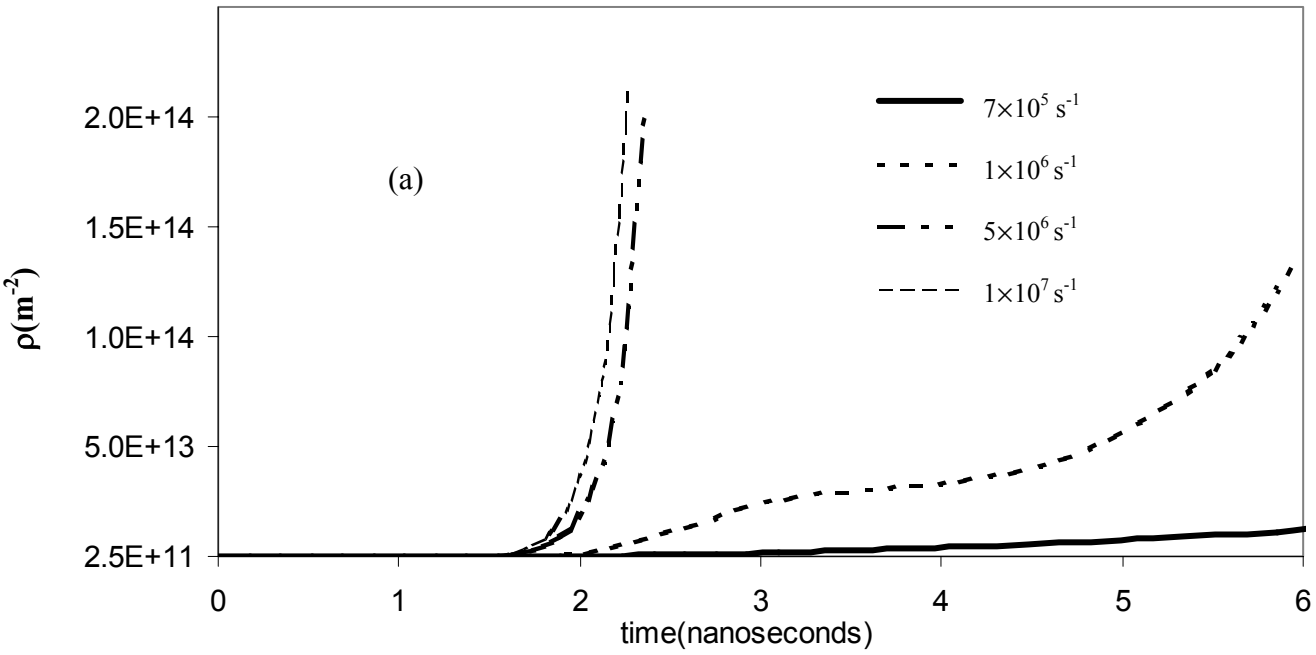

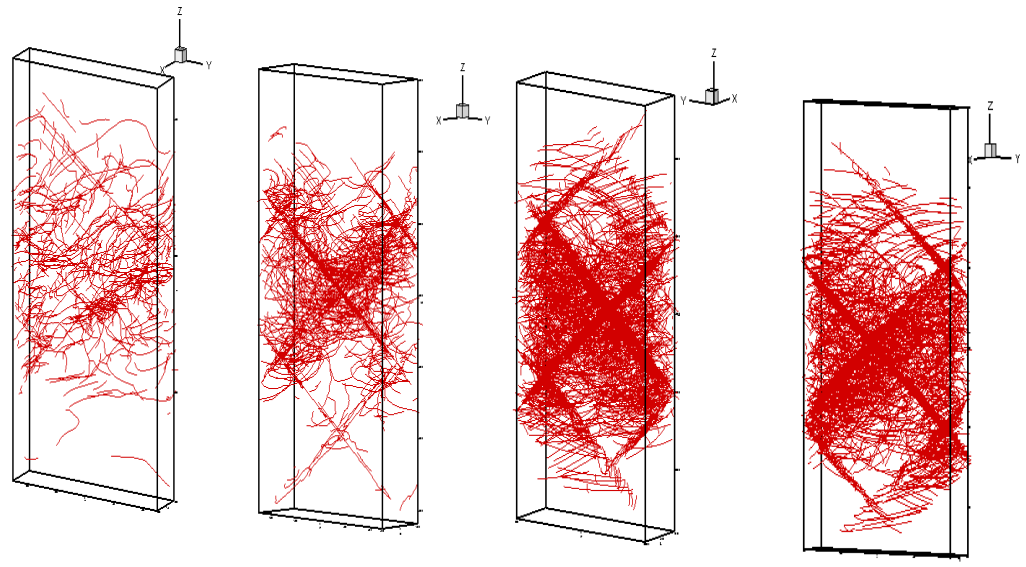

(b)

Figure 8. The influence of strain rate on (a) the dislocation density history in copper single crystal shocked for 1.3 nanoseconds. (b) the resulting dislocation microstructures.

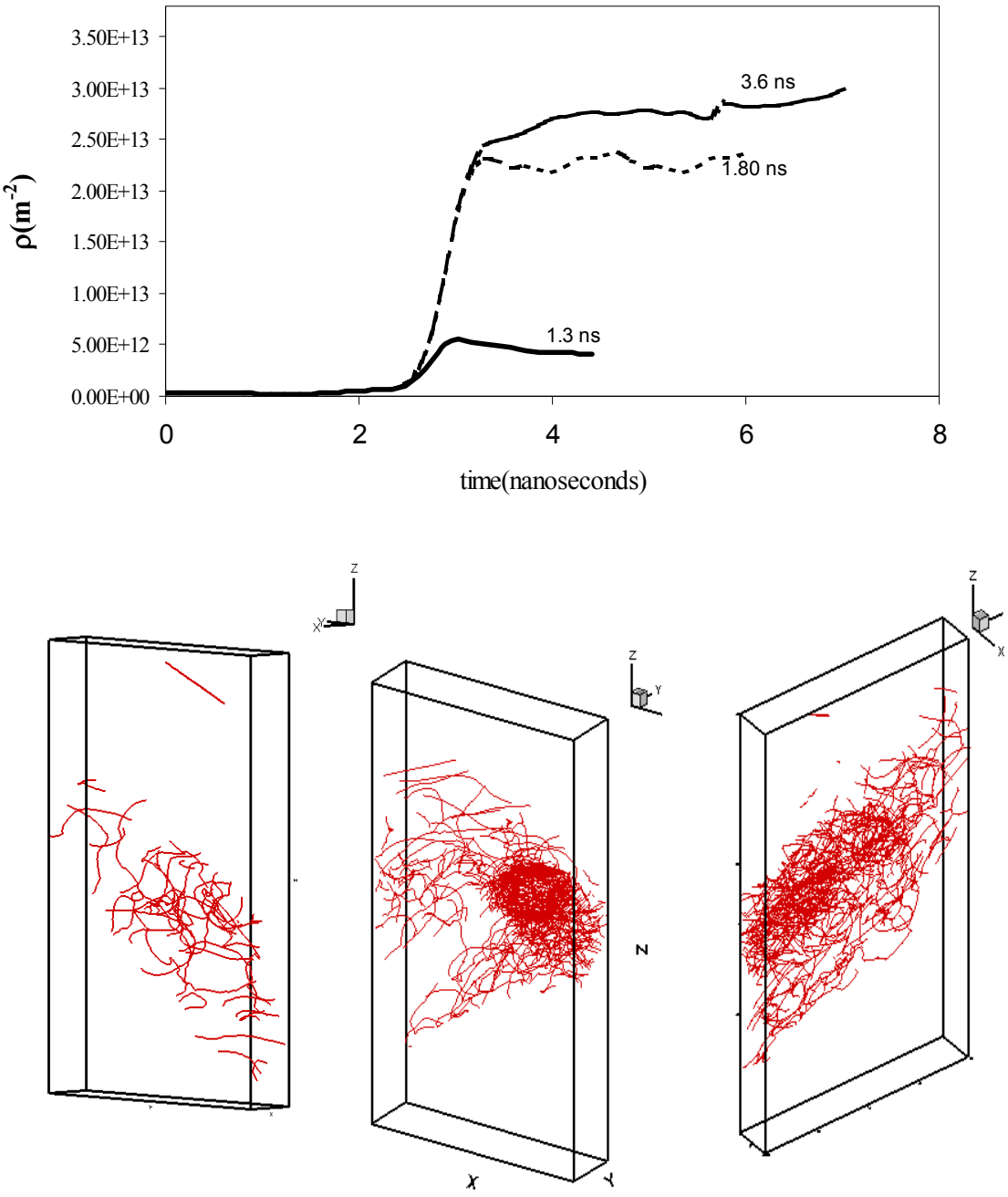

(b)

Figure 2.9. The effect of shock pulse duration on (a) the dislocation density histories in

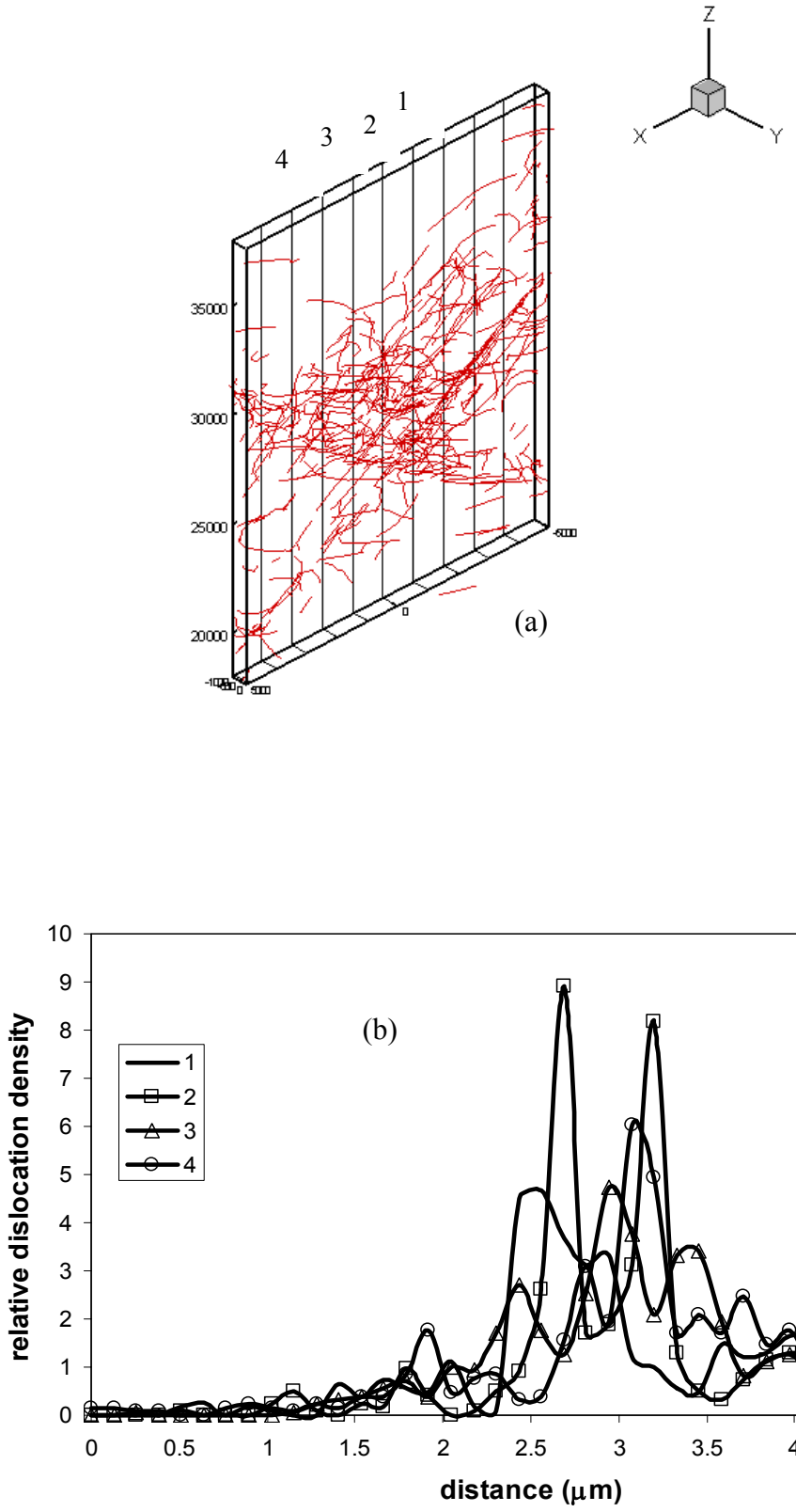

Figure 2.10. (a) Thin slice in the x-z plane, the numbers 1, 2, 3 and 4 are the lines on which the dislocation density was calculated. (b) the calculated relative dislocation density.

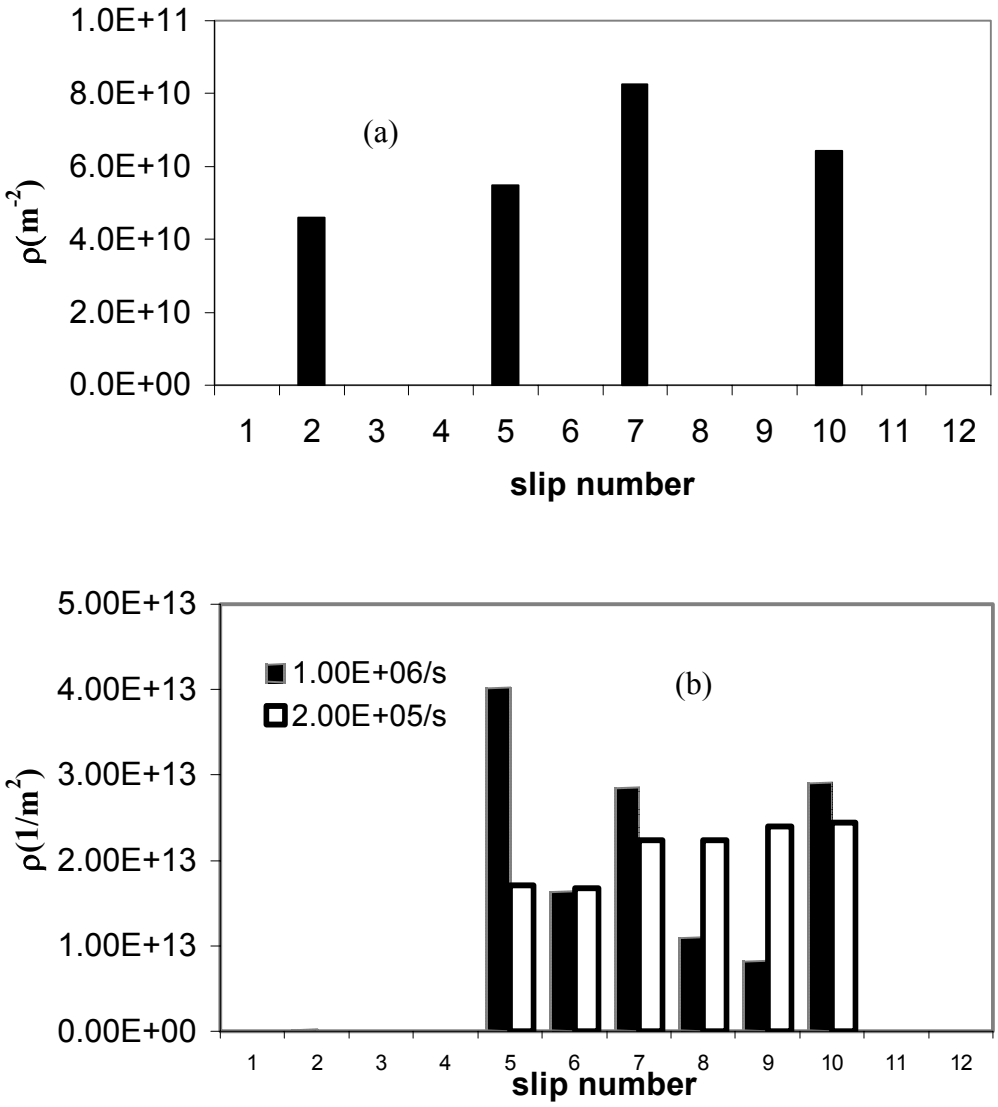

Figure 2.11. (a) The initial dislocation density contributions of each slip system (b) The relaxed dislocation density contributions of each slip

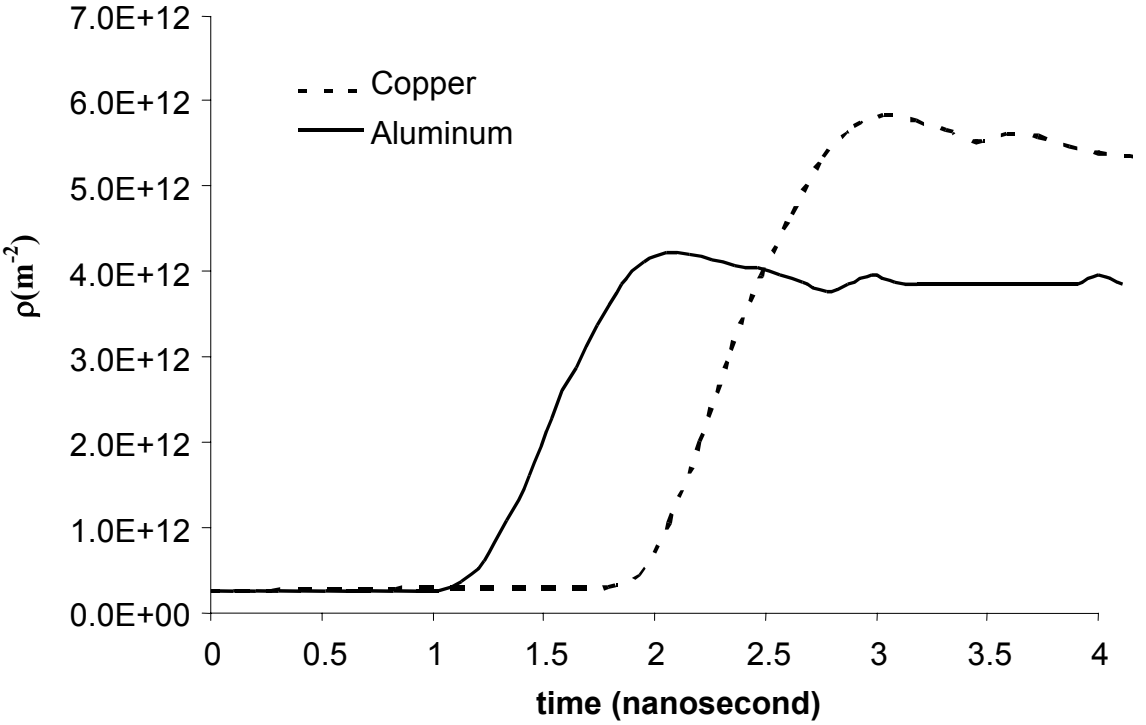

Figure 2.12. Dislocation density histories for aluminum and copper single crystals.

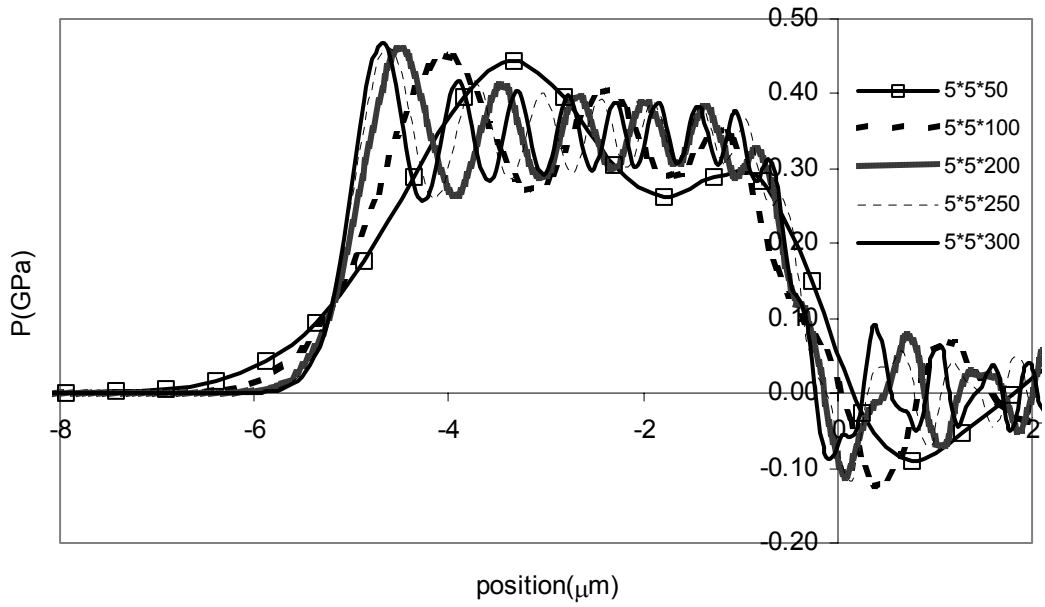

Figure 2.13. The influence of FE mesh size on the wave profile.

CHAPTER 3

Multiscale Dislocation Dynamics Simulations of Shock Compression in Copper Single Crystal: Crystal Anisotropy and Pressure Decay Effects

3.1 Introduction

The response of metal single crystals to high strain rate loading depends on many parameters such as crystal structure, peak pressure, pulse duration, crystallographic orientation, and stacking fault energy (*SFE*). Most metallic single crystals exhibit cubic symmetry that leads to anisotropy in their physical properties such as the elastic constants and wave propagation speed. This anisotropy leads to a more complex wave propagation behavior as well as variations in shock-induced deformation. In the case of high strain rate loading, interaction between shock waves and dislocations plays a major role in determining the material behavior and the resulting microstructure (Gray 1993).

Shock waves are supersonic disturbances that lead to large changes in compression, particle velocity and internal energy almost instantaneously (Gupta 1999). Under shock conditions, a one dimensional compression is induced in the material

resulting in the propagation of high pressure wave. When the applied pressure exceeds the Hugoniot elastic limit, the material deforms plastically as a result of dislocation motion and multiplication. In general, dislocations move on their slip planes with velocities that increase with the rate of deformation. However, due to the relativistic effect, the dislocations are limited to move at velocities less than the shear wave velocity. The dislocations accommodate this velocity restriction by high rates of multiplication. The dislocation density was observed to increase with both peak pressure and pulse duration (Meyers *et al.* 2003, Murr 1981, Wright and Mikkola 1985) and the observed dislocation microstructures of the recovered samples consist of dislocation cells, deformation microbands and deformation twins (Rivas *et al*. 1995, Mogilevskii and Bushnev 1990, Meyers *et al*. 2003).

Deformation process under high strain rate is a complex multiscale dynamic problem. Therefore, different experimental techniques have been used to probe the material response at different levels of strain rates. For high strain rate (~10^6 /s) plate impact technique and high explosive facilities have been used. In the recent years, intense laser with ultra short pulse duration (2-10 nanoseconds) has been used to probe single crystal response to strain rates > 10^7 /s (Kalantar *et al.* 2000, Kalantar *et al.* 2001, Loveridge-Smith *et al.* 2001, Meyers *et al.* 2002, Meyers *et al*. 2003). High intensity laser experiments on copper single crystals showed that the dislocation microstructures of recovered samples are very sensitive to crystallographic orientation and level of pressure. While Meyers *et al.* (2003) found that there is a threshold pressure at which the deformation mechanism changes from glide to twining, Schneider *et al.* (2003) observed

that the pressure at which the deformation mechanism changes from glide to twinning is orientation dependent.

Pressure profile used in shock wave studies is often step wave with very sharp leading edge and relatively long time at uniform pressure. In general, the peak pressure of shock waves is independent of pulse duration and inversely proportional to rise time. In laser-generated shock waves of thin films, shock rise time as low as 10 picoseconds can be generated (Gahagan *et al.* 2000, McGrane *et al*. 2002). In solid anisotropic materials however, steep and planar shock front cannot be achieved (Liber 2000) due to the difference in local velocities at different orientations, in this case, shock waves have finite rise.

Along with the experimental techniques discussed above, computer simulations methodologies have been used to study various dynamic deformation phenomena by attempting to bridge the length scales from atomistic to macroscopic scales. In the atomistic scale, molecular dynamics (MD) simulations have been used to investigate the response of single crystals to high strain rate loading at different crystal orientations (Horstemeyer *et al.* 2001, Horstemeyer *et al.* 2002). Germann *et al.* (2000) carried out MD simulations to study shock wave propagation in fcc single crystals in three different orientations. They found that wave characteristics and pattern formation are orientation dependent. Kum (2003) conducted MD simulations using three potentials to study the anisotropic features of shock wave propagation in Nickel single crystals. He found that shock wave induced plasticity patterns depend on the crystallographic directions.

Current MD capabilities can simulate sizes in the submicron scale over a sub-nanosecond time period. Dislocation dynamics (DD) however, can simulate sizes of few

microns, over nanoseconds (ns) period of time exceeding by an order of magnitude the capabilities of MD simulations. DD has emerged as an excellent numerical tool to simulate the collective behavior of dislocations in a bulk material. Over the last 15 years, DD has been used to address various plastic deformation problems including hardening mechanisms, size effects, and dislocation-particles interaction.

The purpose of this work is to investigate the effect of peak pressure, pulse duration, crystal anisotropy and shock rise time on wave characteristics and shock-induced plasticity in copper single crystals. A multiscale dislocation dynamic plasticity model (MDDP) developed at Washington State University by Zbib and coworkers (Rhee *et al.* 1998, Zbib *et al*. 1998, Yasin *et al.* 2001, Zbib and Diaz de la Rubia 2002, Zbib *et al.* 2003) is used to examine the interaction between shock waves and dislocations in copper single crystals oriented in (001), (011) and (111) orientations. The results are compared to experimental data found in the literature.

3.2 Multiscale Dislocation Dynamics Plasticity (MDDP)

MDDP merges two length scales, the nano-microscale where plasticity is determined by explicit three dimensional DD analyses providing the material length scale, and the continuum scale where energy transport is based on basic continuum mechanics laws. The result is a hybrid elasto-viscoplastic simulation model coupling discrete DD with finite element analysis (FE). In the macro level, it is assumed that the material obeys the basic laws of continuum mechanics, i.e. linear momentum balance and energy balance:

$$div\, S = \rho \dot{v}_p \tag{3.11}$$

$$\rho\ C_v \dot{T} = K\nabla^2 T + S.\dot{\varepsilon}^p \tag{3.2}$$

where S is the stress, T is the temperature, v_p is the particle velocity, ρ, C_v and K are mass density, specific heat and thermal conductivity respectively. For elasto-viscoplastic behavior, the strain rate tensor $\dot{\varepsilon}$ is decomposed into an elastic part $\dot{\varepsilon}^e$ and plastic part $\dot{\varepsilon}^p$ such that:

$$\dot{\varepsilon} = \dot{\varepsilon}^e + \dot{\varepsilon}^p \tag{3.3}$$

For most metals, the elastic response is linear and can be expressed using the incremental form of Hooke's law such that:

$$\overset{\circ}{S} = \left[C^e\right]\dot{\varepsilon}^e \tag{3.4}$$

where $\overset{\circ}{S}$ is the corotational stress rate, and C^e is in general the anisotropic elastic stiffness tensor for cubic symmetry. Combining (3.3) and (3.4) leads to:

$$\overset{\circ}{S} = \left[C^e\right]\left[\dot{\varepsilon}\text{-}\dot{\varepsilon}^p\right] \tag{3.5}$$

In the nano-microscale, DD analyses are used to determine the plasticity of single crystals by explicit three-dimensional evaluations of dislocations motion and interaction among themselves and other defects that might be present in the crystal, such as point and cluster defects, microcracks, microvoids, etc. In DD, dislocations are discretized into segments of mixed character. The dynamics of the dislocation is governed by a "*Newtonian*" equation of motion, consisting of an inertia term, damping term, and driving force arising from short-range and long-range interactions. Since the strain field of the dislocation varies as the inverse of distance from the dislocation core, dislocations interact among themselves over long distances. As the dislocation moves, it has to

overcome internal drag, and local barriers such as the Peierls stress. The dislocation may encounter local obstacles such as stacking fault tetrahedra, defect clusters and vacancies that interact with the dislocation at short ranges and affect its local dynamics. In summary, the dislocation may encounter the following set of forces:

- Drag force, $B\boldsymbol{v}$, where B is the drag coefficient and $\boldsymbol{v}$ is the dislocation velocity.
- Peierls stress $\boldsymbol{F}_{Peierls.}$
- Force due to externally applied loads, $\boldsymbol{F}_{external.}$
- Dislocation-dislocation interaction force $\boldsymbol{F}_{D.}$
- Dislocation self-force $\boldsymbol{F}_{self.}$
- Dislocation-obstacle interaction force $\boldsymbol{F}_{obstacel.}$
- Image force $\boldsymbol{F}_{image.}$
- Osmotic force $\boldsymbol{F}_{Osmotic}$ resulting from non-conservative motion of dislocation (climb) and results in the production of intrinsic point defects.
- Thermal force $\boldsymbol{F}_{thermal}$ arising from thermal fluctuations.

As mentioned above, the velocity $\boldsymbol{v}$ of a dislocation segment is governed by a first order differential equation consisting of an inertia term, a drag term and a driving force vector such that:

$$m_s \dot{v} + \frac{1}{M_s(T,p)} v = F_s \qquad \text{with} \qquad m_s = \frac{l}{v}\left(\frac{dW}{dv}\right) \tag{3.6}_1$$

$$F_s = F_{Peirels} + F_D + F_{Self} + F_{External} + F_{Obstacle} + F_{Image} + F_{Osmotic} + F_{Thermal} \tag{3.6}_2$$

In the above equation the subscript s stands for the segment, m_s is defined as the effective dislocation segment mass density, M_s is the dislocation mobility which could

depend both on the temperature T and the pressure P, and W is the total energy per unit length of a moving dislocation (elastic energy plus kinetic energy). Hirth *et al.* (1998) derived the following expressions for the effective mass per unit dislocation length for screw $(m_s)_{\text{screw}}$ and edge $(m_s)_{\text{edge}}$ dislocations when moving at a high speed;

$$
\begin{aligned}
(m_s)_{screw} &= \frac{W_0}{v^2}\left(-\gamma^{-1}+\gamma^{-3}\right) \\
(m_s)_{edge} &= \frac{W_0 C^2}{v^4}\left(-16\gamma_l-40\gamma_l^{-1}+8\gamma_l^{-3}+14\gamma+50\gamma^{-1}-22\gamma^{-3}+6\gamma^{-5}\right)
\end{aligned}
\tag{3.7}
$$

where $\gamma_l = (1-v^2/C_l^{\,2})^{\frac{1}{2}}$, $\gamma = (1-v^2/C^2)^{\frac{1}{2}}$, C_l is the longitudinal sound velocity, C is the transverse sound velocity, v is the dislocation velocity, $W_0 = \frac{Gb^2}{4\pi} ln(R/r_0)$ is the rest energy for the screw per unit length, and G is the shear modulus. The value of R is typically equal to the size of the dislocation cell (about 1000 *b,* with *b* being the magnitude of the Burgers vector), or in the case of one dislocation is the shortest distance from the dislocation to the free surface. In the non-relativistic regime when the dislocation velocity is small compared to the speed of sound, the above equations reduce to the familiar expression $m = \beta\rho b^2 \ln(R/r_0)$, where β is a constant dependent on the type of the dislocation.

The motion of each dislocation segment contributes to the macroscopic plastic strain and spin via the relations:

$$\dot{\varepsilon}^p = \sum_{i=1}^{N} \frac{l_i v_{gi}}{2V}\left(n_i \otimes b_i + b_i \otimes n_i\right) \tag{3.8}$$

$$W^p = \sum_{i=1}^{N} \frac{l_i v_{gi}}{2V}\left(n_i \otimes b_i - b_i \otimes n_i\right) \tag{3.9}$$

where W^p is the plastic spin, l_i is the dislocation segment length, v_{gi} is the dislocation glide velocity, n_i is a unit normal to the slip plane, V is the volume of the representative volume element (RVE), and N is the total number of dislocations segments within a given element.

Determination of the time step under extreme dynamic loading conditions is critical. The time step in this analysis is dictated by the shortest flight distance for short range interaction between dislocations in DD and the time step used in the dynamic FE. The critical time (t_c) and the time step (δt) for both DD and FE which yield a stable solution are given by $t_c = (l / C_0)$, $\delta t = (t_c / 10)$ where l is the characteristic length which is the shortest dimension in the FE mesh. In our calculations, t_c can be as small as 10^{-10} second and thus δt is one order of magnitude less. This time step is very suitable to simulate ultra high strain rate, short pulse duration conditions involved in laser based experiments.

It is apparent that the momentum equation generates elastic stress wave with a specific shape by applying certain boundary conditions in the FE code. The elastic wave exerts a driving force on the dislocations giving rise to $\boldsymbol{F}_{external.}$ which, can be expressed as:

$$F_{External} = \left(\sigma^a . b\right) \times \zeta \tag{3.10}$$

where σ^a is the stress applied on the dislocation by the stress wave and ζ is the line sense of the dislocation line. An interaction process between the dislocations and the stress wave takes place resulting in changes in the wave profile and the formation of

dislocation microstructure. Peierls force ($\boldsymbol{F}_{Peierls}$) is also related to Peierls stress ($\sigma^{Peierls}$) by a similar relation as given in equation (3.10).

3.3 MDDP Simulations

MDDP simulations are performed to investigate the deformation process in copper single crystals under shock loading. The simulations are designed to mimic uniaxial strain loading at extreme conditions of high strain rates > 10^6/s, and short pulse durations of few ns. The simulation setup as illustrated in figure 3.1 consists of a block with dimensions 2.5 μm ×2.5 μm ×25 μm. In order to achieve the uniaxial strain involved in shock experiments, the four sides are confined so that they can only move in the loading direction while the bottom surface is rigidly fixed. To generate the stress wave a displacement-controlled boundary condition is applied on the upper surface such that the resulting velocity history $v_p(t)$ consists of a ramp part where the velocity increases from zero to its maximum value ($v_{p\,max}$) over a finite rise time (t_{rise}). The velocity is then kept on its maximum value for a period of time equals to the wave holding time (t^*). In this case, $\frac{v_p}{L_z}$ corresponds to the macroscopic strain rate. The upper surface is then released and the simulations continue for the elastic transmitted wave to interact with the existing dislocation sources.

The loading and the boundary conditions are summarized in the following equations:

$$
\begin{aligned}
u_z(t) &= -a_p t^2 && 0 \le t \le t_{rise}, \quad \text{at } z = \frac{L_z}{2} \\
u_z(t) &= -a_p t_{rise}{}^2 - v_{p\,max}\left(t - t_{rise}\right) && t_{rise} \le t \le t^*, \quad \text{at } z = \frac{L_z}{2}
\end{aligned} \tag{3.11}
$$

$$
\begin{aligned}
&u_z(t) = 0 \qquad \text{at } z = -\frac{L_z}{2} \\
&u_x(t) = 0, \quad at \quad x = -\frac{L_x}{2}, \frac{L_x}{2} \\
&u_y(t) = 0, \quad at \quad y = -\frac{L_y}{2}, \frac{L_y}{2}
\end{aligned} \tag{3.12}
$$

where L_x, L_y, and L_z are the lengths of the computational cell in the x, y and z directions respectively, u_x, u_y, and u_z are the displacement components and a_p is a constant that is related to particle velocity by $v_p(t) = \dot{u}_z(t) = -2a_p t$ for $0 \le t \le t_{rise}$.

When loading crystalline materials under extreme uniaxial compression, the deviatoric stresses at the wave front may attain or even exceed the theoretical strength of the material in pure shear under normal conditions. The lattice responds to that by nucleating dislocation loops at the wave front. A homogenous nucleation mechanism was proposed by (Meyers 1978) in which he assumed that dislocations are homogenously generated at the front to accommodate the deviatoric stresses. The insertion of dislocations relaxes the deviatoric stresses and as the wave propagates, new layers of dislocation loops are nucleated. Currently, a nucleation criterion is under implementation in our framework so that the simulations can be started from a defect free cell and end with high dislocation densities. Results of the rule of dislocation nucleation on the deformation process under shock loading condition using both DD and MD analyses will be presented in chapter 5. Alternatively, one can start from a random initial distribution of small dislocations loops that may act as dislocation sources.

In the present analyses, Frank-Read dislocation loops randomly distributed on different slip planes are used as agents for dislocation generation. For copper, sources length ranging between 0.30 μm to 0.80 μm are used. It is worth mentioning here that the boundary conditions of the computational cell sides are different in FE and DD parts of the code. In DD, periodic boundary condition for the RVE is used to ensure both the continuity of the dislocation curves and the conservation of dislocation flux across the boundaries, by that we take into account the periodicity of single crystals in an infinite media. In FE analysis however, the sides are constrained to move only in the z direction so that a uniaxial strain consistent with shock experiments is achieved. In passing, we point out that other FE boundary conditions, namely free and periodic boundary conditions have been investigated and discussed, but it turns out that the boundary condition defined in (3.11) and (3.12) is the best one that mimics shock experiments (Shehadeh and Zbib 2005).

The main focus of this work is to investigate the interaction between the *transmitted* wave and dislocation sources. However, when the stress wave hits the rigid base, it reflects to the block and interacts with the dislocations again. In order to minimize the effects of the reflected wave, the dislocation sources were placed in locations such that their activities are confined in the upper one-fifth part of the sample and so once the wave front reaches the bottom surface, the value of the stresses in the positions where the dislocations are located will be small allowing dislocation relaxation process to take place. Our calculations of the dislocation density therefore are carried out assuming that the sample size is one-fifth of the simulation cell. A better solution to

isolate the effect of the reflected wave would be by implementing a suitable non-reflective FE boundary condition.

Under high strain rate loading, the elastic properties of metals depend on the applied pressure. In order to better simulate the physical problem, any constitutive model must account for this effect. In the MDDP code, the experimental results of Hayes *et al.* (1999) for the shear modulus (G) and Poisson's ratio (ν^*) of isotropic copper are fitted in the constitutive equation to account for the dependence of elastic properties on pressure such that:

$$G = \begin{cases} G_0 + 0.89P & 0 < P < 60 \\ G_0 + 53.4 + 0.40P & 60 < P < 100 \end{cases} \tag{3.13}$$

$$\nu^* = \nu^*_0 + 1.70 \times P \times 10^{-12} \tag{3.14}$$

where, P is in GPa, G_0 and ν^*_0 are the shear modulus and Poisson's ratio under normal static loading conditions. The implementation of the above nonlinear elastic model in the FE framework required the adjustment of the stiffness matrix at every time step. In passing we point out that here the pressure is given by $P = -\sigma_{33}$ as usually defined in the shock wave community, this definition is used through out this paper. In the continuum mechanics community, however, pressure is usually defined as $P = -(\sigma_{33} + \sigma_{22} + \sigma_{11})/3$. It can be shown that these two definitions coincide only in the case of uniaxial strain of isotropic linear elastic material with Poisson's ratio of ½.

3.4 Results and Discussion

3.4.1 Wave characteristics

Figure 3.2 shows pressure snapshots and contour plot of a wave propagating in copper single crystal shocked to a peak value of 4.5 GPa for 1.50 ns. Clearly, three distinct regions are seen in the wave profile; 1) a leading wave front in which the pressure increases from zero to the peak value over a period equivalent to the rise time, 2) a plateau of the peak pressure which stays for a period equivalent to the pulse holding time, and 3) a release part where the pressure decreases almost instantaneously from its peak value to zero. The tail of the release wave shows fluctuations that are attributed to the FE mesh. The frequency of these fluctuations is proportional to the FE density (Smirnova *et al.* 1999, Shehadeh *et al.* 2005). Under shock loading conditions, the release wave moves at speed faster than that of the wave front, which leads to a decrease in the width of the plateau part as can be seen in figure 3.2. As the shock wave propagates in the material, attenuation in the peak pressure occurs as the release wave surpasses the wave front. Snapshots of the calculated pressure profiles in copper shocked to 145 GPa are shown in figure 3.3a. It can be seen that there is a considerable decrease in the peak pressure. The peak pressure as a function of distance shows a decay of -1.25 (GPa/μm) corresponding to a decay rate of – 4.04 (GPa/ns) as shown in figures 3.3b, c. Meyers *et al.* (2003) showed that the rate of attenuation is pressure dependent.

The effect of the pressure dependent elastic properties as given in (3.13) and (3.14) on the wave profile is illustrated in figure. 3.4. The wave profiles generated by linear and nonlinear (pressure dependent) models reveal that while the qualitative

features of the two profiles are similar, the nonlinear model leads to faster wave propagation and higher values of peak pressure.

For cubic symmetry materials, three independent elastic properties that are orientation dependent are required to describe the mechanical behavior of the material. This anisotropy effect increases significantly the number of nonzero elements in the FE stiffness matrix leading to alteration in the calculated stress components and the wave speed. In order to test these anisotropy effects, the wave profiles of three different orientations and that of an isotropic medium (assuming (001) orientation in its DD calculations) are shown in figure 3.5. We observed that under the same loading condition, the peak pressure of (111) and (011) orientations are slightly higher than those of the (001) which is lower than that of the isotropic material. Furthermore, the wave speed varies moderately with orientation with the fastest moving wave in the (111) followed by (011), isotropic medium and (001) respectively.

As the shock wave advances in the material, it encounters the dislocation sources and an avalanche of dislocations occurs the instant the wave hits the sources. The dislocations continue to emit from the sources at very high speeds causing the stress to have different values than those predicted by elasticity theory (Weertman 1981). The wave profiles of two simulations using perfectly elastic (no dislocations) and elastic-plastic (with dislocation) models are shown in figure 3.6a. Obviously, significant deviations in the plateau and the release part are observed, revealing that plastic deformation resulting from dislocation motion and multiplication causes material's softening. The energy used to generate plastic strains is converted into heat, which results in local temperature increase as shown in figure 3.6b.

Snapshots of shock-induced plasticity are presented in figure 3.7a by plotting the effective plastic strain along the central line of the simulation cell in the z-direction. The local values of plastic strain in the location where the dislocations are interacting with the shock wave keep changing till the relaxation process takes place and therefore, the dislocation density saturates and so does the plastic strain. Moreover, several peaks appear in the plastic strain profile suggesting the existence of localized deformation regions and the formation of dislocation patterns, as the dislocation density in these regions is very high relative to other locations. The profiles of the effective plastic strain for different orientations show that the number of peaks and the separation distance between two consecutive peaks are orientation dependent as illustrated in figure 3.7b.

The deformed shape resulting from shock induced plastic strain is presented in figure 3.8 by plotting the deformed shape of a slice within the RVE. The deformed shape shows the formation of bands in the region where dislocation microbands are formed. This indicates that dislocation activities under high strain rate loading can be considered as sources for shear banding.

3.4.2 Dislocation density and slip activation

In fcc materials, there are 12 different slip systems, which can contribute to the deformation process. Table 3.1 lists the 12 slip systems as combinations of the slip planes and slip directions. Dislocation density histories at a peak stress of 5.0 GPa and pulse duration of 1.5 ns with a rise time of 0.50 ns for (001), (011) and (111) orientations and isotropic case were calculated and plotted in figure 3.9. These plots suggest the existence of three distinct regimes of interaction between dislocations and the propagating shock waves, namely; 1) no interaction regime, where the wave has not yet impacted the

dislocation sources, 2) the interaction regime, where the wave impacts the dislocation sources leading to avalanche in the dislocation density, and 3) the relaxation regime, in which, the wave surpasses the region where the dislocation sources are located. In this regime, the contribution of dislocation annihilation becomes noticeable, curved dislocations retract to stable configurations and therefore, dislocation density saturates. Furthermore, these plots show that that the dislocation density is very sensitive to crystal orientation with the highest density exhibited by an isotropic media oriented in the (001) followed by (111), (011) and (001) anisotropic media respectively. This may be attributed to the number of slip systems activated and the way these systems interact. The (001) orientation has the highest symmetry among all orientations with four possible {111} slip planes that have identical Schmid factor of 0.4082, which leads to immediate work hardening (Meyers *et al.* 2003). The (111) orientation also exhibits symmetry with three possible slip planes that have Schmid factor of 0.4082. The (011) orientation has the lowest symmetry among these three orientations with two possible slip planes.

The contribution of each slip systems to plastic deformation is investigated by plotting the dislocation density distribution of the slip systems as shown in figure 3.10. As expected, (001) orientation shows the largest number of activated slips (8 systems) on all four slip planes followed by and the (111) orientation, which shows four slips activated on three different slip planes and finally (011) in which three slip systems on two slip planes are activated.

3.4.3 Dislocation microstructure

The dislocation microstructure generated by shock waves depends on a number of shock wave and material parameters (Meyers 1994). Among shock wave parameters,

pressure (strain rate) and pulse duration are very important. Pulse duration is related to the time required for the dislocations to reorganize. For the case of dislocation cell structure, it was observed that as the pulse duration increases, the cell walls become better defined (Wright *et al.* 1981).

We found previously that the dislocation microstructure at strain rates on the order of 10^6/s or higher consists of deformation bands within which the dislocation densities are very high (Shehadeh *et al.* 2004). Here, morphologies of the dislocation microstructures obtained from slices within the computational cell at different crystal orientation are shown in figure 3.11. The figure clearly shows the formation of band-like dislocation cell walls coincident with the slip planes. The main features of these bands does not seem to change with crystal orientation, however, the number, thickness and the dislocation density in these bands differ from one orienatation to another. In fact while (001) orientation shows multiple bands running on all four slip planes, (011) orientation shows bands crossing each other suggesting the activation of dislocations on two slip planes, whereas (111) orientation shows bands running on three slip planes.

The thickness of these band like walls is determined by a double cross-slip mechanism (Figure 3.11d). Because of the high level of resolved shear stress on all possible slip systems, cross-slip may easily be activated. Therefore, a screw dislocation segement can cross-slip to a secondary plane and glide on that plane for a short distance and subsequently it may return to its primary plane again by cross-slip. This cross-slip mechanism results into the generation of Frank-Read sources on adjacent and parallel slip planes. The dislocation on these parallel planes are of the same type and they have strong mutual attraction, therefore they stabilize.

Although the thickness of the cell wall is physical as explained above, the same cannot be said about the spacing between the wall. The spacing is directly related to the computational cell size, periodicity and initial distirbution of the dislocation sources.

The dislocation density within the deformation bands is calculated at different values of peak pressure and pulse duration. The calculated dislocation densities are plotted at different pressures and compared with the experimental observations of Murr (1981) and the analytical predictions of Meyers *et al.* (2003). Figure 3.12 reveals that the dislocation density varies as a power law with pressure such that; $\rho_{dis} = 3.33 \times 10^{7} (P^{1.70})$. These results conform very well with the predications of Meyers *et al*. (2003) for moving dislocations when the pressure is less than 70 GPa. The experimental observations of Murr (1981) however, exhibit lower values of dislocation density compared to DD calculations. This maybe attributed to the nature of recovery experiments in which the recovery process occurs at much lower pressure than the maximum in the plot (Meyers *et al.* 2003).

Calculations of the effect of pulse duration at constant pressure on the dislocation density were also performed and compared with available experimental results. Figure 3.13 illustrates that there is an increase in the dislocation density with pulse duration to a certain duration beyond which the dislocation density saturates. These results are in good qualitative agreement with the observations of Wright *et al.* (1981) and Wright and Mikkola (1985) using plate impact experiment with pulses in the microsecond time scale.

3.4 Summary and Concluding Remarks

Multiscale simulations were carried out to study shock wave propagation and interaction with dislocations in copper single crystals. These simulations were designed to mimic the loading conditions in recent laser based experiments, where the pulse duration is few ns. It is shown that avalanche of dislocation density is a natural consequence of shock wave dislocations interaction. Our calculations show that dislocation density has a power law dependence on pressure with a power of 1.70. Dislocation microstructure consisting of microbands coincident with the {1 1 1} planes were formed. The inclusion of pressure-dependent elastic properties for isotropic media leads to faster wave propagation speed. Incorporating the effect of crystal anisotropy in the elastic properties results in an orientation dependent wave speed and peak pressure. Computer simulations of dislocation motion under impact loading hold a great promise for investigating deformation process of metals in regimes that cannot be probed by current experiments.

References

Clifton, R. J., and Bathe, N., 1999. In: Furnish, M. D., Chhbildes, L. C. and Hixson, R. S., (Eds.), Shock Compression of Condensed Matter, Melville, New York, pp. 19-26.

Coffey, C. S., 1992, In: Meyers, M. A., Murr, L. E., Staudhammer, K. P., (Eds.), Shock Waves and High Strain Rate Phenomena in Materials, Marcel Dekker, New York, pp. 669-690.

Gahagan, K. T., Moore, D. S., Funk, D. J., Reho, J. H., and Rabie, R. L., 2002, *Journal of Applied Physics* **92 (7)**, 3679

Germann, T. C., Holian, B. L., and Lomdahl. P. S., 2000, *Physical Review Letter* **84(24)**, 5351.

Gray, G. T., 1993, In: Asay, J. R., Shahinpoor. M., (Eds.), High Pressure Shock Compression of Solids, Springler-Verlag, New York, pp. 187-213.

Gupta, Y.M., 1999, In: Bulatov, V., de la Rubia, T., Philips, R., Kaxiras, E., Ghoniem, N., (Eds.), Multiscale Modeling (Material Research Society, 1998) pp. 139-149.

Hayes, D., Hixson, R. S., and McQueen, R.G, 1999, In: Furnish, M. D., Chhbildes, L. C., Hixson, R. S., (Eds.), Shock Compression of Condensed Matter, Melville, New York, pp. 483-488.

Hirth J. P., Zbib, H. M., and Lothe, J., 1998, *Modeling Simul. Mater. Sci. Eng*. **6**, 165.

Horstemeyer. M. F., Baskes, M. I., and Plompton, S. J., 2001, *Acta Mater*. **49**, 4363.

Horstemeyer, M. F., Baskes, M. I., Godfrey, A., and Hughes, D. A., 2002, *Int. J. Plasticity* **18**, 203.

Kalantar, D. H., Belak, J., Bringa, E., Budil, K., Colvin, J., Kumar, M., Lorenz, K. T., Rudd, R. E., Stolken, J., Allen, A.M., Rosolankova, K., Wark, J. S., Meyers, M. A., and Schneider, M. S., 2003, *Physics of Plasmas* **10, n 5 II**, 1569.

Kalantar, D. H., Allen, A. M., Gregori, F., Kad, B., Kumar, M., Lorenz, K. T., Loveridge, A., Meyers, M. A., Pollaine, S., Remington, B. A., and Wark, J. S., 2001, In: Furnish, M. D., Thadhani, N. N., Horie, Y., (Eds.), Shock Compression of Condensed Matter, pp 615-618.

Kum, O., 2003, *Journal of Applied Physics* **93(6),** 3239.

Leiber, C. O., 2000, *Propellants, Explosives, Pyrotechnics,* **25**, 288.

Loveridge-Smith, A., Allen, A., Belak, J., Boehly, T., Hauer, A., Holian, B., Kalantar, D., Kyrala, G., Lee, R.W., Lomdahl, P., Meyers, M. A., Paisley, D., Pollaine, S., Remington, B., Swift, D. C., Weber, S., and Wark, J. S., 2001, *Phys. Rev.Lett.* **86(11)**, 2349.

McGrane, S.D., Moore, D. S., Funk, D. J., and Rabie, R. L., 2002, *Applied Physics Letter* **80**, 3919.

Meyers, M. A., 1978, *Scripta Metallurgica* **12(1)**, 21.

Meyers, M. A., 1994. Dynamic Behavior of Materials, (New York: John Wiley & Sons).p. 2, 386, 394, 108.

Meyers, M. A., Benson, D. J., Vohringer, O., Kad, B. K., Xue, Q., and Fu, H.-H., 2002, *Materials Sciences and Engineering* **A322**, 194.

Meyers, M. A., Gregori, F., Kad, B. K., Schneider, M. S., Kalantar, D. H., Remington, B. A., Ravichandran G., Boehly, T., and Wark, J., 200, *Acta Materialia* **51**, 1211.

Mogilevskii, M. A., and Bushnev L. S., 1990, *Combustion, Explosion, and Shock Waves* **26**, 215.

Murr, L. E., 1981, in: Meyers, M. A., Murr, L. E., (Eds.), Shock Waves and High Strain Rate Phenomena in Metals, Plenum, New York, pp. 607-673.

Rhee, M., Zbib, H. M., Hirth, J.P., Huang, H., and de la Rubia, T.D., 1998, *Modeling and Simulations in Maters.Sci. & Eng*. **6**, 467.

Rivas, J. M., Quinones, S. A., and Murr, L. E., 1995, *Scripta Metallurgica et Materialia* **33(1),** 101.

Schneider, M. S., Kad, B. K., Gregori, F., Kalantar, D., Remington, B.A., and Meyers, M.A. (Private communication).

Shehadeh, M. A., Zbib, H. M., and de la Rubia, T. D., 2005, *Phil. Mag*., in press.

Shehadeh, M. A., Bringa, E., Zbib, H. M., McNaney, J., and Remington, B. A., 2005, Submitted for publication.

Shehadeh, M. A., and Zbib, H. M., 2005, In preparation.

Smirnova J. A., Zhigilei L. V., and Garrison B. J., 1999. *Computer Science Communications* **118**, 11.

Weertman, J., 1981, In: Meyers, M. A., Murr, L. E., (Eds.), Shock-Wave and High Strain Rate Phenomena in Metals, Plenum press, NewYork, pp. 469-486.

Wright, R. N., Mikkola, D. E., and LaRouche, S., 1981, In: Meyers, M. A., Murr, L. E., (Eds.), Shock Waves and High Strain Rate Phenomena in Metals, Plenum, New York, pp. 703-716.

Wright, R. N., and Mikkola, D. E., 1985, *Metallurgical Transactions* **16 A**, 891.

Yasin, H., Zbib, H. M., and Khaleel, M. A., 2001, *Material Science and Engineering* **A309**, 294.

Zbib, H. M., Rhee, M., and Hirth, J. P., 1998, *Int. J. Mech. Sci*. **40**, 113.

Zbib, H. M., and Diaz de la Rubia, T., 2002*, Int. J. Plasticity* **18**, 1133.

Zbib, H. M., Shehadeh, M., Khan, S.M, and Karami, G., 2003, *International Journal for Multiscale Computational Engineering* **1**,73.

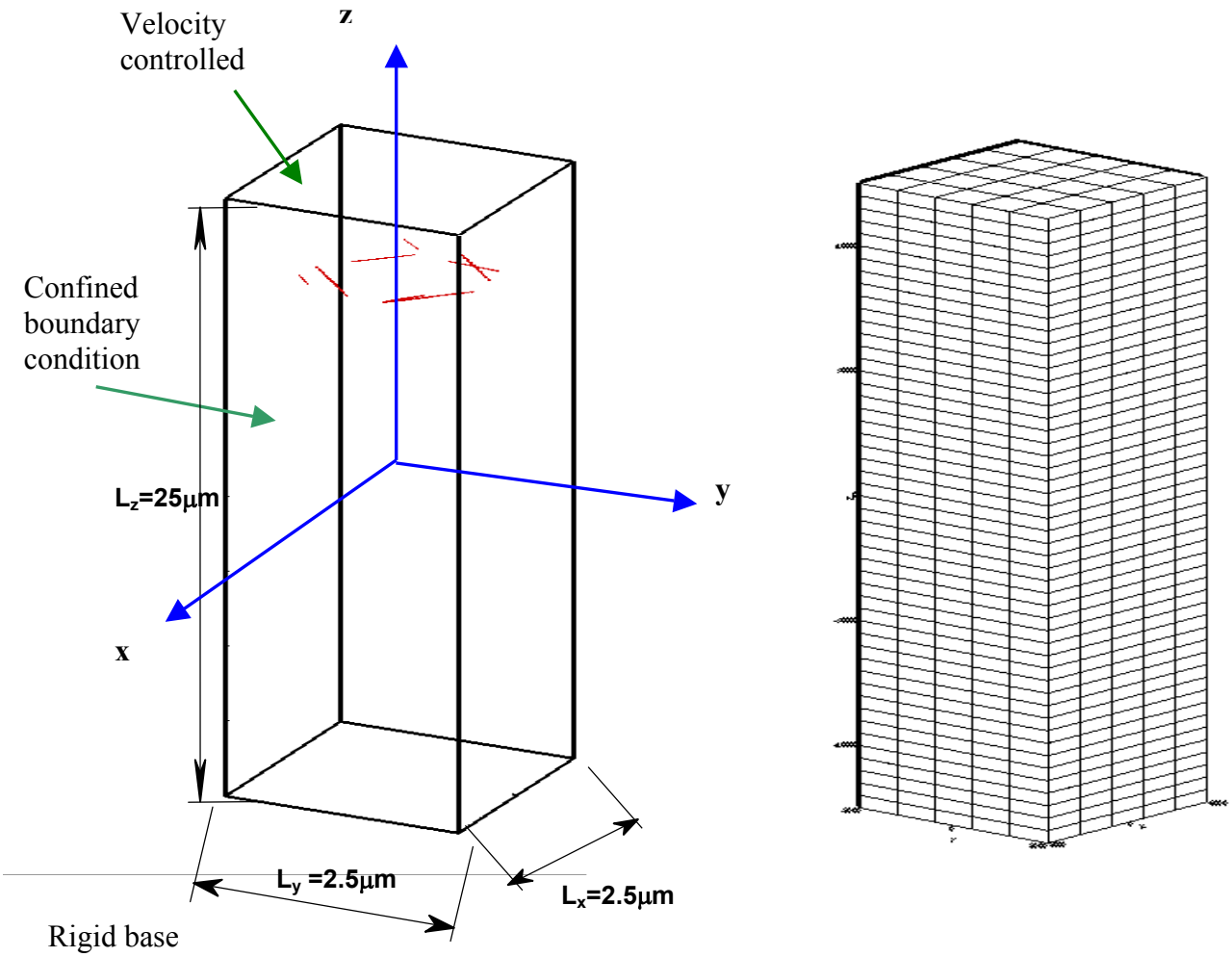

Figure 3.1. Setup of the simulation cell and the finite element mesh.

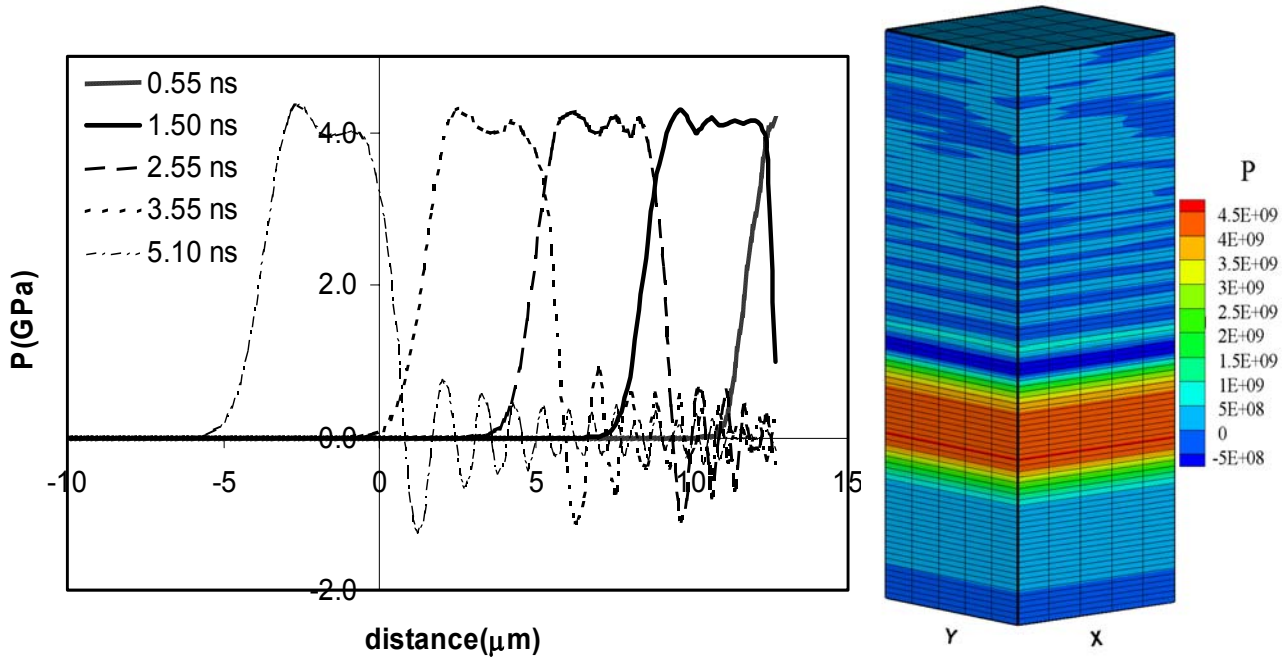

(a) (b)

Figure 3.2. Shock wave propagating in copper single crystal shocked to 4.5 GPa peak pressure for 1.50 ns pulse duration.(a) snapshots (b) contour plot at 5.10 ns.

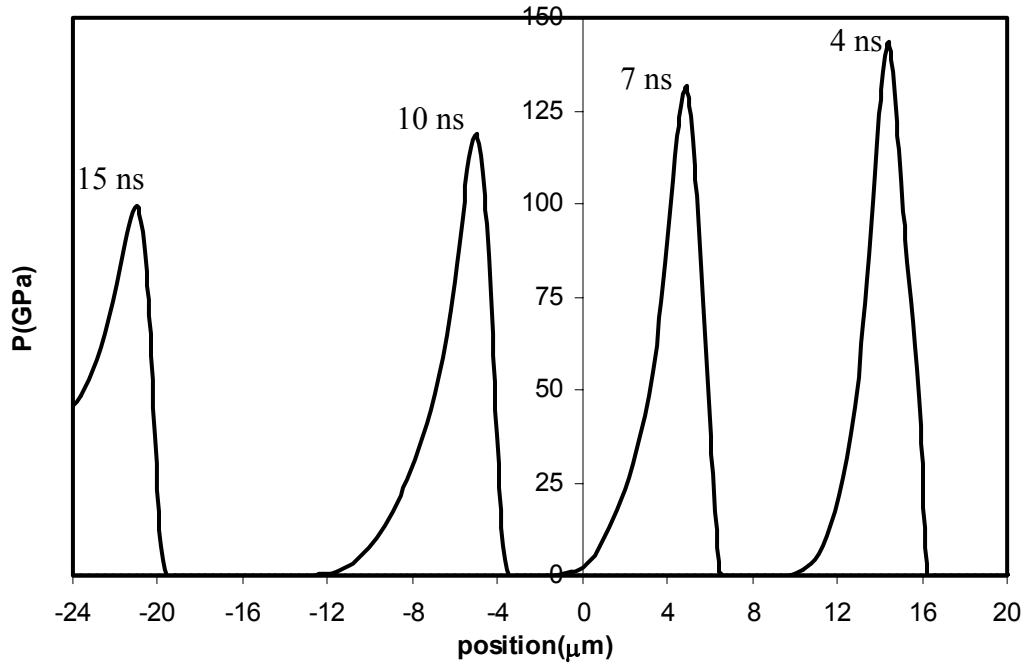
150
125
100
75
50
25
0
P(GPa)
15 ns
10 ns
7 ns
4 ns
-24
-20
-16
-12
-8
-4
0
4
8
12
16
20
position(μm)

(a)

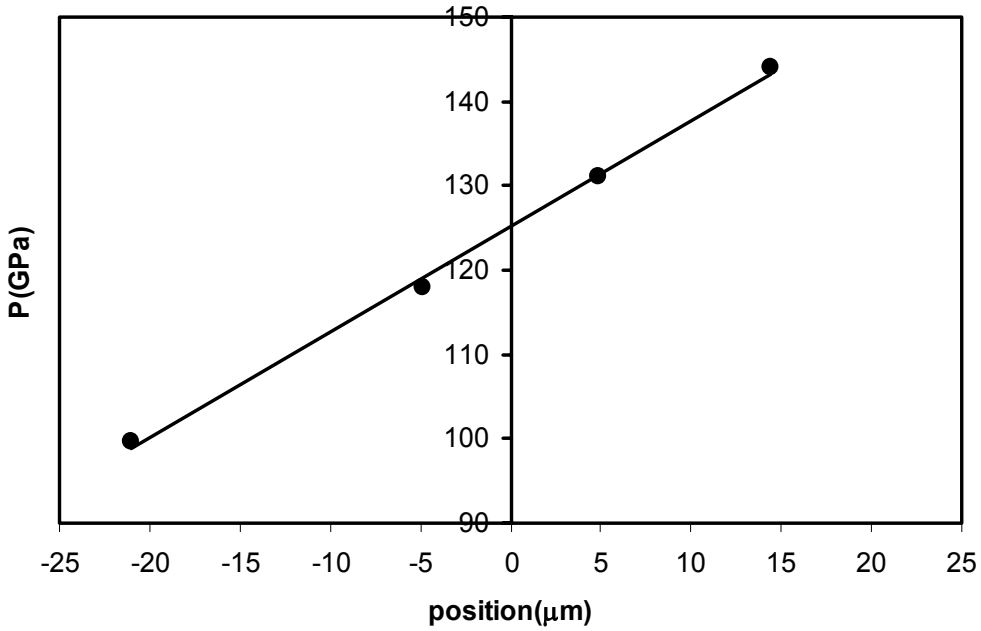

(b)

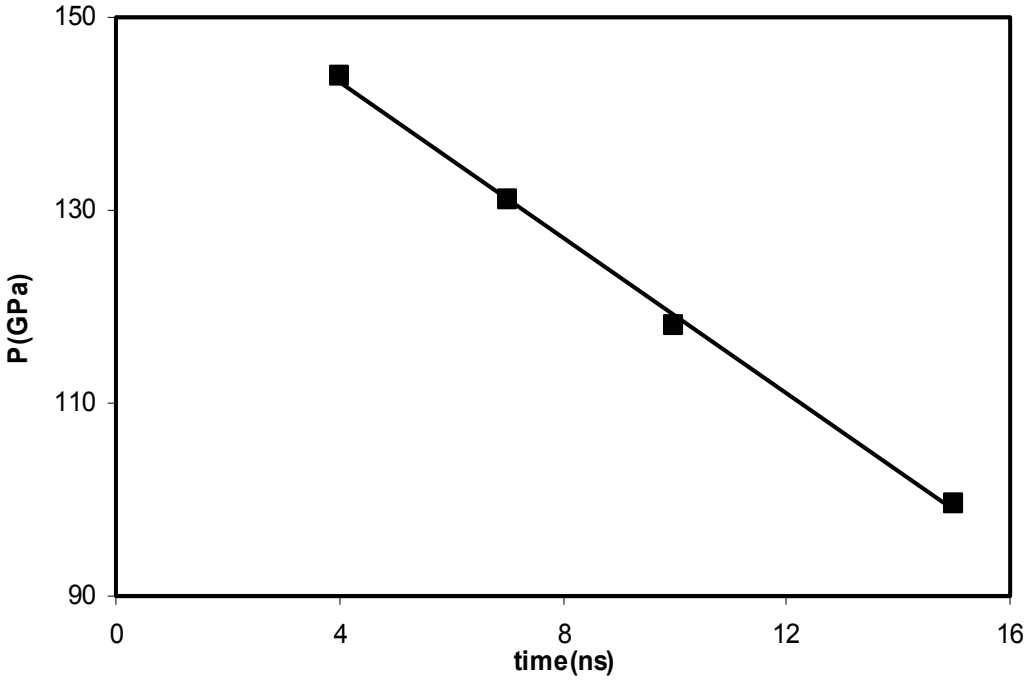

(c)

Figure 3.3. Simulated pressure profiles (a) Wave attenuation in copper at maximum pressure of 145 GPa. (b) Pressure decay as a function of distance (c) Pressure decay

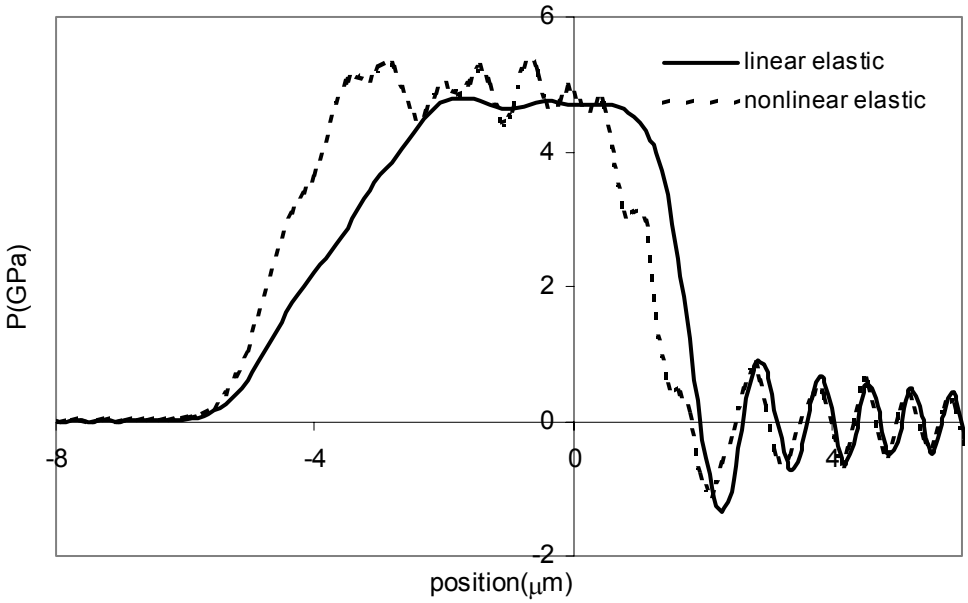

Figure.3.4. The effect of pressure dependent elastic properties on the wave profile

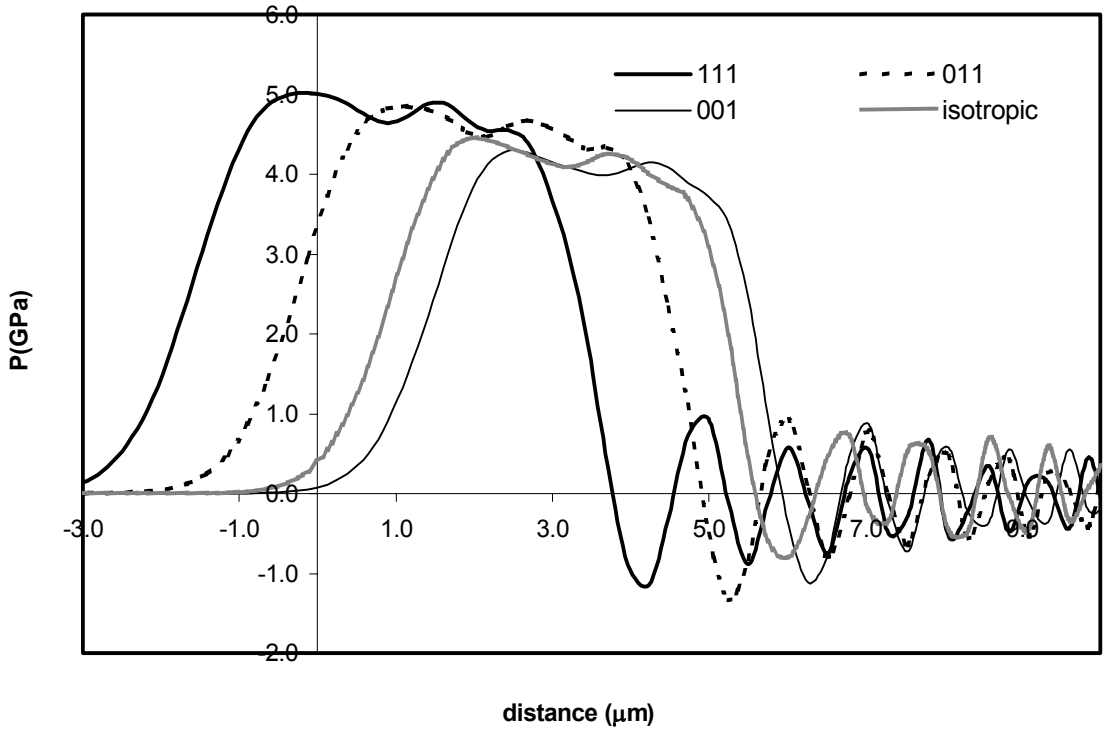

Figure 3.5. Wave profiles for (111), (011), (001) orientations compared to the isotropic media oriented in (001) in copper shocked to 5.0 GPa peak pressure for 1.50 ns pulse duration.

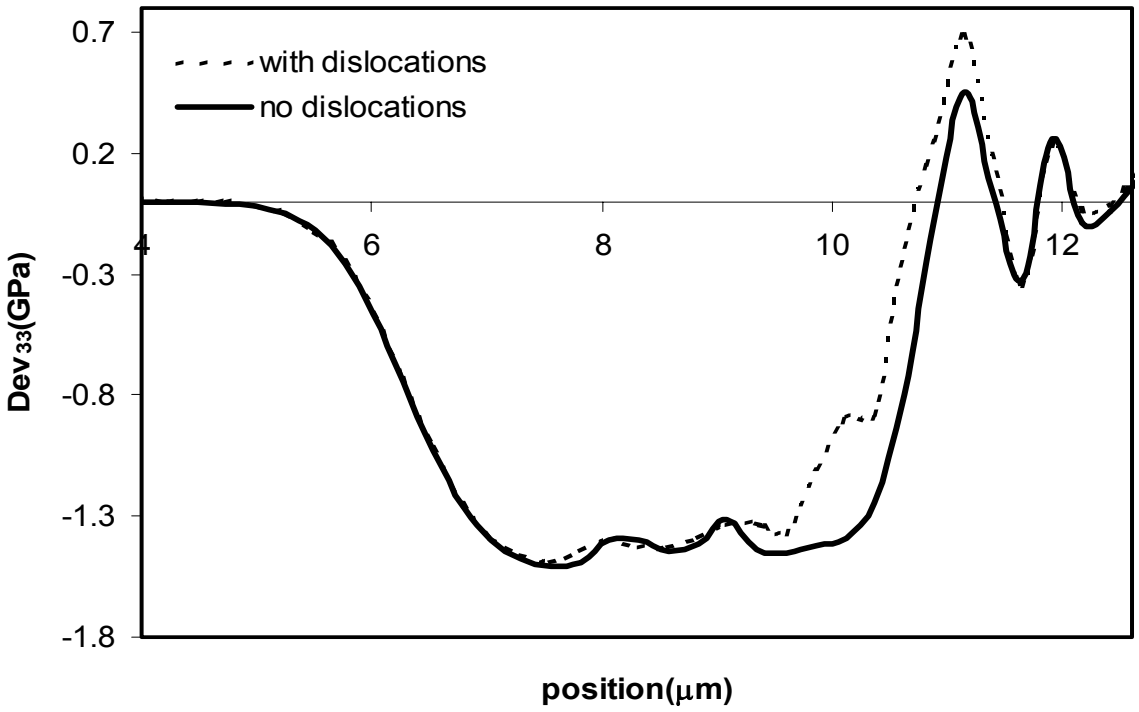

(a)

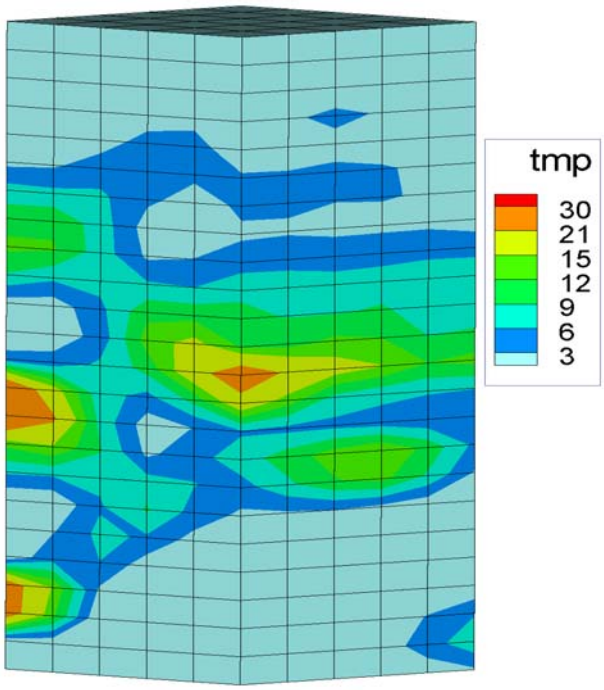

(b)

Figure. 3.6: (a) The effect of dislocations activities on the deviatoric stress for copper shocked at 4.5 GPa peak pressure for 1.5 ns, (b) temperature rise (K) from plastic deformation

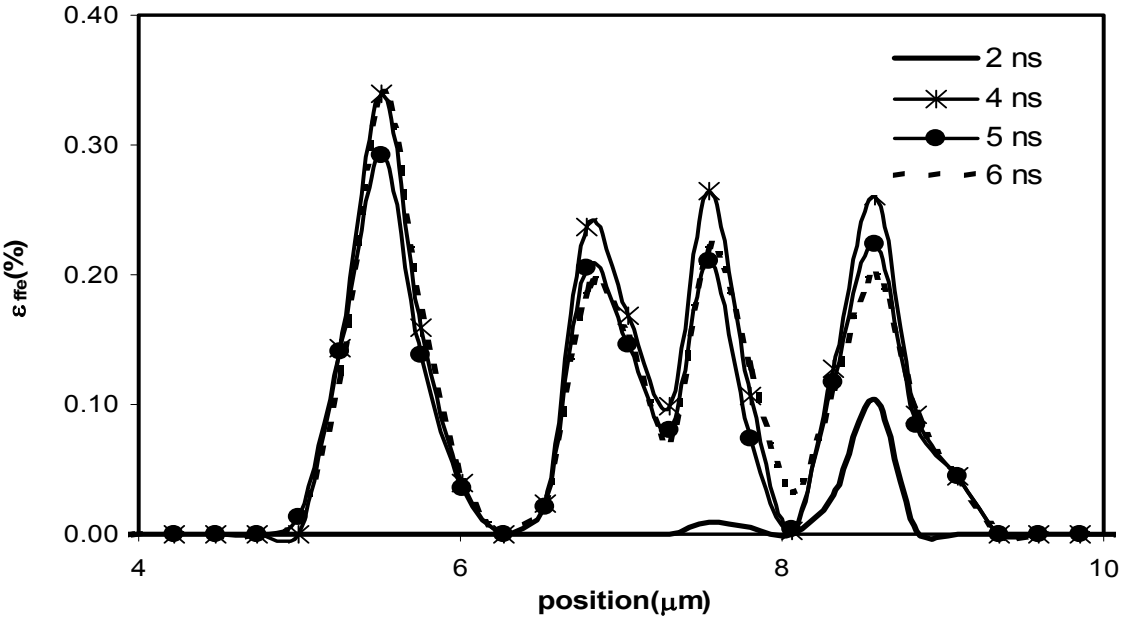

(a)

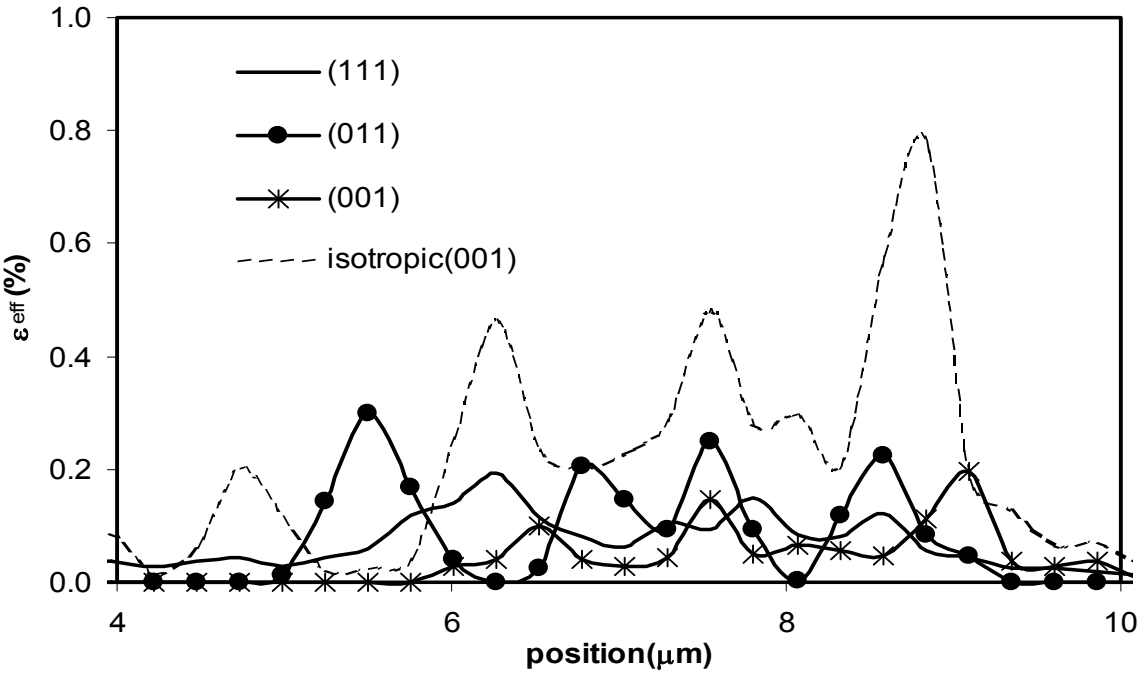

(b)

Figure. 3.7. (a) Evolution of effective plastic strain in crystal oriented in the (011) shocked to 5.0 GPa peak pressure. (b) the effect of crystal orientation on the plastic strain.

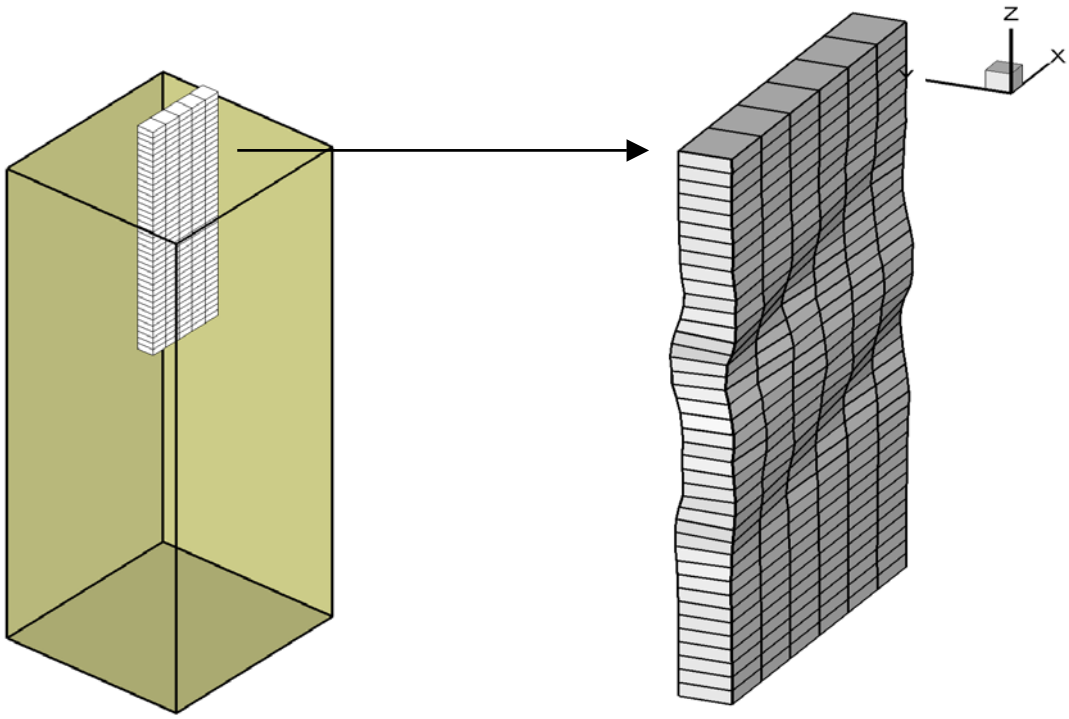

Figure. 3.8. The deformed shape of a slice within the RVE, showing the formation of localized deformation bands coincident with regions with high dislocation density.

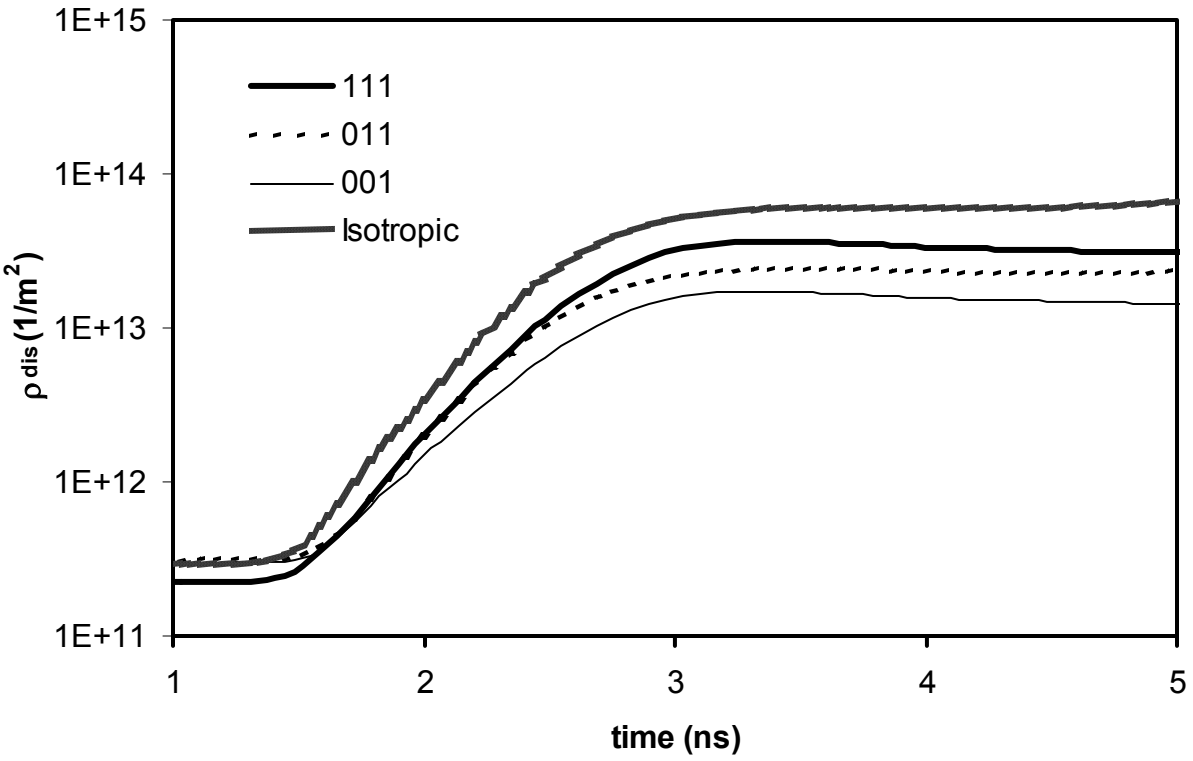

Figure. 3.9. The influence of crystal orientation on the dislocation density history in copper single crystal shocked to 5.0 GPa peak pressure for 1.5 ns.

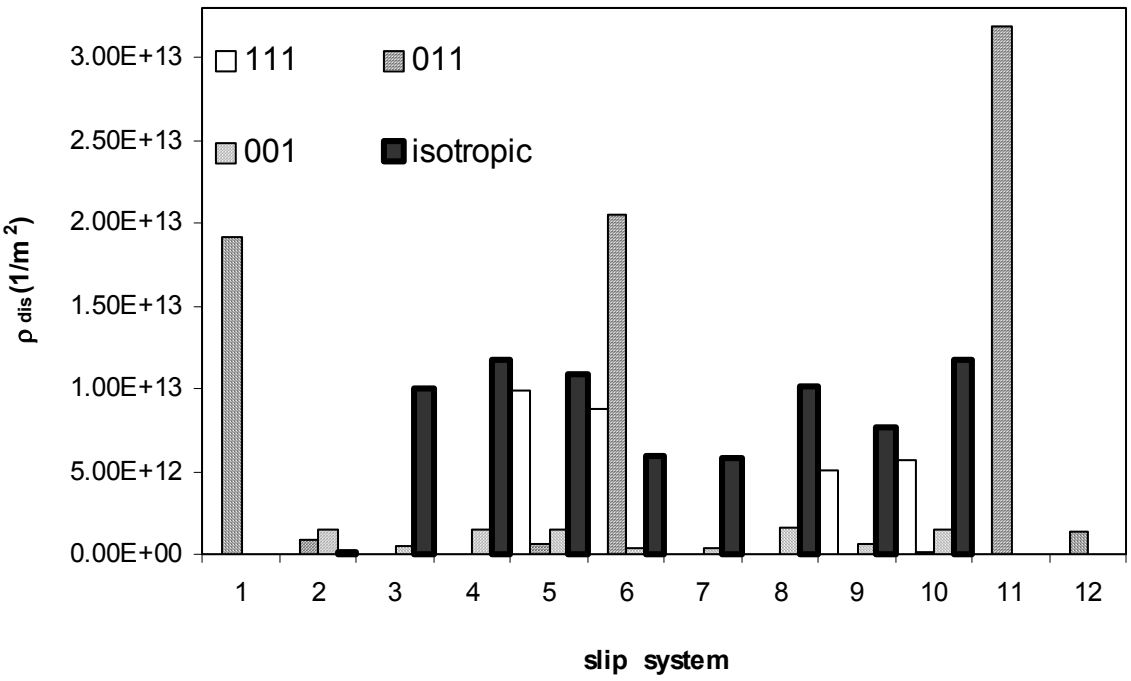

Figure. 3.10. The influence of crystal orientation on the slip activation.

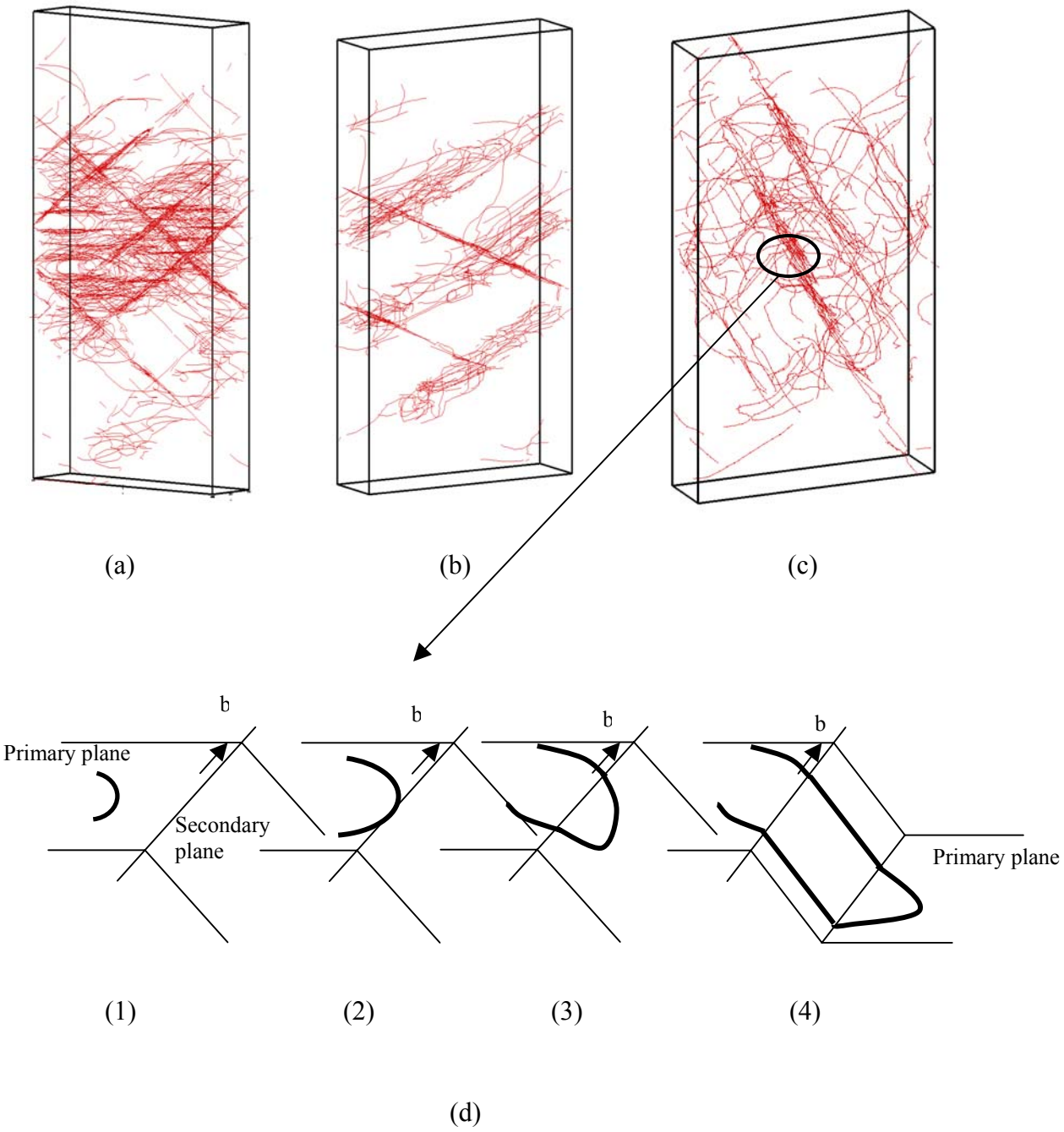

Figure. 3.11. The dislocation microstructure in copper crystal at 5.0 GPa peak pressure and 1.50 ns pulse duration for crystal oriented in (a) (001) (b) (011) (c) (111) and (d) subsequent events that lead to the activation of the cross slip mechanism

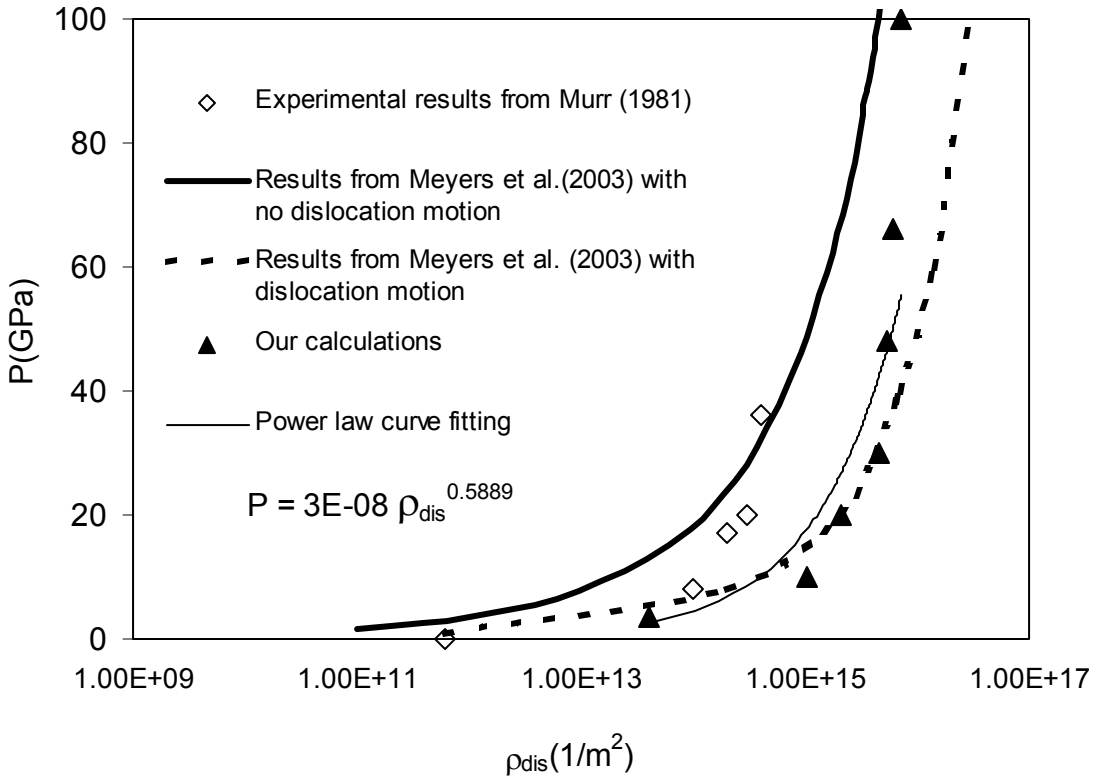

Figure. 3.12. The variation in the dislocation density with pressure.

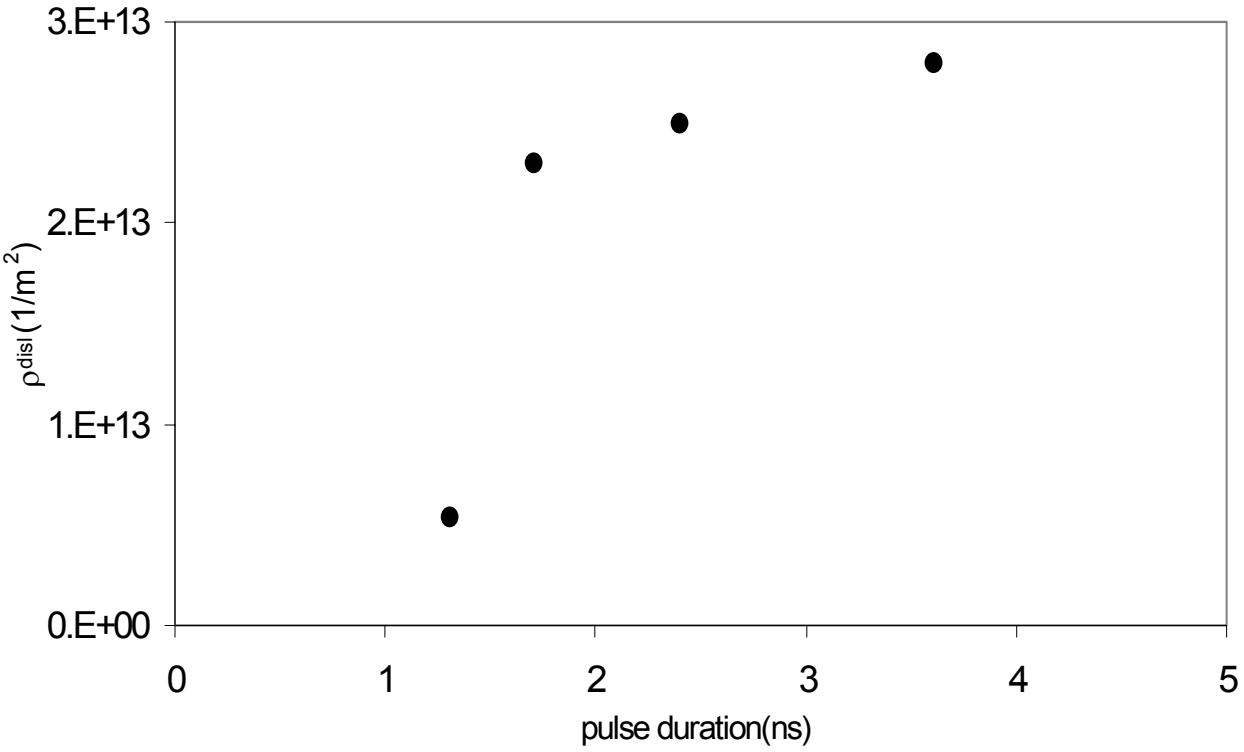

Figure. 3.13. The variation in the dislocation density with pulse duration.

Peak pressure is 9 GPa.

Table 3.1. Slip systems in fcc metals.

Slip System	Burgers Vector	Slip Plane
1	$[\bar{1}10]$	$(\bar{1}\,\bar{1}\,1)$
2	$[\bar{1}10]$	$(1\,1\,1)$
3	$[0\,1\,\bar{1}]$	$(\bar{1}11)$
4	$[0\,1\,\bar{1}]$	$(1\,1\,1)$
5	$[\bar{1}0\,\bar{1}]$	$(\bar{1}11)$
6	$[\bar{1}0\,\bar{1}]$	$(\bar{1}\,\bar{1}\,1)$
7	$[10\,\bar{1}]$	$(1\bar{1}1)$
8	$[10\,\bar{1}]$	$(1\,1\,1)$
9	$[0\bar{1}\,\bar{1}]$	$(1\bar{1}1)$
10	$[0\bar{1}\,\bar{1}]$	$(\bar{1}\,\bar{1}\,1)$
11	$[\bar{1}\,\bar{1}\,0]$	$(1\bar{1}1)$
12	$[\bar{1}\,\bar{1}\,0]$	$(\bar{1}11)$

CHAPTER 4

Multiscale Simulations of Shock-Induced Plasticity: The Role of Homogenous Nucleation

4.1 Introduction

The propagation of shock waves is the most common way to take a material to extreme conditions of pressure and temperature (Nguyen and Holmes 2004, Holian and Lomdahl 1998). Shock waves typically involve uniaxial compression at very high strain rates, which leads to plastic deformation (Holian and Lomdahl 1998, Meyers *et al.* 2003), twinning (Meyers *et al.* 2003), and phase transformations (Nguyen and Holmes 2004, Kadau *et al.* 2002, Belonoshko 1998). Plastic deformation is induced when the applied pressure exceeds a threshold value, the Hugoniot elastic limit (HEL), above which there is multiplication and motion of pre-existing dislocations as well as the nucleation of new dislocations if the stress is high enough. Several experimental techniques have been used to study the response of materials to shocks, such as plate impact, explosives and pulsed laser loading. Recently, high intensity laser facilities coupled with the X-ray diffraction technique have been used to study the dynamic deformation process in crystalline fcc materials (Meyers *et al.* 2003, Loveridge-Smith *et al*. 2001). These experiments showed that: 1) the microstructures in the recovered samples are very similar to those generated

in plate impact experiments where the pulse duration is two orders of magnitude longer; 2) large dislocation and twin densities were observed in the recovered samples; and 3) transition from one dimensional to three dimensional compression occurs in a time scale of less than a ns. Due to the high stress level in these experiments, it would be expected that homogeneous nucleation of dislocations was the dominant deformation mechanism, as suggested by several researchers (Holian and Lomdahl 1998, Smith 1958, Meyers 1978, Weertman 1981, Germann *et al.* 2004, Tanguy *et al.* 2003, Tanguy *et al*. 2004). However, most models of shock-induced plasticity do not include homogeneous dislocation nucleation as a way to relax the huge stress induced by the shock wave. Here we present a new model, based on atomistic simulations, to include homogeneous nucleation in a dislocation-dynamics/finite elements method framework of crystal plasticity. We are able to reproduce several experimental trends and make predictions about isentropic loading of materials, compared to shock loading.

Smith (1958) proposed that the lattice of a crystal responds to the uniaxial compression by nucleation of an array of infinite edge dislocations that travel supersonically with the wave front. Meyers (1978) suggested the nucleation of subsonic dislocation loops that are left behind the wave front to account for the residual plastic strain. Weertman (1981) postulated that in strong shock waves, supersonic dislocations could propagate in the material along with the generation of subsonic dislocations behind the shock front. Along with these theoretical efforts, computer simulations have been used to investigate shock phenomena at different length scales. At the atomistic scale, molecular dynamics (MD) simulations have been used to investigate shock-induced plasticity in single crystals. Holian and Lomdahl (1998) showed that the mode of

plasticity in shocked fcc single crystals changes from heterogeneous nucleation at low shock strength to homogenous nucleation of stacking faults at high shock strength. Germann *et al*. (2004) used large-scale MD simulations to investigate the dislocation structure behind the shock front in fcc single crystals. Tanguy *et al*. (2003, 2004) performed extensive MD simulations, which showed that there is a critical size of the nucleated dislocation loop, below which it becomes unstable and annihilates. Bringa *et al.* (2004, 2005) found that embedded atom method potentials can reproduce the experimental Hugoniot of single crystal copper. Current non-equilibrium MD capabilities can simulate only sub-micron spatial scales and sub-nanosecond time scales, even using the world's most-powerful parallel computers. However, most laser-induced shock experiments involve shock pulses at least a few ns long, travelling over a distance of many microns. Dislocation dynamics (DD) simulations are able to capture these time and length scales.

Shehadeh *et al*. (2005a, 2005b) have recently used multiscale dislocation dynamics plasticity simulations (Zbib and Diaz de la Rubia 2002) to study the effects of different parameters such as peak pressure, pulse duration and crystal orientation on the interaction between shock waves and dislocation sources in copper and aluminium single crystals. However, the problem of homogenous nucleation under shock loading has not been addressed in the context of DD simulations. Here we present results on the role of homogeneous dislocation nucleation on the deformation process under shock loading condition using DD simulations informed by MD simulations (see Methods).

4.2 Method

4.2.1 Multiscale dislocation dynamics plasticity (MDDP)

In the macro scale, the governing equations of MDDP are based on the representative volume element (RVE) over which the deformation field is assumed to be homogenous. The material obeys the basic laws of continuum mechanics, i.e. linear momentum balance and energy balance. In the nano-microscale, DD analyses are used to determine the plasticity of single crystals by explicit three-dimensional evaluations of dislocations motion and interaction among themselves and among other defects. In DD, dislocations are discretized into segments of mixed character. As the dislocation moves, it has to overcome internal drag, and local barriers such as the Peierls stress. The dynamics of the dislocation is governed by a "*Newtonian*" equation of motion, consisting of an inertia term, damping term, and driving force arising from short-range and long-range interactions. The momentum equation is used to generate an elastic stress wave by modifying the boundary conditions in the FE code. The elastic wave exerts a driving force on the dislocations, which in turn results in changes in the wave profile and the formation of dislocation microstructures (Shehadeh *et al.* 2005a, b). We have carried out several MDDP simulations of shocked copper single crystals with [0 0 1] orientation to compare with MD results. The simulation setup consists of a block with dimensions 0.25 μm × 0.25 μm × 1.0 μm and larger. To achieve the 1-D compression involved in shock experiments, the four sides are confined so that they can only move in the loading direction. A velocity-controlled boundary condition with piston velocity U_p and finite

linear rise time t_{rise} is applied on the upper surface to generate the shock wave. The bottom surface is fixed. A number of simulations were carried out, including (10-70) GPa shocks with 2 and 50 ps rise times, with and without dislocation sources. In the DD code, periodic boundary conditions are applied to ensure the conservation of dislocation flux across the boundaries and continuity of dislocation lines.

4.2.2 Homogeneous nucleation model

Following MD results, dislocation loops are nucleated at random positions all over the wave front when a critical value of shear stress, τ_{crit}, is achieved. This critical shear stress was taken to be 2 GPa. If this stress is changed in the range 1-3 GPa, the results are qualitatively the same. Dislocations are nucleated in all available slip planes with a probability proportional to their Schmid factor. This is similar to a criteria previously used in 2D DD dynamics simulations of deformation (Van der Giessen and Needleman, 1995). In principle, one can select a more complex stress condition, like the one presented by Li *et al*. (2002), for nano-indentation simulations. There is a second condition imposed in the DD simulations, based on numerous MD shock simulations: even if the shear stress is above the critical stress to nucleate a dislocation loop, a large initial stress along the shock direction (σ_{33}) is also required. For instance, for the EAM Cu used here (Li *et al*. 2002), the critical shear stress for loop nucleation is reached at σ_{33} ~10 GPa, but dislocation nucleation does not occur until σ_{33}~30 GPa (i.e., a compressive strain of ~12%). This large stress needed for nucleation is consistent with estimates based on nucleation of vacancy loops (Hirth and Lothe 1982).

4.2.3 Standard nucleation theory

Below we present detailed calculations of the pressure required for homogenous nucleation of prismatic dislocation loops under shocks for high *SFE* materials. These calculations are based on standard nucleation theory that gives a nucleation number. In general, the free energy of loop formation (ΔG^*) increases with increasing the size of the loops till a critical size (r^*) is reached and the loop formation becomes stable and a steady state rate nucleation process can take place according to the following relationship:

$$JVt = Vt\omega Z n_0 \exp(-\frac{\Delta G^*}{KT}) \exp(-\frac{t}{\tau}) = N \tag{4.1}$$

where J is the steady state nucleation rate $\left[number/(volume \times time)\right]$, Z is a non-equilibrium factor known as Zeldovich factor, V is the observable volume, t is the time since the onset of stressing (observable time in the experiment), τ is the rise time to establish a quasi-equilibrium distribution of embryos and it is proportional to the size of the nucleated loop ($\tau \propto r^*$), n_0 is the concentration of atom sites, ΔG^* is the free energy of formation of a critical sized loop, N is the observable number of events (dislocations sweeping a grain or a specimen) and ω is frequency factor given by:

$$\omega = \frac{8\pi r^* v}{b} \tag{4.2}$$

$$Z = \frac{1}{2}\left[(\frac{\partial^2 G}{\partial^2 x})/(2KT)\right]^{1/2} \tag{4.3}$$

where v is the Debye frequency.

For the case of a crystal under external applied stress (σ), the change in the free energy of formation neglecting the elastic energy of dislocations per unit volume is:

$$\Delta G^* = \Delta G_0{}^* - W_e \tag{4.4}$$

Where $\Delta G_0{}^*$ is the free energy of formation under zero applied stress and W_e is the external work done to nucleate the prismatic dislocation loop, and it is given as:

$$W_e = \sigma \times \pi \ r^{*2} b \tag{4.5}$$

Assuming a loops size of few lattice parameters say 2b, and combining 4.4 and 4.5 yields:

$$\Delta G^* = \Delta G_0{}^* - \sigma \times 4\pi \ b^3 \tag{4.6}$$

4.2.4 Calculation of nucleation stress under shock loading

In this section we carry out calculations to compute the stress required to homogenously nucleate dislocation loops in copper single crystal under shock loading. Based on both MD and DD simulation that have been performed, we have the following numerical values: $Z = 10^{-2}$, $V = 10^{-15} cm^3$, $t = 5 \times 10^{-11} s$, $\tau = 5 \times 10^{-12} s$, $N = 10^2$, $b = 0.30nm$, $r^* = 0.6nm$, $c = 10^{16} cm^{-3}$, $v = 10^{15} s^{-1}$, $n_0 = 10^{16}$ and $KT = 0.03 \ eV$.

Substituting these values in equation 4.1 and 4.2 yields: $\omega \sim 10^{32}, Z\omega = 10^{-2} \times 10^{33} = 10^{31}$

and from equation 4.2 $\Rightarrow J = \dfrac{N}{Vt} = \dfrac{10^2}{10^{-15} \times 5 \times 10^{-11}} \sim 10^{28}$.

As one can see the system under consideration gives a huge steady state nucleation rate. It is worth mentioning here that for bulk nucleation under normal tensile test, J has a value of ~1 which yields a value of $\dfrac{\mu}{50}$ for the nucleation stress. Therefore it is expected because of the huge increase in J that the nucleation stress will increase dramatically. Equation 4.2 can be rearranged such that:

$$(\frac{\Delta G^*}{KT}) \times \frac{t}{\tau} = \log_n (\frac{J}{n_0 \omega Z}) = log_n (\frac{10^{28}}{10^{16} \times 10^{31}}) \sim -43$$

$$(\frac{\Delta G^*}{KT}) = -43 \ , \ (\Delta G^*) = -43KT$$

This will switch the value of stress in stress calculations see 4.6 assuming that $\Delta G_0^* = 0$.

Which mean that

$$\sigma = 40 \times 0.01 \times 1.6 \times 10^{-19} / 200 \times 10^{-32} \sim 32 \text{ GPa}$$

A detailed understanding of this condition from the atomistic viewpoint is still lacking, but similar strain conditions have been observed for Lennard-Jones solids. This second condition is only relevant in the DD simulations for "long" rise-time shocks, where homogenous nucleation when triggered by the ramped shock results in higher dislocation and junction densities and smaller amount of plastic relaxation.

4.2.5 MD simulation details

The massively parallel molecular-dynamics code MDCASK (Bringa. *et al*. 2004), using domain decomposition with a combination of cells and linked lists was run on the Multi-programmatic Capability Resource (MCR) Linux cluster (11 TF, http://www.top500.org) at Lawrence Livermore National Laboratory, using 256-2048 CPU's. The embedded atom method (EAM) potential for Cu due to Mishin *et al*. (2001) was used. This potential has been fitted to experimental lattice parameter (0.3615 nm), *SFE* and ab-initio P-V curve, among other parameters. Our samples were prismatic with free surfaces along the shock direction and periodic boundary conditions (PBC) in the directions transverse to the shock wave. They were equilibrated at 5 K for several ps before applying the shock. The first nm on one side was chosen as a piston and atoms there were moved at the desired piston velocity, U_p. Using centro-symmetry parameter (CSP) filtering (Kelchner *et al.* 1998) we have been able to obtain dislocation densities at

different pressures, as a function of time, for two different rise times. Recent MD simulations (Germann *et al.*

2004, Tanguy *et al.* 2003, Tanguy *et al.* 2004) for materials with SFT much lower than the experimental SFT for copper show that: a) <001> shocks produce a set of partial loops that grow, following the shock front, as in Smith model (Smith 1958); b) <111> shocks produce dislocations that nucleate at the shock front, as in Meyers model (Meyers 1978). Our MD simulations for shocks in EAM Cu which has been fitted to the experimental *SFE* are similar, but display a more mixed behavior, including the nucleation of some full dislocations for <100> shocks.

4.3 Results and Discussion

Snapshots of MDDP simulations of homogenous dislocation nucleation for a wave launched into copper single crystal at 35 GPa with a 50 ps rise time are shown in figure 4.1. As the wave travels through the material new loops are nucleated while the previously nucleated ones grow quickly behind the front. The loops continue to form at the wave front while relaxation of the grown dislocation loops takes place, and dislocation-dislocation interactions become dominant leading to the development of a three dimensional pattern of intersecting loops in all available {111} slip planes with large numbers of jogs and junctions. Figure 4.2 shows MD simulations of two shocks (sub-ps rise time) launched at 21GPa and 48 GPa crossing a sample with one pre-existing dislocation loop that acts as a dislocation source. These snapshots were taken after ~50 ps and show only atoms belonging to dislocations, for a sample size of 0.07x0.07x0.21 μm^3

(200x200x600 a_o^3, where a_o is the lattice parameter of copper). In the case of the 21 GPa shock wave, which is below the threshold for homogeneous nucleation, the pre-existing loop is "activated" and the growing dislocation density is entirely due to this activation process. On the other hand, when the shock is launched at 48 GPa, above the homogenous nucleation threshold of ~30 GPa, we observe that the density of dislocations is immense, and the homogenous nucleation mechanism overwhelms any dislocation production from the pre-existing source for shocks with short rise time.

From MD and MDDP calculations at several pressures we observe that: a) the dislocation density saturates at very high dislocation densities and b) the value of this saturation density increases with pressure. Dislocation saturation has been seen in previous MD simulations as well (Bringa *et al.* 2005), and is a result of I) relaxation of the material as dislocations are produced and grow, leading to a decreased driving force for nucleation/multiplication of dislocations and II) formation of junctions that impede dislocation multiplication. The dislocation density at different pressure using DD, MD calculations and the predictions of the semi-analytic model of Meyers *et al*. (2003) are shown in figure 4.3. While the calculated dislocation density using DD is higher than that from the analytic model by about an order of magnitude (for pressures greater than 40 GPa), it is one order of magnitude lower than the prediction of MD calculations. We note that the MD result using a centro-symmetry parameter (Kelchner *et al.* 1998) filtering (see Methods) which allows analysis of large datasets, is only a rough upper limit on dislocation motion. More accurate calculations, analyzing individual atomic positions in small volumes behind the shock front, gave dislocation densities smaller by a factor of 3 compared to that method.

For an fcc crystal compressed along the <001> direction the shear stress is defined as $\tau=0.5[\sigma_{33}-0.5(\sigma_{11}+\sigma_{22})]$, where σ_{33} is the stress in the loading direction, and σ_{11} and σ_{22} are the stresses in the lateral directions. Therefore, if $\sigma_{33}\sim\sigma_{11}\sim\sigma_{22}$, the shear stress is zero, as in a fluid, and this state can be approximately described as "hydrostatic", with a 3D strain (compression). On the other hand, if $\sigma_{33}>>\sigma_{11}\sim\sigma_{22}$, the shear stress can be large, and the strain is "uniaxial", or "1D". For a shock wave launched at 35 GPa peak pressure, a volumetric strain of about 15% was induced in copper single crystal. The plastic strain generated by loop nucleation and growth results in shear stress relaxation that transforms the state of stress from "uniaxial" to almost "hydrostatic" as shown in figure 4.4a. Stress relaxation occurs by means of plastic deformation mechanisms leading to a transition from 1D strain to 3D compression as depicted in figure 4.4b. This relaxation process occurred over less than 100 ps, as suggested in previous experiments (Loveridge-Smith *et al.* 2001) due to the extremely high rate of dislocation generation. MD simulations however, show a rapid decrease in dislocation activity due to the formation of junctions, leading to only a partial transition from 1D to 3D before dislocation activity largely stops. The lack of full 3D relaxation in MD is also consistent with the larger dislocation density as compared to DD. In MD simulations, the initial velocity of nucleated dislocations is close to the sound velocity, much faster than in DD simulations. This leads to an "early" fast multiplication rate, and fast junction formation, which reduces the mobility at longer times compared to DD calculations. If dislocation multiplication rate and mobility were changed in our DD simulations to match that in the MD simulations, the MD and DD relaxation rates would be closer, and full 3D relaxation may not be reached.

The process of dislocation nucleation, growth and motion is dissipative. High percentage of plastic work resulting from dislocation activities is converted into heat leading to abrupt increase in temperature. In MDDP model, the increase in temperature is accounted for from the energy equation (3.2). In the current calculations however, the heat conductivity term is neglected. Therefore, the adiabatic temperature increase can be expressed as:

$$dT = \frac{\mathrm{S.d}\varepsilon}{\rho\ \mathrm{C_v}} \tag{4.7}$$

The temperature and the effective plastic strain histories in a slice within a copper sample shocked to 35 GPa is presented in figure 4.5a. The calculations show a rapid increase in temperature in the first few ps. This corresponds to the time at which the homogenous nucleation dominates the deformation process. As the time passes, the rate of temperature time evolution decreases and eventually diminishes leading temperature to saturate at a maximum value of about 350 K. The saturation in temperature is attributed to the relaxation process that takes place during which dislocation-dislocation interaction dominates the dislocation interaction processes. The adiabatic calculations of temperature increase at different pressure using DD and MD show a very good agreement between the two methods as can be seen in figure 4.5b.

As the dynamics of dislocations under shock loading is of Newtonian type, it is expected that the dislocation relaxation time, which is related to the ratio (m_e/B) increases with increasing this mass-damping ratio. In DD simulation we carried out calculation of the relaxation time at different shock pressures as depicted in figure 4.6. These results how that as the peak pressure increases, the time required for the crystal to

relax (1D→3D) decreases. This is mainly attributed to the increase in the rate of dislocation nucleation with pressure. Another thought of looking at the relationship between relaxation time and pressure is from the first order approximation for relaxation in creep process which relates the saturation density and the rate of dislocation generation such that; $\tau_{relax} = \rho_{sat} / \rho^{\bullet}$. Our calculations show that both ρ_{sat} and $\rho^{\bullet}$ increase, however, their ratio which gives τ_{relax} decreases and this is in agreement with figure 4.6.

Shock rise time is one of the most important parameters in specifying pulse shapes. The importance of this parameter under shock loading comes about as it is inversely related to peak pressure. Generally speaking, as the peak pressure increases the rise time decreases, therefore, the knowledge of the rise time is extremely important as it includes information on the extremity of the shock. In order to investigate the effect of rise time on the deformation process, we carried our DD and MD simulation for both perfect and real copper crystals.

The rate of dislocation nucleation in copper crystal shocked to a peak pressure of 35 GPa at three different rise times of 5, 25 and 50 ps is shown in figure 4.7. From these simulations we observe the following:

1- The onset of nucleation takes place first in the 5 ps sample followed by the 25 and the 50 ps samples respectively. This is obviously because the width of the wave front is inversely proportional to shock rise time and therefore the nucleation pressure is reached in shorter rise time shocks first.

2- For short rise time, the rate of dislocation multiplication is higher. After the dislocation loops are nucleated at the wave front, they start to grow at rates that

are proportional to the increment of pressure at each time step. Apparently, this increment of pressure is the largest for the shortest rise time.

3- The rate of dislocation density saturates to a value that is also inversely proportional to shock rise. This is also attributed to the reasons we mentioned above.

Real single crystals have pre-existing dislocation sources, which are typically assumed to play the dominant role in shock-induced plasticity. Recent MD simulations have explored the role of prismatic loops acting as dislocation sources (Bringa *et al.* 2005). The simulations found that: a) for "short" rise time the dislocation density for a system with/without sources was the same; b) for a 50 ps rise time the dislocation density near the sources was ~3 times lower, due to stress relaxation induced by dislocation multiplication during the ramp of the stress wave. We have carried out DD simulations where in addition to homogeneous nucleation we had embedded dislocation sources. As in the MD simulations, we observe two main regions of dislocation activity, as shown in figure. 4.1. Homogenous dislocation dominates the deformation process before the leading part of the ramp wave hits the dislocation sources. A mixed mode of deformation appears when the critical shear stress for source activation is reached. In this region a few sparse dislocation lines emitted from the embedded sources interacting with the already nucleated loops hamper the process of homogenous nucleation in the location where they are located. The time evolution of dislocation density in a crystal with pre-existing sources is shown in figure 4.8. Note that this is the average over both regions mentioned above, and the difference in dislocation density between those two regions gets mostly washed out in figure 4.8. It is clear from figures 4.1 and 4.8 that homogeneous nucleation

is the mechanism that dominates plastic deformation under shock loading conditions for these relatively short rise times, because the source activation mechanism has a relatively small effect on the overall evolution of the dislocation density. On the other hand, for 50 ps rise time the dislocation density near the sources is much lower, as found in the MD simulations.

Shock-induced dislocation densities are generally inferred from recovered samples that have experienced significant thermal processing and stress unloading. The times involved in these processes are prohibitive even for DD simulations. However, one can relax the final state of our simulations to mimic the recovery process. We find that the deformation microstructure of a relatively relaxed sample shows uniform features consisting of weak dislocation cells. This compares well with experimental results (Meyers *et al.* 2003) as can be seen in figure 4.9. MD simulations of shock induced twinning in copper show that twinning proceeds by production of partial dislocations in adjacent planes, as predicted earlier by Zaretski (1995). Once three partial dislocations are nucleated, a twin forms and can grow rapidly. The twinning threshold found in the MD simulations also agrees with the experimental estimates (Schneider *et al.* 2004). The probability of twin formation is therefore directly proportional to the dislocation density: at a given peak pressure above the twinning threshold, one would expect to see more twins for higher dislocation density during loading. Given that longer rise times imply lower dislocation densities we would also expect less twinning. New, preliminary, experimental results using isentropic loading seem to confirm our average spacing and line senses of the dislocations.

4.4 Conclusions

In summary we have carried out the first MDDP simulations of shock loading of single crystals at large stress taking into account homogeneous nucleation as predicted by atomistic simulations. Shock waves with strength ranging from 30 to 60 GPa were launched in copper single crystals resulting in the nucleation of large number of dislocation loops at the wave front. Once the dislocation loops are nucleated, they grow in all directions in their slip planes forming a three dimensional microstructure consisting of dislocation entanglements and weak cellular structures. These simulations show a number of novel features:

(a) The material is rapidly relaxed to a "hydrostatic", shear-free state. This 3D relaxation has been seen in recent experiments (Loveridge-Smith *et al.* 2003). Current MD simulations using sub-ps shock rise times achieve only a partial 3D relaxation due to the fact that dislocation rate production in the MD simulations is somewhat higher that in these DD simulations, mostly due to differences in the early dislocation mobility at large applied stress. Higher rates lead to more dislocation junctions and obstacles, which make achieving a fully relaxed 3D state with MD simulations more difficult. However, MD simulations with 50 ps shock rise-time do achieve a ~3D state, but at somewhat longer times than the DD simulations.

(b) In agreement with recent MD simulations, the initial micro-structure of the copper single crystal is not important for short rise time shocks (up to few ps), above the homogeneous nucleation threshold, since the dislocation density due to homogeneous nucleation overwhelms the density due to multiplication of pre-existing dislocation

sources. This may be true for other materials if dislocation hardening is the dominant mechanism.

(c) Also in agreement with recent MD simulations, the initial microstructure is extremely important for long rise times. Activation of pre-existing dislocation sources will relax the material impeding significant dislocation nucleation. Dislocation and twin densities would be much lower for long-rise time pulses, in agreement with recent experiments (McNaney *et al*. 2005).

In this paper we explore a new, powerful, model for shock conditions that can be also simulated with atomistic simulations. The degree of agreement with the atomistic simulations is promising and opens up the possibility of confidently simulating shocks and ramped compression waves that are impossible to model with atomistic methods, even with the current most powerful parallel computers. For instance, a significant number of experiments actually deal with "long" rise time pulses of a few ns. These are the kind of pulses used for isentropic compression experiments (ICE), and our model could be useful to plan future experiments at the National Ignition Facility (NIF) and the Z-machine, where ICE loading will become routine (Remington *et al.* 2004*,* Remington *et al*. 2005, Cauble *et al*. 2002).

References

Belonoshko, A. B**.**, 1997, *Science* **275**, 955.

Bringa E.M. *et al.*, 2005, submitted to Nature.

Bringa, E.M., Cazamias, J. U., Erhart, P., Stölken, J., Tanushev, N., Wirth, B. D., Rudd, R. E., and Catural, M. J., 2004, *J. App. Phys.* **96**, 3793.

Cauble, R. Reisman, D. B. Asay, J. R. Hall, Knudson, C. A. Hemsing, M. D. Goforth, J. H., and Tasker, *D. G.* 2002, *J. Phys. Condens. Matter* **14**, 10821.

Germann, T.C., Tanguy, D., Holian, B. L., Lomdahl, P. S., Mareschal, M., and Ravelo, R., 2004, *Met. Mat. Trans.*, **35 A,** 2609.

Hirth, J. P, Lothe, J., *Theory of dislocations* (Wiley, New York, ed. 2, 1982), and J.P. Hirth, private communication.

Holian, L., and Lomdahl, P. S., 1998, *Science* **280**, 2085.

Kadau, K., Germann, T. C., Lomdahl, P. S., and Holian, B. L., 2002, *Science* **296**, 1681.

Kelchner, C.L., Plimpton, S.J., and Hamilton, J.C., 1998, *Phys. Rev. B* **58**, 11085.

Li, J., Van Vliet, K. J., Zhu, T., Yip, S., and Suresh, S., 2002, *Nature* **418**, 307.

Loveridge-Smith, A., Allen, A., Belak, J., Boehly, T., Hauer, A., Holian, B., Kalantar, D., Kyrala, G., Lee, R.W., Lomdahl, P., Meyers, M. A., Paisley, D., Pollaine, S., Remington, B., Swift, D. C., Weber, S., and Wark, J. S., 2001, *Phys. Rev.Lett*., **86(11)**, 2349.

McNaney, J.M. *et al*., 2005, to be submitted.

Meyers, M. A., 1978, *Scripta Met*., **12**, 21.

Meyers, M. A., Gregori, F., Kad, B. K., Schneider, M. S., Kalantar, D. H., Remington, B. A., Ravichandran G., Boehly, T., and Wark, J., 2003, *Acta Materialia*, **51(5),** 1211.

Mishin Y., Mehl, M. J., Papaconstantopoulos, D. A., Voter, A. F., and Kress, J. D. 2001, *Phys. Rev.* B **63**, 224106.

Nguyen, J. H., and Holmes, N. C., 2004, *Nature* **427**, 339.

Remington, B.A., Bazan, G., Belak, J., Bringa, E., Caturla, M., Colvin, J.D., Edwards, M.J., Glendinning, S.G., Ivanov, D.S., Kad, B., Kalantar, D.H.; Kumar, M., Lasinski, B.F., Lorenz, K.T., McNaney, J.M., Meyerhofer, D.D., Meyers, M.A., Pollaine, S.M., Rowley, D., Schneider, M., Stolken, J.S., Wark, J.S., Weber, S.V., Wolfer, W.G., Yaakobi, B., and Zhigilei, L. V., 2004, *Met. Mat. Trans. A* **35**, 2587.

Remington, B.A. *et al*., 2005, *Astrophysics and Space Science* **298**, No. 1-2 (July), in press.

Schneider, M.S., Kad, B., K., Gregori, F., Kalantar, D., H., Remongton, B. A., And Meyers, M. A., 2004, *Explosion, Shock Wave and Hyper Velocity Phenomena in Materials*. Materials Science Forum 465-466: 27-34 2004, in press.

Shehadeh , M.A., Zbib, H.M., and Diaz de la Rubia, T., 2005a, *Int. J. Plasticity*, in press.

Shehadeh, M.A., Zbib, H.M., and Diaz de la Rubia, T., 2005b, *Phil. Mag*., in press.

Smith, C. S., 1958, *Trans. Met. Soc. AIME*. **212**, 574.

Tanguy, D., Mareschal, M., Lomdahl, P. S., Holian, B. L., Germann, T. C., and Ravelo, R., 2003, *Phys. Rev. B,* **68,** 144111.

Tanguy, D., Mareschal, M., Germann, T. C., Holian, B. L., Lomdahl, P. S., and Ravelo, R., 2004, *Mat. Sci. Eng.* **387-389***,* 262.

Van der Giessen, E,. and Needleman, 1995, *Modelling Simul. Mater. Sci. Eng.* **3**, 689-735.

Weertman, J., *Shock Waves and high Strain Rate Phenomena in Metals*, edited by M. Meyers, L.E., and Murr (Plenum, NewYork), pp. 469-486 (1981).

Zaretsky, E., 1995, *J. Appl. Phys.* **78**, 3740.

Zbib, H.M., & Diaz de la Rubia, T.D., 2002, *Int. J. Plasticity*. **18**, 1133.

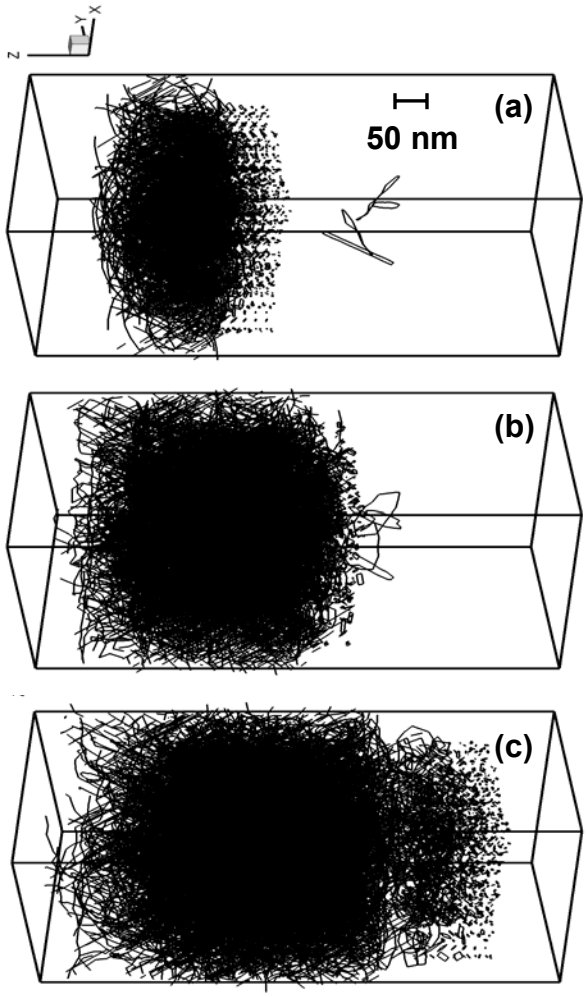

Figure 4.1. MDDP simulation of a 35 GPa, 50 ps rise time shock in copper. Sample contains few pre-existing loops, which interact with the homogeneous nucleation front. (a) 67 ps, (b) 90 ps, and (c) 122 ps. Shock front moves from left to right of the viewer.

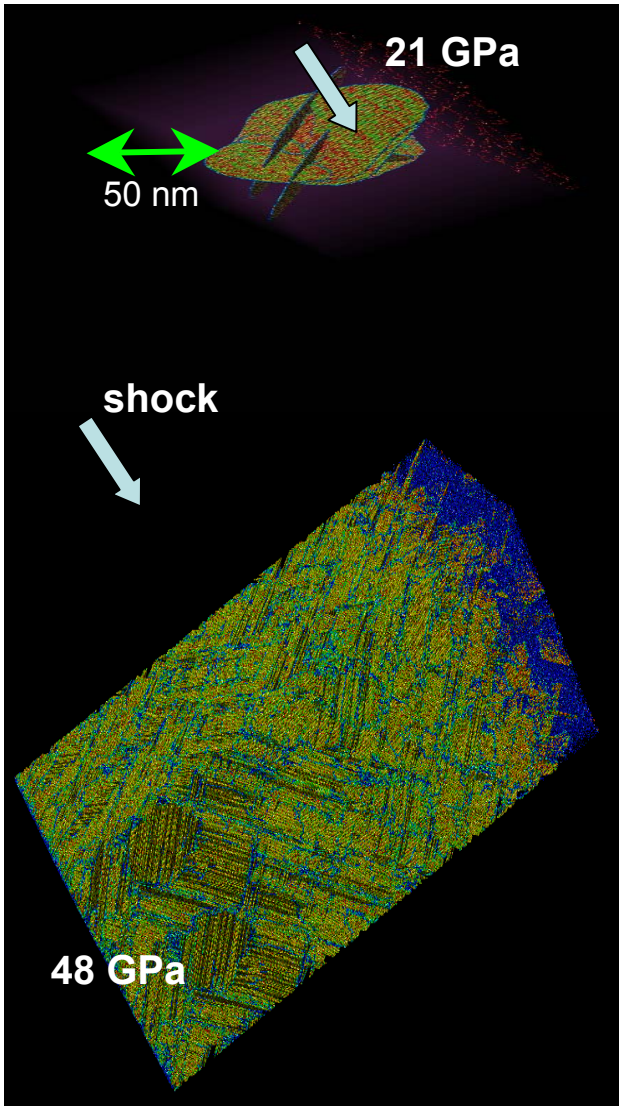

Figure 4.2. MD simulations of shocked copper, below (21 GPa) and above (48 GPa) the homogeneous nucleation threshold (30 GPa). Sample contains one pre-existing dislocation loop, which interacts with the homogeneous nucleation front.

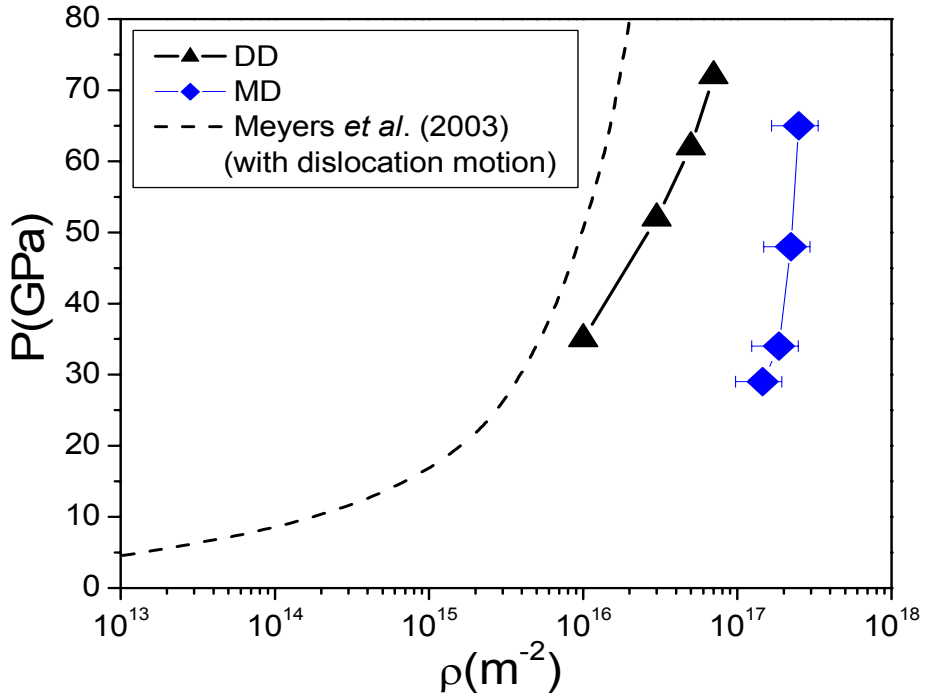

Figure 4.3. Variation of the dislocation density, ρ, with shock wave pressure. DD simulations used a 5 ps rise time.

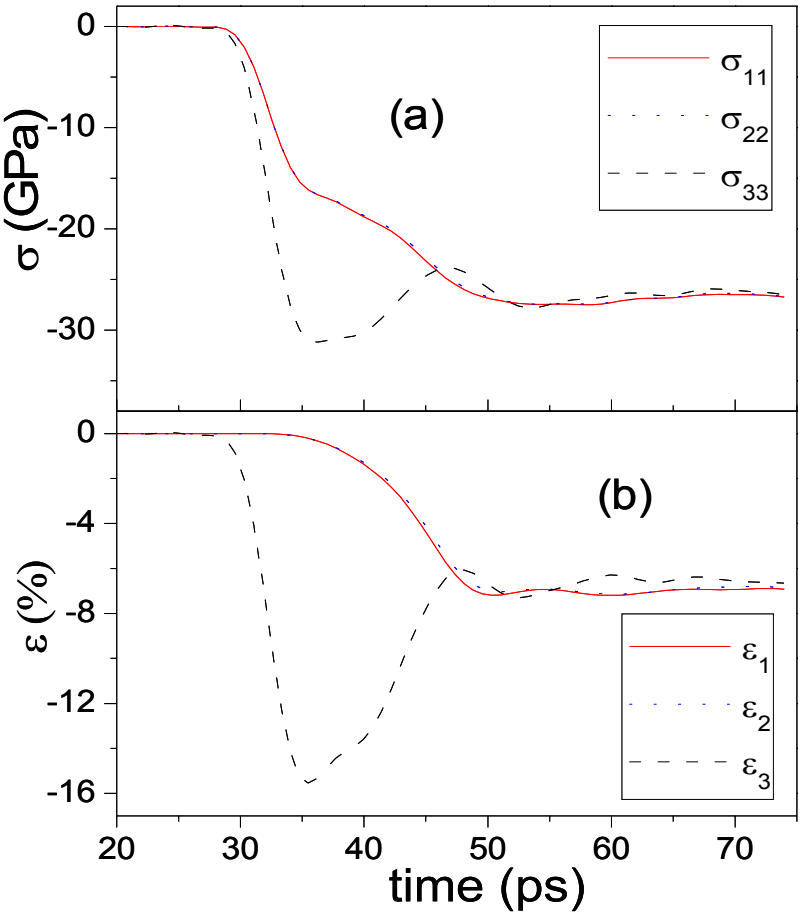

Figure 4.4. DD simulations of a 35 GPa shock, 5 ps rise time, showing plastic relaxation. (a) stress history in a slice where the dislocation is first nucleated showing fluid-like like behaviour (shear stress~0) at "long" times. (b) Strain history showing 1D → 3D transition.

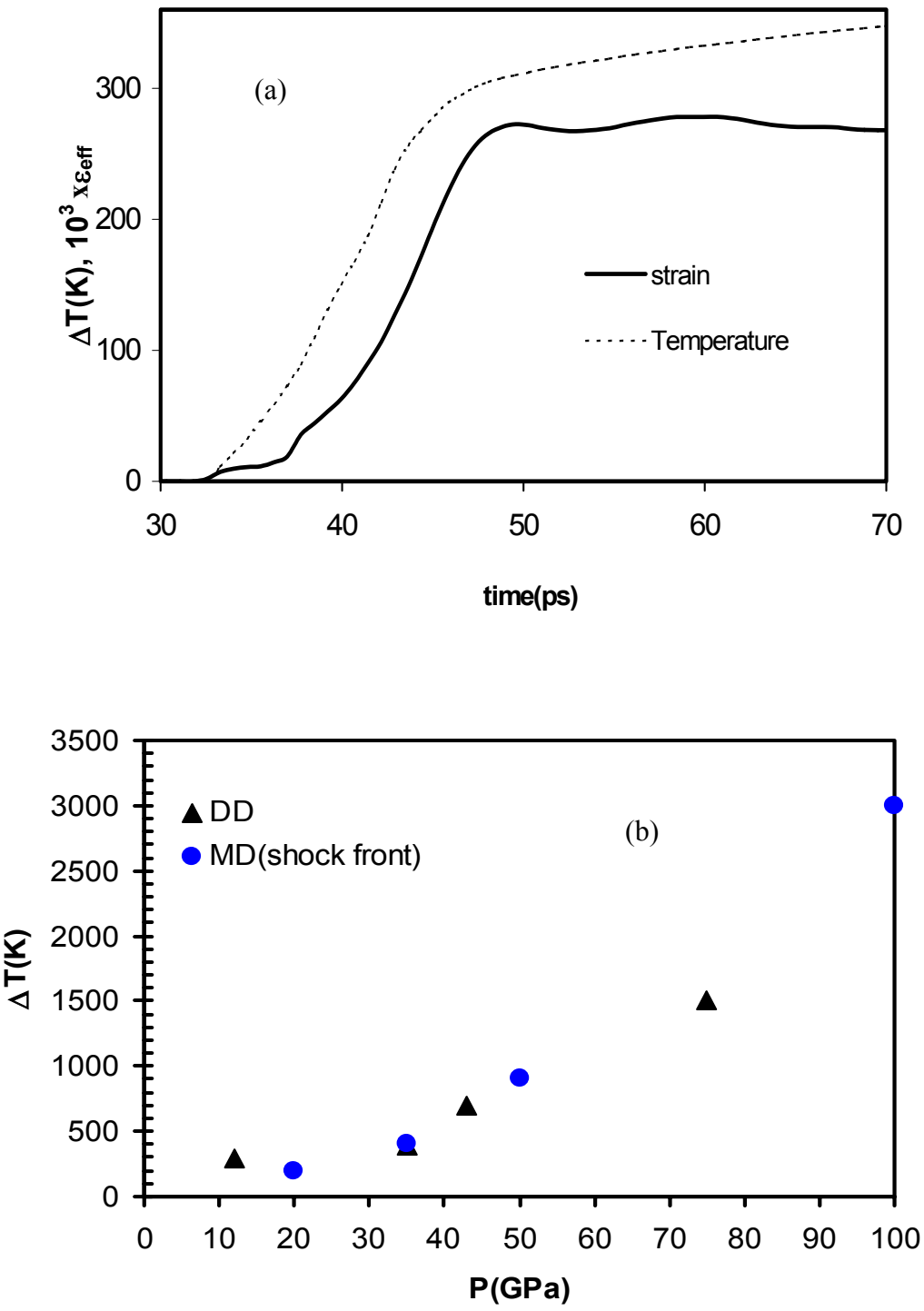

Figure 4.5. (a) Adiabatic temperature increase and effective plastic strain calculations in a thin slice in copper single crystal using MDDP model (b) Variation of the local temperature increase dislocation density, ΔT, with shock wave pressure. DD simulations used a 5 ps rise time.

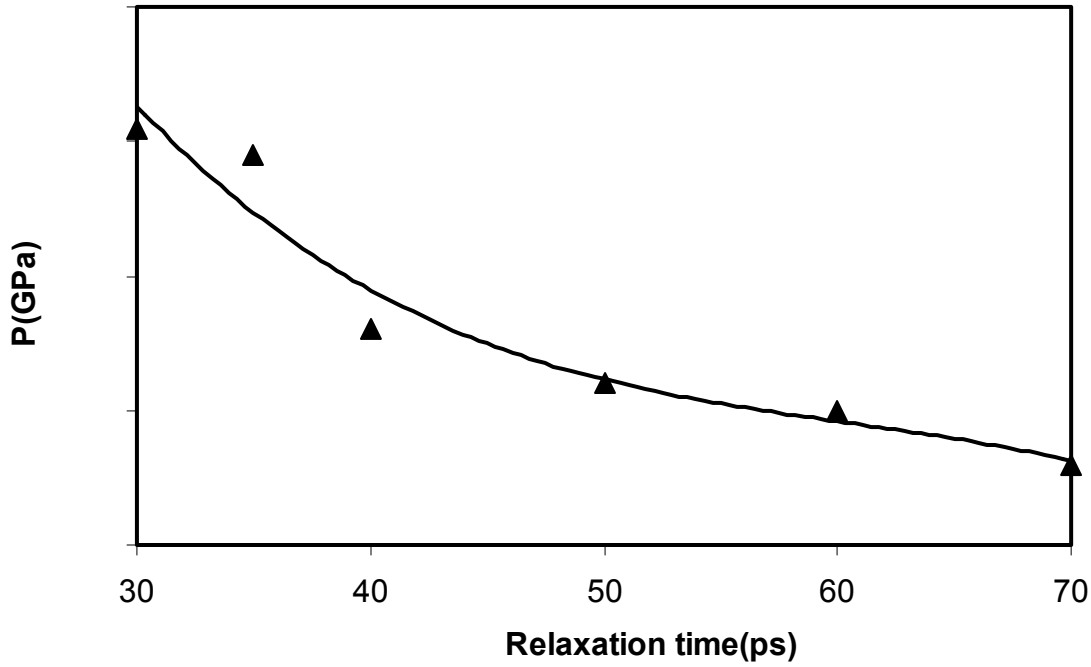

Figure 4.6. Variation in relaxation time with pressure in copper single crystal. During this time, 1D → 3D transition occurs

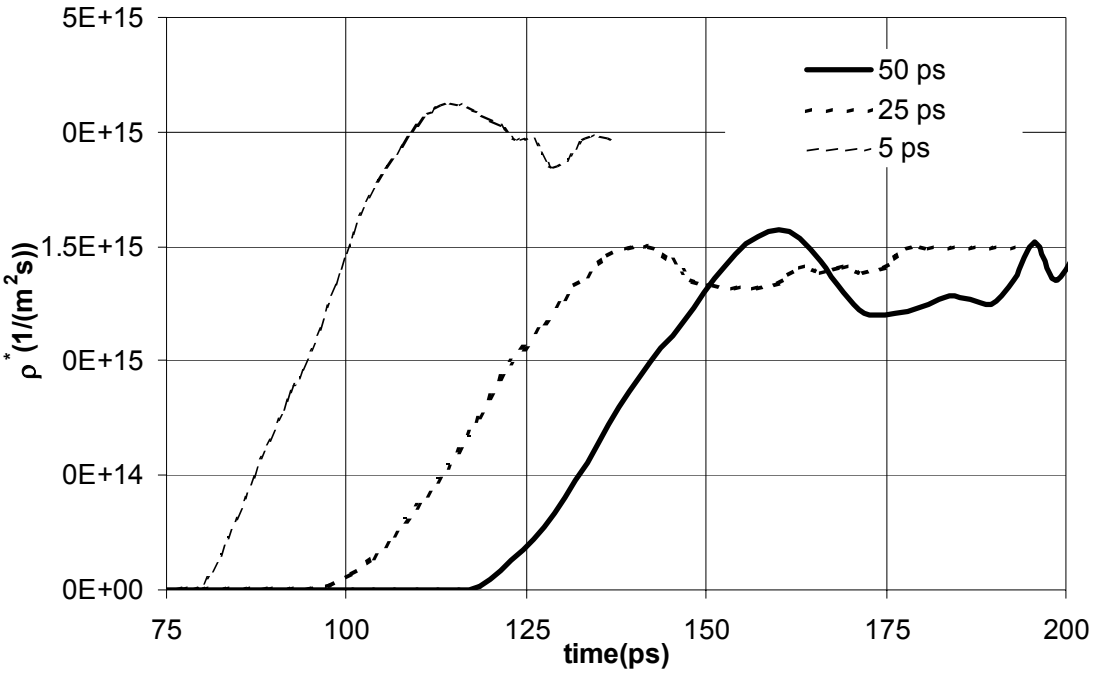

Figure 4.7. DD calculations of the effect of shock rise time of the rate of dislocation nucleation and growth in copper single crystal shocked to a peak pressure of 35GPa.

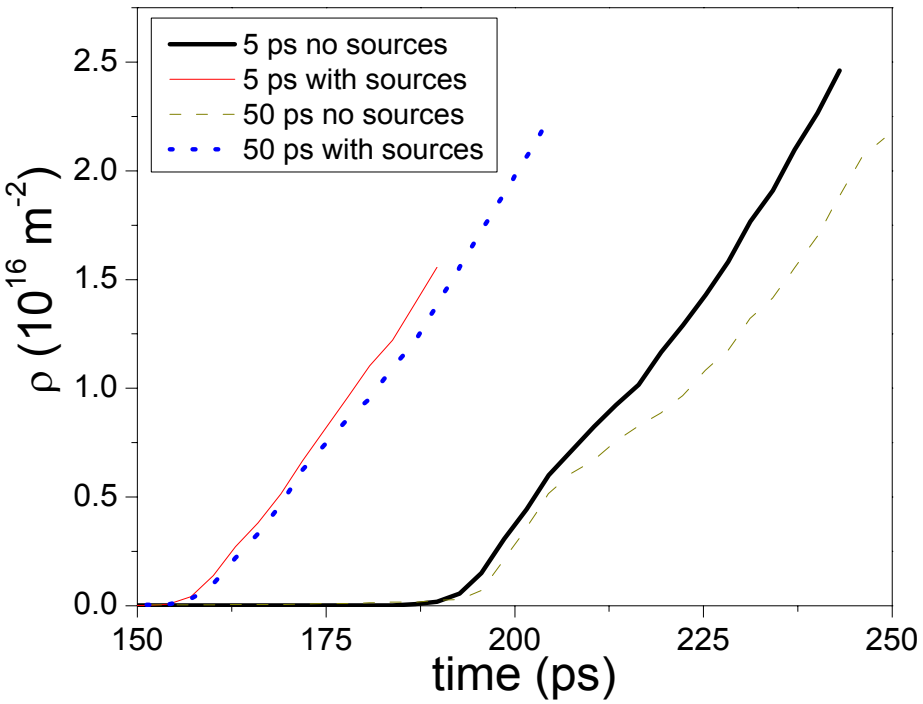

Figure 4.8. Average dislocation density from MDDP simulations of 35 GPa shocks, 5 ps and 50 ps rise time. A short rise time does not give a large difference between samples with or without pre-existing sources, while a longer rise time does show a larger effect.

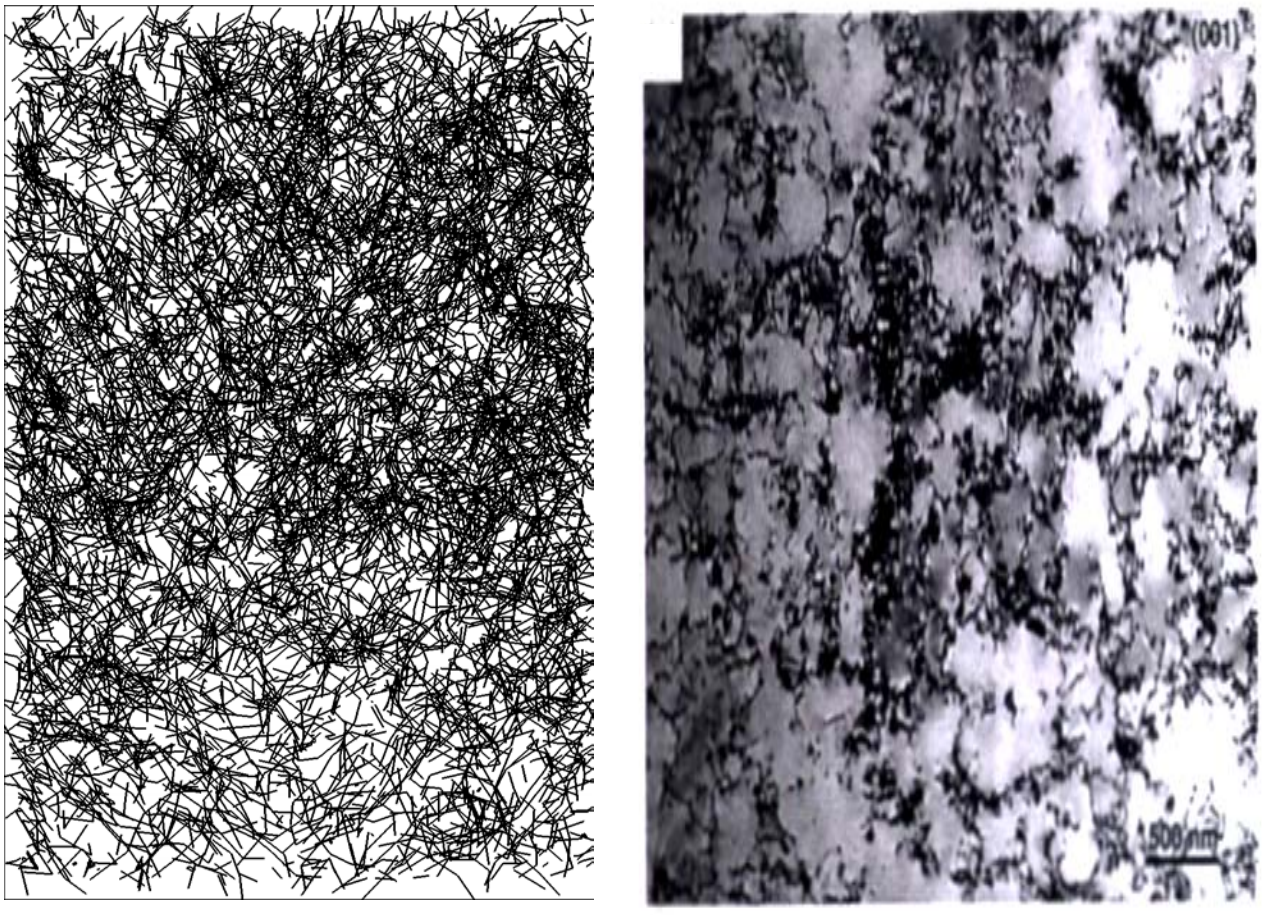

(a) (b)

Figure 4.9. Dislocation microstructure in copper (a) DD results (b) Laser shock experiment by Meyers et al (2003).

CHAPTER 5

Numerical and Strain Localization Issues in Modeling High Strain Rate Shock Loading

5.1 Introduction

Most of the work that has been carried out in the area of shock compression of solids is experimental in nature. This can be attributed to the transient nature of shocks, complexities of geometries and the nonlinearities of the material behavior (Zukas and Scheffler 2000), which make the numerical simulations of shock-induced deformation quite complex. However, there has been a considerable progress in studying the dynamic response of materials using finite element (FE), finite difference, molecular dynamics, dislocation dynamics and multiscale simulations. In this chapter, we address several numerical issues that may enhance numerical modeling of shock-induced plasticity. On top of these issues is the effect of FE boundary conditions on wave profile characteristics and dislocation density.

The implementation of a relevant boundary condition is of great most importance for successful modeling of the material response under different loading condition. In particular, the assumption of periodic materials is commonly used in the area of micromechanics (Kistensson *et al.* 2003). Based on that assumption, periodic boundary

condition is commonly imposed in the micro scale system as in the case of MD and DD simulations.

As mentioned in chapter 1, planar shock waves are generated when the material is compressed uniaxially by loading of half space with lateral dimensions extending to infinity " No edge effects". It is of great importance to minimize these edge effects in the numerical modeling. Periodic boundary condition has been traditionally used in MD simulations of shock waves. It has been proven that this type of boundary conditions minimizes the edge effects of the simulated sample (Holian *et al.* 1998) and therefore, the uniaxial compression of shocks can be achieved. In MDDP simulations, the uniaxial compression has been achieved using confined boundary condition by restricting the sides of the computational cell to move in the wave propagation direction.

In multiscale modeling, different boundary conditions maybe used on different length scale models. In MDDP simulations of shocks, periodic boundary condition was used in DD while confined boundary condition was used in FE analysis. The use of different boundary conditions in MDDP has raised a question of inconsistencies between DD and FE results. Furthermore, numerical simulations by means of FE method are known to lead to mesh sensitivity when using classical continuum mechanics models (Liu *et al.* 2005).

It is commonly known that high strain rate deformation leads to strain localization, which is considered to be a precursor to failure. In the case of large deformation (>20%), slip rotation is expected to occur in order to accommodate the imposed shear strain (Meyers *et al.* 2003). Localized deformation can be in the form of heavy deformation bands coincident with the slip planes (Mogileviskii and Bushnev

1990, Rivas *et al*. 1995). The thickness and orientation of these bands generally depend on material parameters, geometry, boundary condition and loading history (Liu 2005). The analysis of lattice rotation therefore, is of great importance for developing better understanding of the deformation mechanisms under extreme conditions. In this work the following issues has been addresses:

1- The effect of using different boundary condition on wave profile characteristics. This issue is addressed by carrying out MDDP simulations using free, confined and periodic boundary conditions in the FE code.

2- The effect of loading history on the convergence of the wave profile. This issue is addressed by performing mesh sensitivity analysis using both steep and ramp loading histories.

3- The effect of slip rotation of strain localization. Here preliminary results are presented.

5.2 Method

In the current analysis, MDDP model discussed in sections 2.2 and 3.2 is used. Here we present the modifications that have been done to implement 1) periodic boundary condition in FE code. 2) slip rotation in DD.

5.2.1 Dynamic FE formulation:

The general form of the dynamic FE code is:

$$[M]\{\ddot{U}\}+[C]\{\dot{U}\}+[K]\{U\}=\{f\} \tag{5.1}$$

where $[M]$ is the mass matrix, $[C]$ is the damping matrix, $[K]$ is the stiffness matrix, $\{U\}$is the nodal displacement and $\{f\}$ is the force vector which includes contributions from the externally applied force, body forces, and dislocation image stresses. In the dynamic FE, forward explicit integration scheme is used to solve for the displacement vector $\{U\}$ such that:

$$U_i^{k+1} = -U_i^{k-1} + 2 \times U_i^k - \delta t^2 \frac{K_i}{M_i} U_i^k + \frac{f_i \times \delta t^2}{M_i} + \frac{Dfact}{(1 + Dfact)} U_i^{k-1} \tag{5.2}$$

where, $Dfact = \dfrac{C_i \delta t}{2M_i}$

5.2.2 Implementation of periodic boundary condition

The implementation of the periodic boundary condition is based on the idea of master and slave nodes assumption: the displacement of a node on one side "slave" is linearly dependent on the displacement of a node on the opposite side "master" of the computational cell. This dependency of displacements leads to a reduction in the degrees of freedom in the FE model. The idea of master-slave nodes is illustrated in figure 5.1 that shows a 2D cell with ***a*** denoting the master node and ***b*** denoting the slave node. Using the periodicity assumption for the nodal displacement and force yields:

$$U_i^b = U_i^a \qquad i=1, 2, \tag{5.3}$$

$$f_i^b = f_i^a \qquad i=1, 2, \tag{5.4}$$

By combining equations (5.3) and (5.4) with (5.2), the nodal displacement for the master and the slave nodes can be expressed as:

$$U^{a}{}_{i}^{k+1} = U^{b}{}_{i}^{k+1} = -U^{a}{}_{i}^{k-1} + 2\times U^{a}{}_{i}^{k} - \frac{1}{2}\delta t^{2}\left(\frac{K^{a}{}_{i}}{M^{a}{}_{i}} + \frac{K^{b}{}_{i}}{M^{b}{}_{i}}\right)U^{a}{}_{i}^{k} + \frac{1}{2}\left(\frac{Dfact^{a}}{(1+Dfact^{a})} + \frac{Dfact^{b}}{(1+Dfact^{b})}\right)U_{i}^{k-1} \tag{5.5}$$

In using computer program, it is necessary to specify the slave and the master nodes (Soriano and Nunes 1995).

5.2.3 Computation of slip rotation

In DD, equation (2.3) applies to every infinitesimal length along the dislocation line. In order to solve this equation for any arbitrary shape, the dislocation curve may be discretized into a set of dislocation segments. Then the velocity vector field over each segment may be assumed to be linear and, therefore, the problem is reduced to finding the velocity of the nodes connecting these segments. The motion of each dislocation segment contributes to the overall plastic rotation via the relation:

$$W^{p} = \sum_{i=1}^{N} \frac{l_i v_{gi}}{2V}\left(n_i \otimes b_i - b_i \otimes n_i\right) \tag{5.6}$$

$$\dot{n} = \omega\ n \quad , \qquad \omega = W\text{-}W^{p} \tag{5.7}$$

where W^{p} is the plastic spin, l_i is the dislocation segment length, v_{gi} is the dislocation glide velocity, n_i is a unit normal to the slip plane, $\dot{n}$ is the unit normal rotation, ω is the spin of the microstructure and is given as the difference between the material spin W and the plastic spin W^{p}, V is the volume (RVE), and N is the total number of dislocations segments within a given element. A similar relation as the one given in equation. (5.7) is used to account for the burgers vector rotation as well. In DD analysis, the dislocation

lines are sorted in each sub cell to account for the elemental value of W^p. The computation of slip rotation is carried out in each sub cell as within MDDP as follows:

1- At each time step, W^p in each sub-cell is calculated.

2- In fcc crystals, there are 12 possible slip systems as a combination of 4 possible slip planes and 3 possible slip directions. In DD we loop over all the dislocation segments in each sub cell to find their glide planes and directions. A maximum of 8 possible slip systems maybe present in each sub cell. Equation 5.7 is then used to update both *n* and *b* such that:

$$n^{n+1} = n^n + \omega^n n \delta t \tag{5.8}$$

5.2.4 Loading history and mesh sensitivity analysis

Shock waves by definition are steep discontinuities that take the material from its ambient condition to its high-pressure value. This abrupt change in pressure is usually considered to be valid in fluids; therefore, the hydrodynamic treatment of shocks is used there. In solid anisotropic materials however, steep shock front cannot be achieved; the wave peak pressure is achieved over a period equals the rise time. In chapter 4, we investigated the effect of rise time on the interaction between dislocations and sock waves. Here we focus our attention on the effect of shock rise time on the convergence of the wave profile by performing mesh sensitivity analysis using two types of loading histories:

I- Steep wave with zero rise time, where the loading condition can be expressed as:

$$\begin{aligned} u_z(t) &= -v_p t \qquad 0 \le t \le t^* \\ u_z(t) &= 0 \end{aligned} \tag{5.9}$$

Taking the derivative yields a constant velocity history $U_p(t)$ during the rise time such that:

$$U_p(t) = -v_p \tag{5.10}$$

II- Ramp wave with finite rise time

$$\begin{aligned} u_z(t) &= -a_p t^2 && 0 \le t \le t_{rise} \\ u_z(t) &= -a_p t_{rise}^{\ 2} - v_{p\,max}\left(t - t_{rise}\right) && t_{rise} \le t \le t^* \end{aligned} \tag{5.11}$$

Taking the derivative yields a linear velocity history $U_p(t)$ during the rise time such that:

$$U_p(t) = -2a_p t \qquad 0 \le t \le t_{rise} \tag{5.12}$$

5.3 Simulation Cell Setup and Loading Conditions

After the implementation of periodic boundary condition in the FE code, the boundary of the simulation cell sides can be free, confined or periodic. For the periodic boundary condition, three different ways of matching slave-master nodes are used.

1- All the nodes on one side of the computational cell are assumed to be slaves to their corresponding nodes on the opposite side. This is basically a side-to-side relation. This type of periodicity is named "Periodic-Side (PS)"

2- The odd-numbered nodes of one side are assumed to be the master nodes while the even-numbered nodes to be the slaves of their corresponding nodes. This method is called one-to-one node matching; this type of periodicity is named "Periodic-Node (PN)".

3- The third of way is motivated by MD simulations where the selection of slave or master nodes on each side is random. We call this type of periodicity "Periodic-Random (PR)".

The geometry and loading conditions of the computational cell are similar to the ones discusses in sections 2.3 and 3.3 (see figure 2.1). The only difference here is that the boundary condition of the cell sides are not restricted to be confined. A number of simulations were carried out, including (2-10) GPa shocks with steep and ramp waves at different rise times. In the FE code, different boundary conditions have been used including free, confined and periodic. In the DD code, periodic and symmetric boundary conditions are used.

5.4 Results and Discussion

5.4.1 On the role of boundary conditions

Figure 5.2 compares the wave profiles generated using free and PS boundary conditions with the one generated using confined boundary condition. In theory, free boundary condition results in the propagation of uniaxial stress wave similar to the one generated using Hopkinson bar experiment for moderate strain rate (10^4/s), consequently free boundary condition is not suitable for the shock wave (uniaxial strain) loading. This is confirmed in our simulation in figure 5.2a, which shows that using free boundary condition results in much lower peak pressure compared to confined boundary condition. The implementation of PS boundary condition however, yields a relaxed state of stress with low peak pressure when compared to the experiment as illustrated in figure 5.2a.

Furthermore, both shear and longitudinal waves are generated which is discordant with plane wave characteristics as shown in figure 5.2b.

Figure 5.3 shows top views of the deformed shape for free, PS and confined boundary conditions. For the free case, wave propagation leads to bulging of the side surfaces out, while for the confined case, no distortion occurs in the simulation cell as the nodes cannot move normal to wave propagation. However, considerable distortion occurs in the PS case because the nodes on one side of the cell are forced to follow the corresponding node on the opposite side leading to shear mode and shear wave propagation. These results lead to the conclusion that using free or PS boundary condition is not suitable for shock wave propagation simulations. Therefore, wave profiles generated using PN and PR boundary conditions are tested by comparing their results with that generated using confined boundary condition. Figure 5.4 shows that:

a) Wave profile characteristics generated using PN or PR boundary condition are very similar to those generated using confined boundary condition. This suggests that PN and PR can be used in shock simulations with confidence
b) When comparing the shear components of the wave profiles we notice that PN matches almost exactly the confined case, whereas shear components appear in the PR case. The reason behind this shear component is directly related to the number of slave or master nodes in each side. We believe that ultimately if a very fine mesh is used in the PR case, then the number of slave and master nodes in each side will be equal (as in the PN case) and therefore the shear component will be eliminated. Plots of the deformed shaped of the PR and PN cases as shown in figure 5.5b confirm this point.

5.4.2 Mesh sensitivity analysis: The role of rise time on wave profile convergence

In order to examine the influence of rise time on the convergence of the wave profile, we carried out mesh sensitivity analysis for steep (zero rise time) and ramp waves. Figure 5.6a shows the wave profile resulting from using different mesh sizes of 1250, 2500, 3750, and 5000 elements respectively. For the zero rise time case, where a constant velocity is applied on the upper surface, the following has been observed as the mesh size increases: a) more fluctuations appear in the wave profile b) the wave front becomes steeper. For any signal, the velocity (U_p), the bandwidth (λ) and the frequency (ϖ) are related such that:

$$U_p = \lambda \varpi \tag{5.13}$$

The bandwidth is directly related to FE length (mesh size). As the number of FE increases, λ decreases. Since U_p is constant for the steep wave (equation 5.10), ϖ increases leading to more fluctuations in the wave profile. The same reasoning can be used to explain why the wave front becomes steep as well.

For the ramp wave however, the velocity increases linearly with time from zero to its maximum value. As a result, ϖ increases also linearly over the rise time period from zero to the value that corresponds to the frequency at U_p. For the same peak pressure (maximum U_p) the average frequency of fluctuations decreases with increasing the rise time and this explains the small number of fluctuations in the ramp wave compared to the steep wave. It is worth mentioning here that for a steep wave, the width of the wave front is related to the FE length. As the mesh density increases, the FE length decreases and therefore the wave front becomes steeper. Theoretically, a FE of zero length is required to reach the steep shock wave front. This elucidates why a very fine mesh is needed for the

wave profile to converge. For the ramp wave however, the wave front converges even using a coarse mesh as can be seen in figure 5.6b because the wave front is controlled by the rise time which is not affected by the FE size.

5.4.3 Strain localization and slip rotation

The characterization of post-deformation microstructure is very important to develop a better understanding to strain localization. Strain localization is inherently related to dislocation pattern configurations (number and position of peaks) that can be affected by the imposed strain rate and dislocation boundary condition. The change in pattern configuration may be attributed to the highly correlated dislocation motion. The effect of strain rate on the localized deformation in copper was investigated in chapter 2. In this section we investigate the effect of DD boundary conditions and the effect of slip rotation on the localized deformation in copper single crystal. Figure 5.7a shows the local dislocation densities calculated in a thin slab along the z direction using periodic and symmetric DD boundary conditions. Symmetric boundary condition allows the formation of more peaks with higher relative dislocation densities as shown in figure 5.7a. More details of pattern formation can be obtained by studying the contribution of each slip system to the total dislocation density. Figure 5.7b shows the relaxed configuration of the dislocation densities on each slip system when applying periodic and symmetric DD boundary conditions. The distribution of slip activation when using symmetric boundary condition seems to be symmetric around slip system 7, whereas the distribution is concentrated around slip system 9 when applying periodic boundary condition. This may be attributed to the initial distribution of dislocations and the interaction of the slip systems during the process of plastic deformation.

The role of slip rotation on the deformation process under shock loading is investigated in copper single crystal oriented in the [001] direction and shock loaded in $[00\bar{1}]$ direction by carrying out two simulations. In the first simulation, slip rotation according to equation 5.8 is taken into account, while no slip rotation is assumed in the second simulation. A single Frank-Read dislocation sources is located on slip system 7, which is combined from $(1\bar{1}1)$ slip plane and $[10\bar{1}]$ slip direction. The resulting Schmid factor under this loading condition is 0.408. Figure 5.8a shows that higher values of the local dislocation density are resulted when slip rotation is taken into consideration, suggesting that the dislocations experience higher levels of resolved shear stress- compared to no slip case- that lead to higher rate of multiplication. The change in the resolved shear is related to the change in Schmid factor, as the externally applied stress for the two simulations is the same. When the wave propagates in the crystal, the dislocation density increases, inducing plastic deformation that leads to gradual slip rotation, consequently Schimd factor changes as well. In the current simulation the time evolution of Schmid factor of slip system 7 is tracked in one subcell located in the central region of the computational cell. As can be seen in figure 5.8b, Schmid factor keeps increasing with time from its initial value of 0.408 to around 0.47.

A comparison of the contour plot of the effective plastic strain for the two simulations as illustrated in figure 5.9 shows that; a) more well defined localized bands are formed when slip rotation is taken into account compared to the no slip rotation b) a considerable increase in the effective plastic occurs. The maximum value of the effective plastic strain increases from 0.35 in the no slip simulation to a round 0.45 in the slip rotation case. That translates to 20% increase in the strain localization.

5.5 Summary and Conclusions

MDDP simulations were carried out to address several numerical and strain localization issues in modeling high strain rate shock loading in copper single crystal. The effect of FE boundary condition on wave propagation is investigated by implementing periodic boundary condition and comparing its results with free and confined boundary conditions. Furthermore, mesh sensitivity analyses for steep and ramp waves were carried out. In order to gain better understanding of the strain localization issue in the context of MDDP simulations, slip rotation was accounted for in the current simulations. Based on the results of this study, the following conclusions can be drawn:

a) Confined boundary condition is proven to be the best to simulate shock wave propagation as a uniaxial strain condition is achieved.

b) Periodic boundary condition based on side-to-side matching is not suitable for shock simulations. In disagreement with planar shock wave propagation, this boundary condition yields relaxed state of pressure and propagation of shear waves.

c) Wave profile generated using periodic boundary condition based on node-to-node matching are very similar to the one generated using confined boundary condition.

d) Mesh sensitivity analyses for steep and ramp shock waves show that the convergence in the ramp wave occurs at relatively coarse mesh density when compared to the steep wave. Moreover, loading the crystal using ramp wave results in a much smother wave with little fluctuations.

e) Taking into account slip rotation leads to more localized deformation.

References

Holian, L., and Lomdahl, P. S., 1998, *Science* **280**, 2085.

Kistensson, O., Sorenen, N. J., and Andersen, B., S, 2003, *Comp. Methods Appl. Mech. Engrg*., **192**, 1877.

Liu, X., Scaropas, J., and Blaauwendraad, J., 2005, *International Journal of Solids and Structures*. **42**,1883.

Meyers, M. A., Xu, Y. B., Xue. Q., Perez-Prado, M. T., and McNelley, T. R., 2003, *Acta Materialia* **51** 1307.

Mogilevskii, M. A., and Bushnev L. S., 1990, *Combustion, Explosion, and Shock Waves* **26**, 215.

Rivas, J. M., Quinones, S. A., and Murr, L. E., 1995, *Scripta Metallurgica et Materialia*, **33(1)**, 101.

Shehadeh, M.A., Zbib, H.M., and Diaz de la Rubia, T., 2005a, *Int. J. Plasticity*, in press.

Shehadeh, M.A., Zbib, H.M., and Diaz de la Rubia, T., 2005b, *Phil. Mag*., in press.

Soriano, H. L., and Nunes, C. C., 1995. *Computers & Structures*, **57(3),** 439.

Zukas, J. A., and Scheffler, D. R., 2000, *International Journal of Impact Engineering*, **24**, 925.

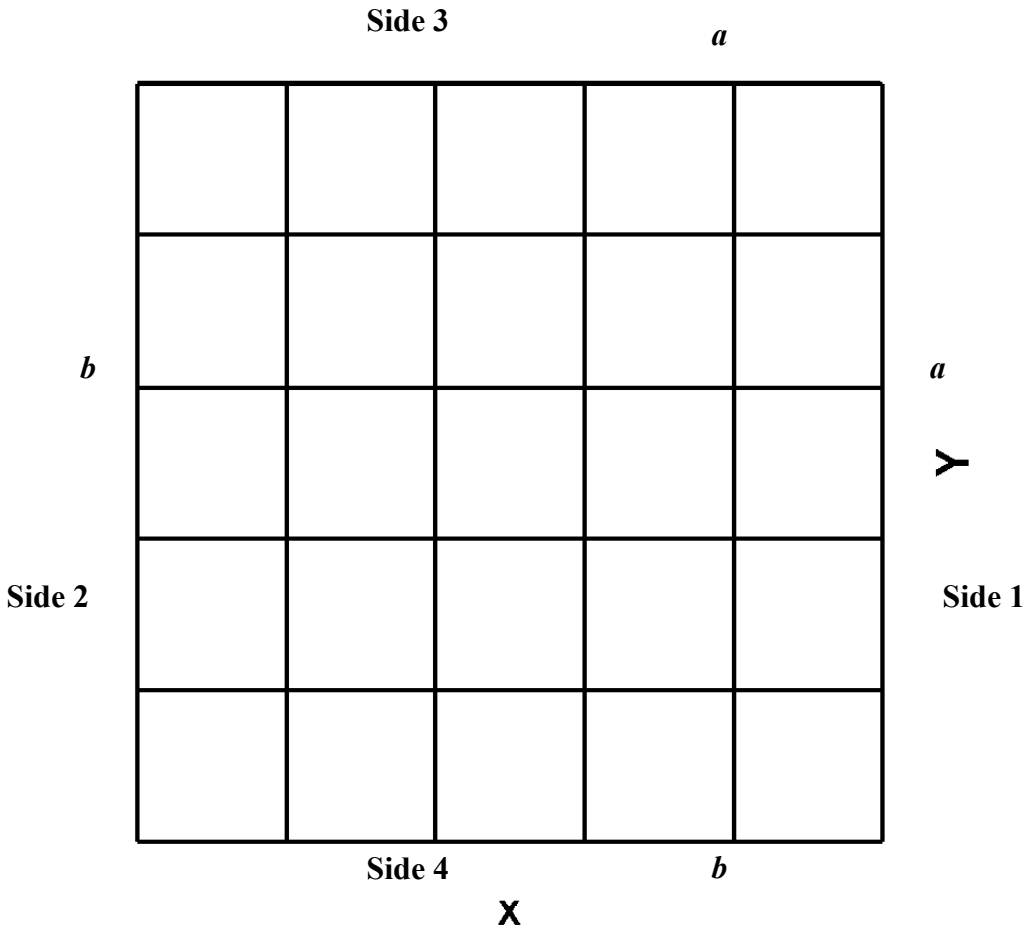

Figure 5.1. 2D unit cell labeled for a matching node pair denoted ***a*** for master and ***b*** for slave.

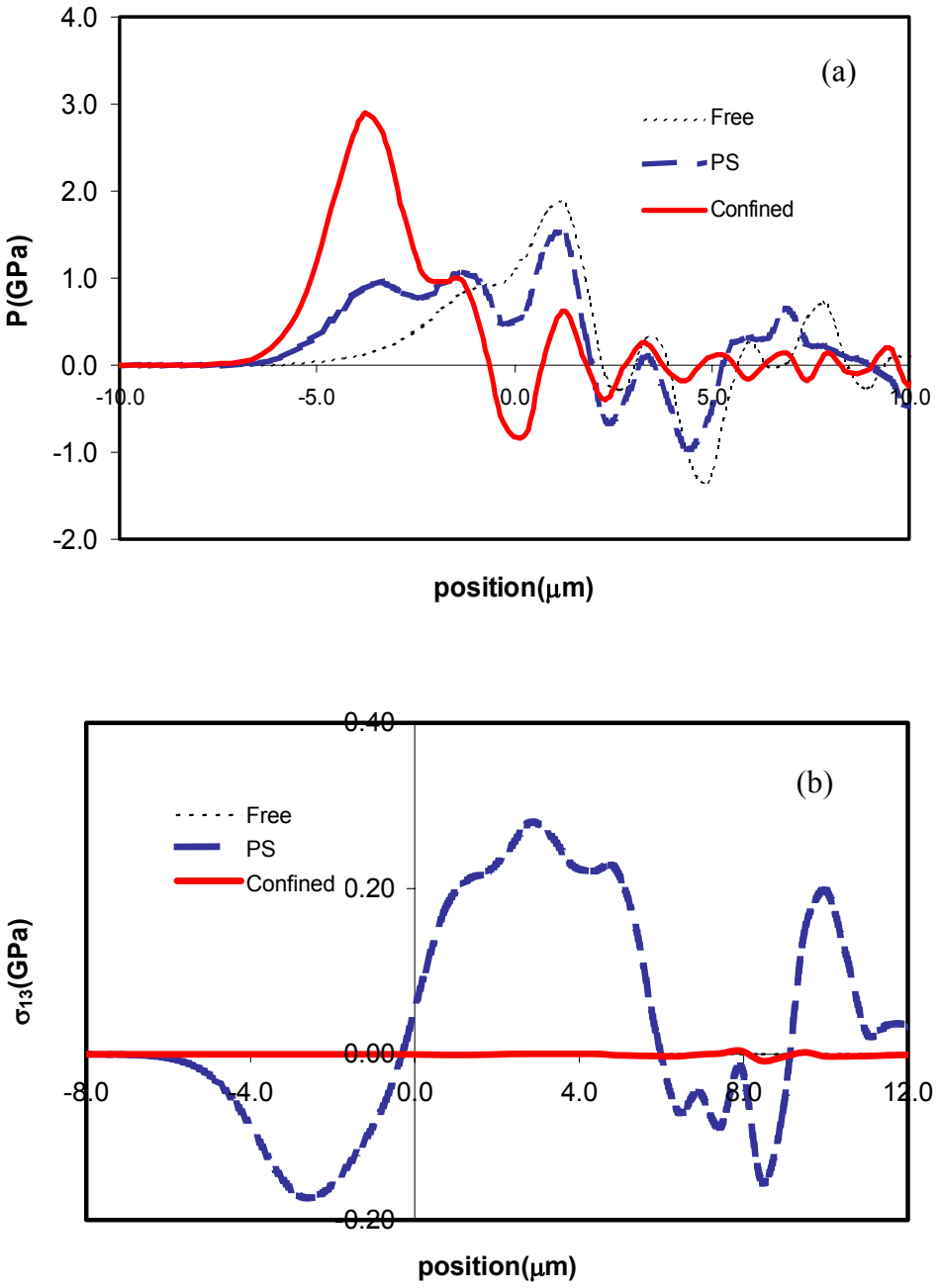

Figure 5.2. The effect of using free, confined and PS boundary condition in FE on (a) the longitudinal wave (b) Shear wave

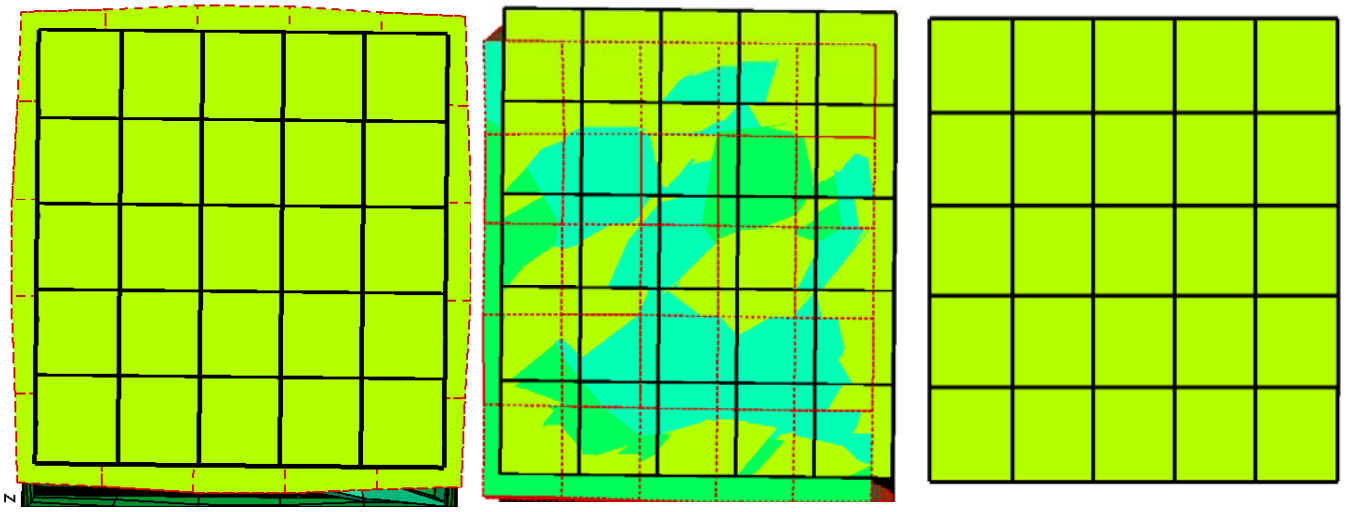

(a) (b) (c)

Figure 5.3. The resulting deformed shapes using (a) free (b) PS (c) confined boundary conditions. These figures are top views of the simulation cell.

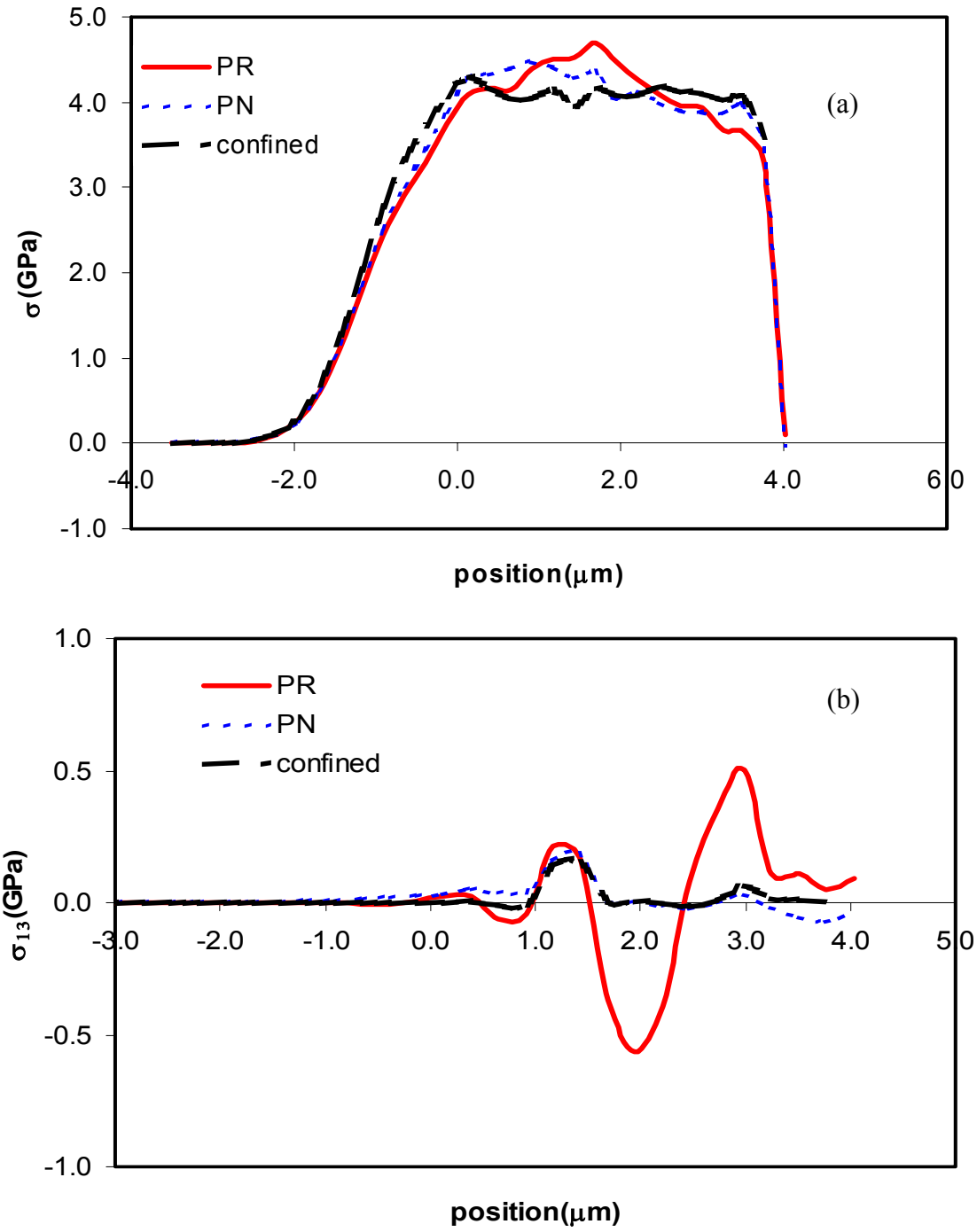

Figure 5.4. The effect of using different types of boundary condition on (a) the longitudinal wave (b) Shear wave

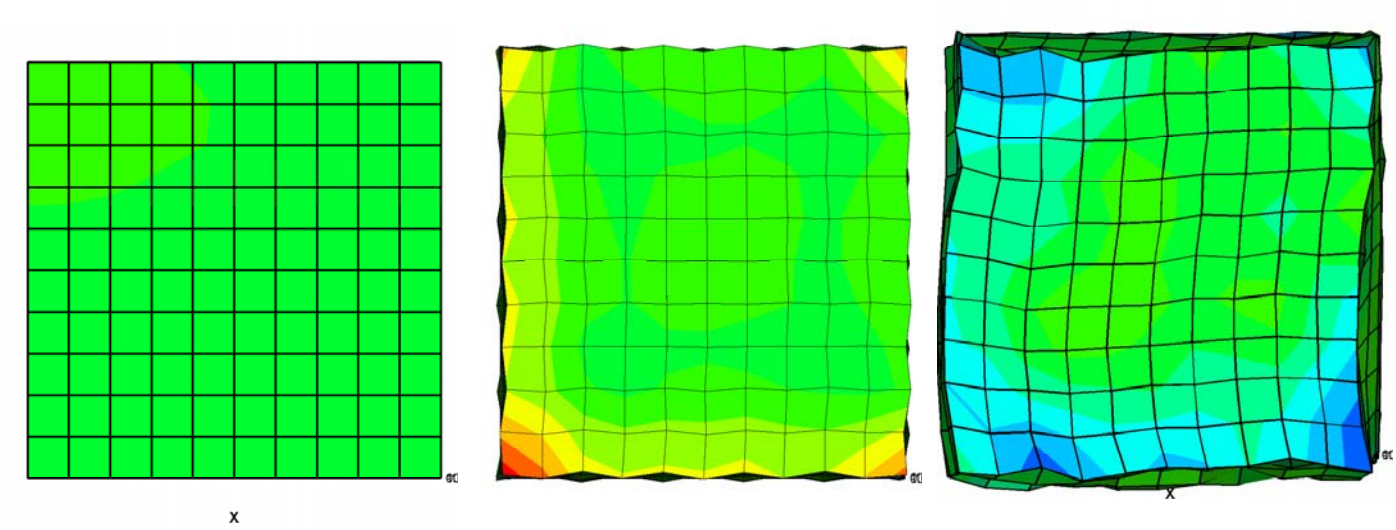

Figure 5.5. The resulting deformed shapes using (a) confined (b) PN (c) PR boundary conditions. These figures are the a top view of the simulation cell

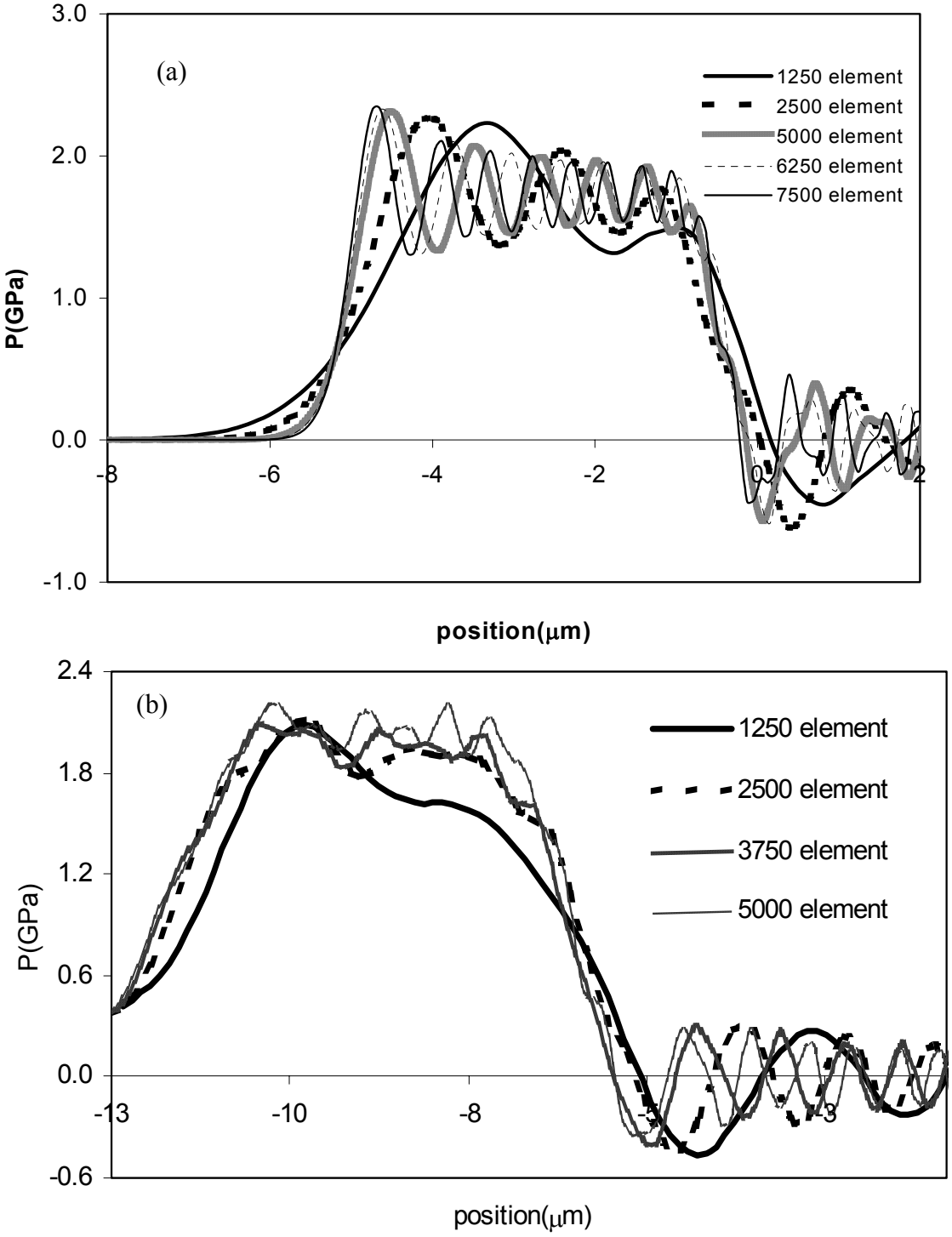

Figure 5.6. The effect of mesh size of the wave profiles for (a) steep wave (b) ramp wave.

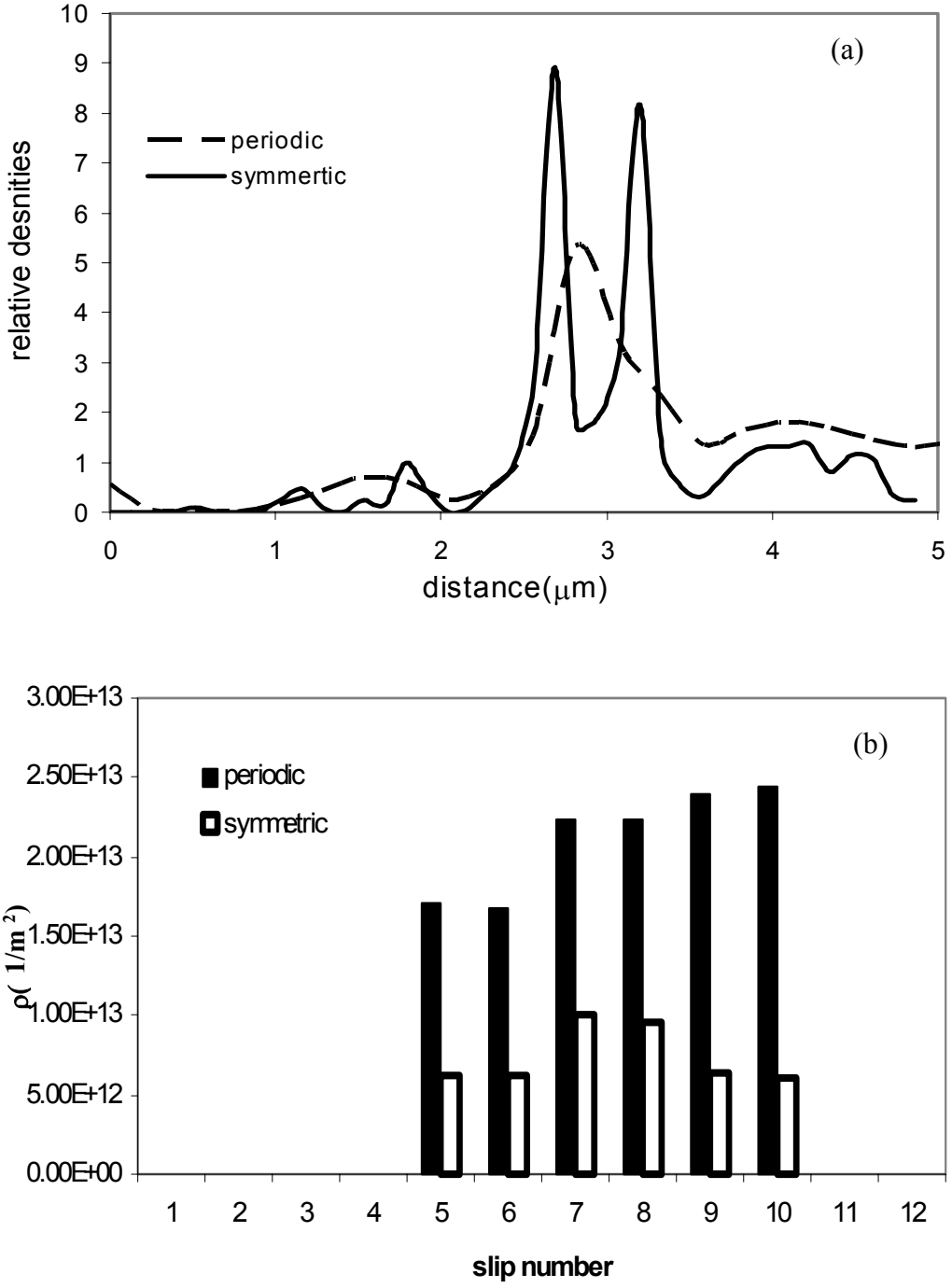

Figure 5.7. The effect of DD boundary condition on (a) relative dislocation densities (b) Slip activation.

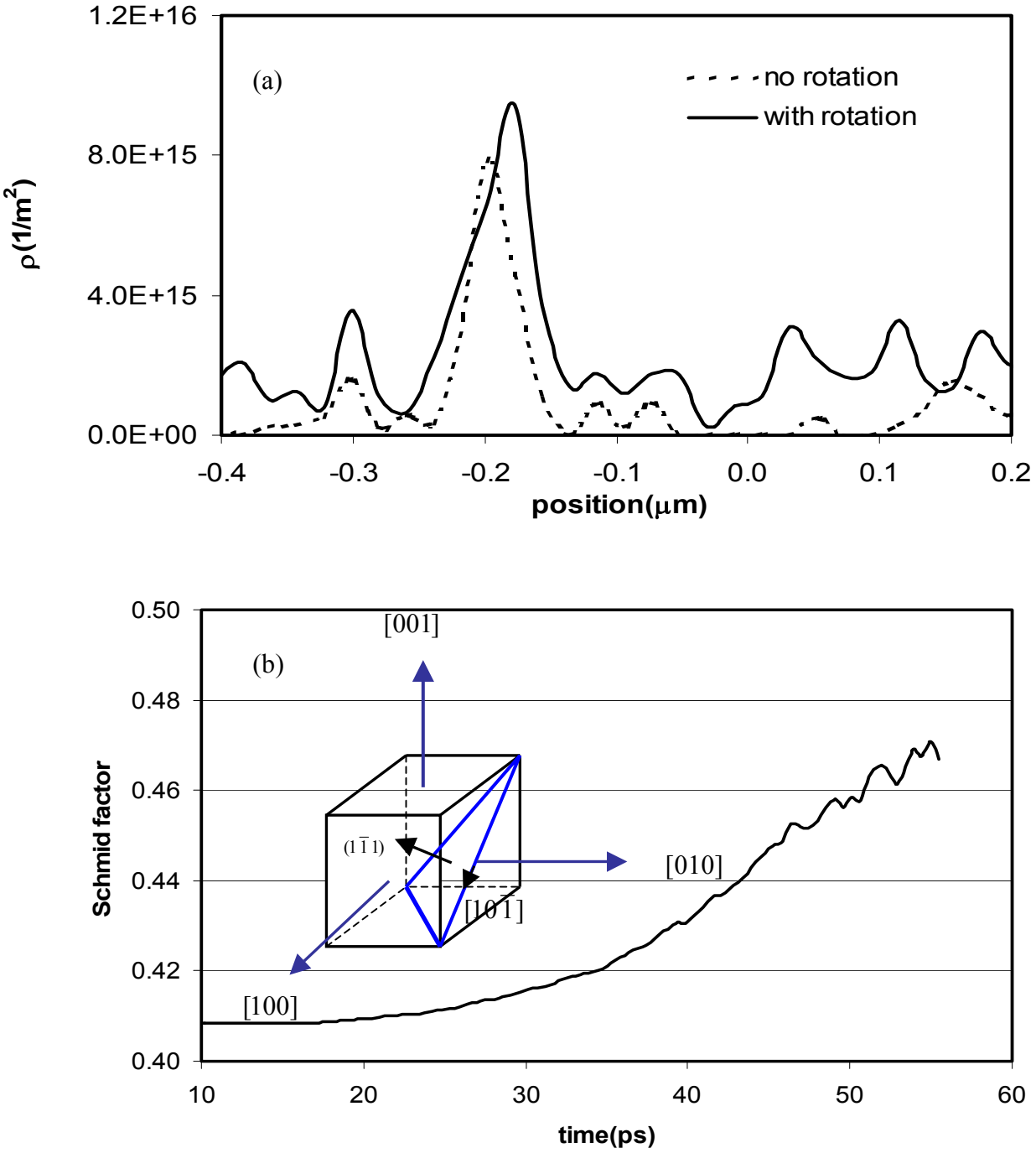

Figure 5.8. The influence of slip rotation on (a) local dislocation density (b) the evolution of Schmid factor. The loading direction is $[00\bar{1}]$.

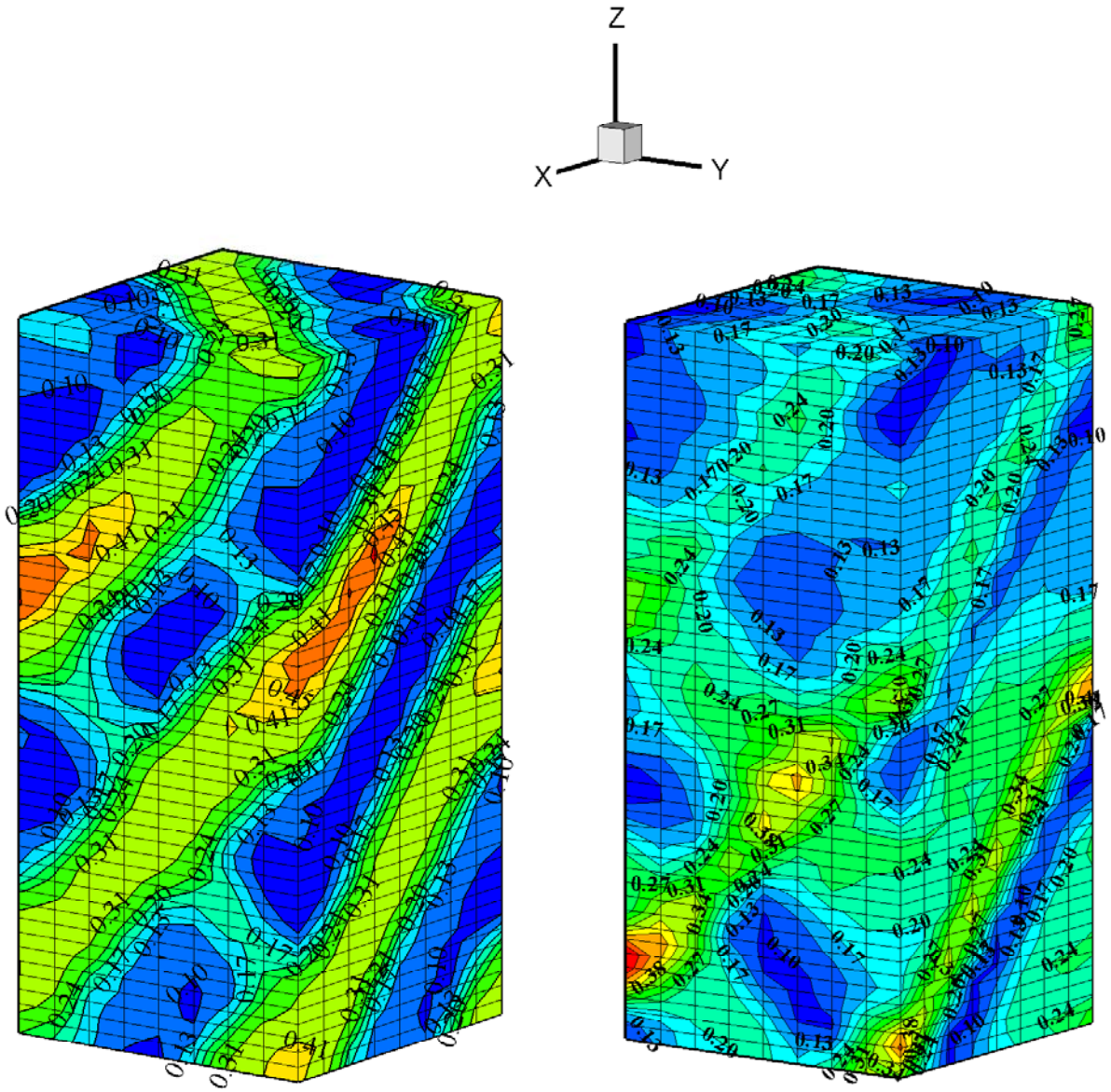

(a) (b)

Figure 5.9. Contour plots of the effective plastic strain in copper (a) with slip rotation (b) no slip rotation.

CHAPTER 6

Conclusions and Future Work

6.1 Summary

This dissertation presents the first piece of work in which MDDP simulations have been used to investigate plasticity induced in fcc single crystals under extreme loading conditions of high strain rate and high pressure. Our understanding of the materials' behavior at high deformation rates has to improve at different length and time scales to resolve the multiple uncertainties still present in this expanding area of materials science. MDDP framework has been modified to account for several important issues in the area of the dynamic response of materials. These modifications include:

I. The implementation of a nonlinear constitutive model to account for pressure-dependent elastic properties and Hugoniot equation.

II. The implementation of cubic symmetry exhibited by fcc single crystal that leads to anisotropy in the elastic properties.

III. A new model for homogeneous nucleation of dislocations based on large-scale atomistic simulations of shock loading has been included.

IV. Numerical and shear localization issues have been addressed. Periodic boundary condition has been implemented in the FE model and calculations of slip systems rotation have been carried out.

6.2 Conclusions

Based on the present MDDP analysis of shock-induced plastic deformation, the following can be concluded:

1. The interaction between dislocation sources and shock waves leads to avalanche of dislocations. The results of our calculations show that dislocation density is proportional to strain rate and pulse duration and that dislocation density has a power law dependence on pressure with a power of 1.70. The instantaneous speed distribution of dislocations interacting with a wave front shows that the speed of a small percentage of the dislocations move at speed approaching the shear wave velocity.
2. The dislocation microstructure is controlled mainly by strain rate. Dislocation micro bands coincident with the {1 1 1} planes are formed at strain rate larger than 10^6 s^{-1}, whereas, dislocation entanglements were formed at strain rates lower than 10^6 s^{-1}. When the homogenous model of nucleation is included, weak dislocation cellular structure was formed.
3. It is observed that the inclusion of pressure dependent elastic properties in the FE constitutive equation influences the shape of the wave profile leading to higher values of peak pressure and faster wave propagation speed. Incorporating the effect of crystal anisotropy in the elastic properties results in an orientation dependent wave speed and peak pressure.
4. The calculations based on the homogenous nucleation model show that the dislocations are produced at and behind the wave front at huge rates taking the

uniaxialy-compressed material to a hydrostatically compressed state (1D→3D) after a few tens of ps. Furthermore, the density of dislocations produced in a sample with pre-existing dislocation sources decreases with shock wave rise time.

5. Calculations based on the homogenous nucleation model show that the dislocations are produced at and behind the wave front at huge rates taking the uniaxialy-compressed material to a hydrostatically compressed state (1D→3D) after a few tens of ps. Furthermore, the density of dislocations produced in a sample with pre-existing dislocation sources decreases with shock wave rise time.
6. The analytical calculations using the standard nucleation theory shows that the threshold pressure for homogenous nucleation is larger than what expected using the continuum theory. This result is in a very good agreement with the 30 GPa threshold pressure predicted by MD simulations.
7. The investigation of wave profile characteristics using different FE boundary conditions illustrates that the confined boundary condition is the best boundary condition for modeling shock wave propagation. However, periodic boundary conditions based on node-to-node matching and random selection of slave and master node has proven to be suitable in multiscale shock simulations.
8. Mesh sensitivity analyses for steep and ramp shock waves show that the convergence in the ramp occurs at relatively coarse mesh density when compared to the steep wave. Moreover, loading the crystal using ramp wave results in a much smother wave profile.
9. Taking into account lattice rotation enhances strain localization.

6.4 Major Contributions of this Work to the Area of Shock Induced Plasticity

Understanding the dynamic plastic response of metals at high strain rate is essential for the understanding of the mechanisms of plastic flow, which is of great technological importance. High rate of loading occurs in many applications such as crash worthiness, high speed machining, and armor penetration. Predicting the material response to such extreme loading condition requires knowledge of mechanical and metallurgical properties at different length scales.

There are many uncertainties involved in the material response under extreme loading conditions, which current constitutive models and experiments cannot resolve. These uncertainties include the lack of information on the material strength, phase transformations and mechanisms of plastic deformation. The current effort is focused on addressing fundamental issues related to interaction process between dislocations and shock waves aiming to resolve some of the uncertainties involved under extreme loading conditions.

In this work, detailed calculations of shock-induced plasticity were carried out for the first time using a multiscale dislocation dynamics model of plasticity. The current modeling method is useful in studying materials processing techniques that use short-pulse lasers. Our results agree and are consistent with several recent laser-loading experimental findings, making our model extremely useful in planning future high-pressure laser experiments. We believe that these simulations can complement the

experiments as they provide information at extremely short time that the most powerful laser facility cannot probe.

The degree of agreement between the dislocation dynamics model with the atomistic simulations is promising and opens up the possibility of confidently simulating shocks and ramped compression waves that are impossible to model with atomistic methods, even with the current most powerful parallel computers.

Many novel materials have heterogeneous microstructures that enhance their mechanical properties. It is widely known that shock waves influence the mechanical properties of the shocked material as a result of the generation pf high density of defects. This work shows that different dislocation microstructures are formed depending on different shock loading conditions such as peak pressure and pulse duration. The effect of the resulting microstructure on the mechanical properties can be investigated by running a new set of multiscale simulations such as simple tensile or nano-indentation simulations. Using this predictive multiscale model can be useful to design new experiments in which samples of enhanced mechanical properties can be produced.

6.4 Future Work and Recommendations

MDDP simulations of shock induced plasticity hold a great promise for investigating deformation process of metals in regimes that cannot be probed by current experiments. Based on these research findings, we recommend the following:

1. Incorporating the effects of temperature and pressure on the dislocation mobility can be very important. This may solve some of the inconsistencies between DD

and MD results that appeared when investigating the role of homogenous nucleation on the mechanism of deformation.

2. Current DD code can be used to simulate the deformation process in fcc and bcc materials. However, extensive research has been carried out of other crystal structures. Therefore, other crystal structures especially hcp and tetragonal will be considered for future research.
3. Under high strain rate loading, there is a threshold pressure beyond which the deformation mechanism changes from dislocation glide to twinning. The mechanism of twining in the context of DD simulations will be considered in the future.
4. In the current simulations, the base of the computational cell was assumed to be rigid. Therefore, when the shock wave hits the base, it reflects to the material block and interacts with the dislocations again. In order to isolate the effect of the reflected waves, we were forced to use a specimen of very high aspect ratio (height/width), increasing the time and the cost of the calculations. A better solution to resolve this problem is by the implementation of FE absorbing (non-reflective) boundary condition.